

For Reference


NOT TO BE TAKEN FROM THIS ROOM

For Reference

NOT TO BE TAKEN FROM THIS ROOM

Ex LIBRIS
UNIVERSITATIS
ALBERTAENSIS





Digitized by the Internet Archive
in 2023 with funding from
University of Alberta Library

https://archive.org/details/Anderson1970_1

THE UNIVERSITY OF ALBERTA

GEOMAGNETIC DEPTH SOUNDING AND THE
UPPER MANTLE IN THE WESTERN UNITED STATES

by



CHESTER W. ANDERSON III

A THESIS

SUBMITTED TO THE FACULTY OF GRADUATE STUDIES
IN PARTIAL FULFILMENT OF THE REQUIREMENTS FOR THE DEGREE
OF DOCTOR OF PHILOSOPHY

DEPARTMENT OF PHYSICS

EDMONTON, ALBERTA

SPRING, 1970

12-1
1970
33

UNIVERSITY OF ALBERTA
FACULTY OF GRADUATE STUDIES

The undersigned certify that they have read,
and recommend to the Faculty of Graduate Studies for
acceptance, a thesis entitled GEOMAGNETIC DEPTH SOUNDING
AND THE UPPER MANTLE IN THE WESTERN UNITED STATES
submitted by Chester W. Anderson III in partial fulfilment
of the requirements for the degree of Doctor of Philosophy.

ABSTRACT

In September 1967 two magnetic variation events, a substorm and storm, were recorded by a two-dimensional array of 42 three-component variometers between latitudes 36°N and 43°N and longitudes 101°W and 116°W . Fourier analysis of these events shows that a complex spectrum with many maxima typify the storm and the substorm has a smooth spectrum. Upper mantle conductivity structure can be seen qualitatively in the original variograms, but is far more sharply defined in maps of Fourier spectral component amplitudes and phases. Separation of the Fourier spectral components into internal and external parts gives further definition to the conductive structures and allows quantitative analysis to be undertaken. A ridge of high conductivity runs at a depth no greater than 200 km. under the Southern Rocky Mountains between the Great Plains and the Colorado Plateau, which marks a low-conductivity region within the Cordillera. A strong conductivity anomaly runs north-south along the Wasatch Front through central Utah, and indicates the presence of an upwelling of highly conductive material at depth no greater than 120 km. along the edge of a step structure which brings the conductive mantle to shallower depths under the Basin and Range province than under the

Colorado plateau. The geomagnetic deep sounding anomalies are found to be in excellent agreement with existing heat-flow data, thus supporting correlation of electrical conductivity with temperature. There is also good correlation with the available seismic velocity information for the upper mantle.

ACKNOWLEDGEMENTS

I wish to thank Dr. D.I. Gough for his invaluable guidance, encouragement and patience during the supervision of my research.

The collaboration of Dr. H. Porath, University of Texas, Dallas, Texas, Dr. J. Reitzel, Arthur D. Little, Co., and Mr. D.W. Oldenburg on this project has been most helpful.

Mr. H. McCullough and Mr. W. Newman receive special thanks for their long hours spent collecting data with the writer during the summer of 1967.

I am also grateful to Dr. J.A. Jacobs for his interest in my academic studies and for his continuous support and encouragement throughout my doctoral studies.

Mrs. Mary Yiu and Mrs. L. Pridham are also commended for their excellent job of typing this thesis.

The writer was financially supported throughout his doctoral studies by a Graduate Teaching Assistantship from the Department of Physics, University of Alberta.

The Southwest Center of Advanced Studies' contribution to this project was supported by the United States National Science Foundation and the University of Alberta's contribution was supported by the National Research Council, the Defence Research Board and the University of Alberta.

TABLE OF CONTENTS

	Page
TABLE OF CONTENTS	i
LIST OF ILLUSTRATIONS	iv
ACKNOWLEDGEMENTS	
ABSTRACT	1
INTRODUCTION	3
OUTLINE OF THE THESIS	7
CHAPTER 1 GEOMAGNETIC DEPTH SOUNDING THEORY	9
1.1 The nature of the geomagnetic depth sounding problem	10
1.2 "Flat-Earth" model with uniform conductivity	10
1.3 Plane-layered model with uniform conductivity	17
1.4 The two-layer model	24
1.5 Electromagnetic induction in non-uniform conductors	28
1.6 Source fields	40
1.7 Two basic geomagnetic depth sounding methods	44
1.8 Fourier transform maps	48
1.9 Separation of the magnetic fields	53
1.10 Limitations of geomagnetic depth sounding	59

CHAPTER 2	PREVIOUS GEOMAGNETIC DEPTH SOUNDING IN THE WESTERN UNITED STATES	66
CHAPTER 3	TECHNIQUES OF OBSERVATION AND INTERPRETATION	84
3.1	The array	84
3.2	Variometers and field procedures	86
3.3	Magnetic variation records	89
3.4	Spectral analysis	90
3.5	Separation of the variation fields	100
CHAPTER 4	ANOMALIES IN THE VARIATION FIELDS AND CONDUCTIVE STRUCTURES	106
4.1	Interpretation procedures	106
4.2	Variograms	108
4.3	Maps of unseparated spectral components	113
4.4	Separated fields in the period domain	126
4.5	Separated storm fields	127
4.6	Conductive structures	146
4.7	Models of conductive structures	156
CHAPTER 5	GEOPHYSICS AND UPPER MANTLE STRUCTURE IN THE WESTERN UNITED STATES	163
5.1	Seismology	163

5.2 Conductivity and thermal structure as a function of time	177
5.3 Electrical conductivity, temperature and heat flow	179
5.4 Conclusions	189
BIBLIOGRAPHY	191

LIST OF ILLUSTRATIONS

Figures		<u>page</u>
1.1	Induction in a conductive half space	16
1.2	Plane layered conductive model	18
1.3	Depth at various frequencies for Lahiri and Price model of the Earth	27
1.4	Conducting sheet insulating crust and conductive mantle	30
1.5	Undulating "perfect substitute conductor"	37
1.6	Possible currents in a polar magnetic substorm	42
1.7	Penetration of electric variation fields, three layer model	62
1.8	Penetration of magnetic variation fields	63
2.1	Geomagnetic deep sounding in the western United States: locations of observation	67
2.2	Schmucker's observations of a bay variation: May 10, 1960	68
2.3	Schmucker's second model for the Rio Grande anomaly	73
2.4	Schmucker's third model for the Rio Grande anomaly	75
2.5	East Front anomaly of Colorado	78
2.6	Magnetotelluric measurement sites of Swift	80
2.7	Conductivity profiles	81
3.1	The 1967 variometer array	85
3.2	Fourier spectral amplitude and phase for vertical component of substorm of September 1, 1967, for stations across the Wasatch Front on Line 1	94

Figures		<u>page</u>
3.3	Fourier spectral amplitude and phase for vertical component of substorm of September 1, 1967, for stations across Wasatch Front on Line 3	95
3.4	Fourier spectral amplitude and phase for vertical component of storm of September 20-21, 1967, at stations of Line 3 on either side of the Wasatch Front	97
3.5	Spectra of three components of field of storm of September 20-21, 1967	99
4.1	Variograms for substorm of September 1, 1967	109
4.2a	Variograms for storm of September 20-21, 1967: two northern lines	110
4.2b	Variograms for storm of September 20-21, 1967: two southern lines	111
4.3	Fourier spectral amplitude maps of vertical component substorm field	114
4.4	Fourier spectral phase maps of the vertical component substorm field	115
4.5	Fourier spectral amplitude maps of horizontal components of the substorm field	116
4.6	Fourier spectral phase maps of horizontal components of the substorm fields	117
4.7	Fourier spectral amplitude maps for three components of the storm field	118
4.8	Fourier spectral phase maps for three components of the storm field	119
4.9	Simplified map of two local internal currents and relationships between external and internal field components	121

Figures		<u>page</u>
4.10	Fourier spectral amplitude map for vertical component of substorm at $T = 120$ minutes	122
4.11	Southern limit of the amoral arc in relation to amplitude of $D_{st}(H)$ for storms	130
4.12	Variation of field components with latitude	131
4.13	Separated fields components for storm along east-west profiles. $T=89$ minutes	133
4.14	Separated storm field profiles. $T = 150$ minutes	134
4.15	Separated storm field profiles. $T = 256$ minutes	135
4.16	Separated substorm field profiles. $T = 89$ minutes	136
4.17	Amplitude of separated external northward horizontal field X_e of the storm	138
4.18	Separated vertical and horizontal eastward storm field at $T = 150$ minutes	139
4.19	Separated Fourier sine transform of storm field components Y and Z at $T = 256$ minutes	
4.20	Isolated cylindrical conductor	148
4.21	Fields of a line current and two-dimensional dipole	150
4.22	Internal parts of Y and Z components of storm field at $T = 150$ minutes	152
4.23	Model fitted to normalized anomalous vertical field of storm at $T = 89$ minutes	158
4.24	Model fitted to normalized anomalous eastward horizontal field of substorm at $T = 89$ minutes	159

Figures		<u>page</u>
4.25	Internal Y and Z fields of storm at T = 150 minutes as compared to con- ductivity model, figure 4.24	161
5.1	P _n velocities in Western United States, after Herrin and Tagart	165
5.2	Station residuals in P arrival times over the United States	169
5.3	Station residuals in S arrival times over the United States	170
5.4	Observational profiles used by Archambeau, Flinn and Lambert (1969)	172
5.5	Velocity profiles in four regions of the United States	174
5.6	Evolution of granites and their electrical conductivities	176
5.7	Heat flow and conductive models	184
5.8	Heat flow and geomagnetic depth- sounding and magnetotelluric stations	185
5.9	Model structure for results of 1967 array	186
5.10	Heat flow and Fourier spectral amplitude contour map	188

INTRODUCTION

Geophysical observations of several kinds indicate that the upper mantle of the earth under North America is laterally inhomogeneous. Upper mantle seismic velocities of 8.0 km/sec or larger are characteristic of the eastern United States and the Great Plains province, while velocities decrease to values of 7.9 km/sec or lower west of the Rocky Mountains (Herrin and Taggart, 1962). A similar pattern is shown by travel time anomalies of seismic waves at vertical incidence. A "time-term" like analysis of P and S waves (Cleary and Hales, 1966; Doyle and Hales, 1967) gives evidence of early arrivals at stations in the eastern United States and predominantly late arrivals in the western United States. As the differences between P and S travel time residuals and the gravity anomalies in the central and western United States cannot be explained by the Birch (1961) relation between velocity and density, Doyle and Hales (1967) suggested that temperature anomalies in the upper mantle, possibly accompanied by partial melting, might cause lower velocities in the western United States by lowering the values of the elastic constants. Archambeau, Flinn and Lambert (1969) substantiate the existence of partial melting by giving evidence of the coexistence of low-Q

zones with zones of low P_n velocities in the western United States.

This interpretation is supported by recent heat flow data (Lee and Uyeda, 1965; Roy, Decker, Blackwell and Birch, 1968; Blackwell, 1969). High heat flow in the Southern Rockies and the Basin and Range province correlates with low upper mantle velocities; normal heat flow is found for the Great Plains and has high upper mantle velocities.

Seismic and heat flow data are not abundant enough as yet to delineate the boundaries of different upper mantle provinces with accuracy. However, temperature anomalies in the upper mantle will cause anomalies in the electrical conductivity, as silicates at upper mantle temperatures show semi-conductor properties (Tozer 1959).

Geomagnetic variations measured at the surface of the Earth are the vector sum of external variations originating in currents in the ionosphere and magnetosphere and of internal variations arising from currents induced by the external part in the conductive regions in the upper few hundred kilometers of the Earth. Lateral inhomogeneities in the electrical conductivity of the upper mantle will give rise to anomalies in the field measured at the surface. Qualitative interpretation of such conductive structures can be made from the amplitudes of geomagnetic variations in both the time and frequency domains if Fourier analysis of the variations is under-

taken, especially of the vertical component. Quantitative interpretation of such conductive structures requires the separation of the internal and external parts of the field. The amplitude and phase relationships in the frequency domain between the internal and external parts can then be fitted by the appropriate conductivity models through the employment of conformal mapping techniques (Schmucker, 1969).

In the summer of 1967 42 variometers designed and built by Gough and Reitzel (1967) to be inexpensive and reliable were set out by the University of Alberta and the Southwest Center for Advanced Studies in a study of the crustal and upper mantle conductive structures in the western United States.

Variation anomalies found during the summer of 1967 have been described, with a qualitative interpretation by Reitzel, Gough, Porath and Anderson (1970). A following paper by Porath, Oldenburg and Gough (1970) presents the results of a three dimensional separation of a polar substorm of September 1, 1967, and a preliminary interpretation by simple conductivity models of the relation between the substorm separated fields. This thesis presents extensions of the qualitative interpretation of the variation anomalies presented by Reitzel et al. 1970. Also presented are results of the separation of the complicated polar storm field of September 20-21, 1967 with conductive models determined from the relationship between the separated storm fields.

The writer joined the project in early 1967 and helped assemble and test twenty-two Gough-Reitzel variometers prior

to the 1967 summer field season. The writer was a member of a team consisting of Dr. D.I. Gough and Mr. W. Newman which installed twenty-one variometers in two east-west lines across the western United States. Regular servicings were carried out by Mr. Newman, Mr. McCullough and the writer at seven day intervals. This servicing routine required some 20,000 miles of driving by each member of the team.

The writer was responsible for the initial data reduction for the substorm of September 1, 1967. The results of this analysis were presented at the 1968 American Geophysical Union meeting in Washington, D.C. and at the 1968 Canadian Association of Physicists meeting at Calgary, Alta. The writer was responsible for all the data reduction and analysis of the storm of September 20-21, 1967. Also the writer prepared maps of unseparated spectral amplitudes and phases of the three-components of both the substorm and storm fields mentioned above. These results were presented to the 1969 A.G.U. meeting in Washington, D.C. in a paper by Reitzel, Gough, Porath and Anderson.

To corroborate the model of the upper mantle under the western United States proposed by Porath et al. (1970) the writer separated three components of the storm field in the frequency domain at periods $T=89$, $T=150$ and $T=256$ minutes. Semi-quantitative interpretation of the storm internal fields at these periods does support Porath's model particularly under the Wasatch Fault zone in Utah.

The writer has also shown in Chapter 5 of this thesis that this model of the upper mantle is consistent with seismic and heat flow results in the western United States.

OUTLINE OF THE THESIS

Chapter 1 develops geomagnetic deep sounding theory pertaining to the determination of conductivity structure under a plane surface starting from Maxwell's equations through to theoretical estimates of depth and conductivity structures in the Earth. The governing equations for electromagnetic induction in a conducting half-space, multi-layered structure and undulating conducting surfaces are presented. Two methods of deep sounding, the "Base Station" and "Array" methods are also presented. The concept of applying fast Fourier analysis to a single event at each station over an entire array is developed with the emphasis on the physical meaning of two-dimensional maps representing the spatial variations of a magnetic event. Separation of the total field into its internal and external parts is discussed on a global basis and over a plane surface.

Chapter 2 covers previous geomagnetic deep sounding investigations in the western United States. The work of Schmucker (1964), Caner et al. (1967), Gough and Reitzel (1967) and Swift (1967) is reviewed with the aim of obtaining correlations with the work of Reitzel et al. (1970), Porath et al. (1970) and this thesis as to the locations of the major magnetic anomalies in the western

United States; primarily the Wasatch Front and East Front anomalies.

Chapter 3 gives a description of the 1967 array, the recording equipment used and the field procedures used. This is followed by a discussion on the processing of the magnetic variation records from analog to digital form. A section on the special spectral analysis techniques along with the method of separation of the magnetic variations is also included.

In Chapter 4, the basic analyses for the stations in the western United States from which magnetograms were obtained are presented and correlated with the results of Reitzel et al. (1970) and Porath et al. (1970).

Chapter 5 discusses the use of seismology and heat flow work as upper mantle investigation techniques compared to the "Array" method of geomagnetic deep sounding. Suggestions for further work are included in this chapter.

CHAPTER 1

GEOMAGNETIC DEPTH SOUNDING THEORY

This chapter develops geomagnetic depth sounding theory as applied to the determination of conductivity structure under a plane surface, starting from Maxwell's equations through to theoretical estimates of depth and conductivity of structures in the Earth. The governing equations for electromagnetic induction in a conducting half-space (flat-earth model), multi-layered structure and undulating conducting surfaces are presented. Two methods of depth sounding, the "Base Station" method and the "Array" method are considered. The concept of applying fast Fourier analysis to a single event at each station over an entire array is developed with the emphasis on the physical meaning of two-dimensional maps representing the spatial variations of a magnetic event. Separation of the total field into its internal and external parts is discussed on a global basis (Rikitake, Yokoyama and Sato 1956, Lahiri and Price 1939) and over a plane surface (Siebert and Kertz 1957, Weaver 1963, Oldenburg 1969). Knowledge of the external field makes possible study of the morphology of the source of the magnetic event. Knowledge of the internal field makes possible the accurate location on the map and estimation of maximum

depths of regions of enhanced conductivity within the Earth.

1.1 The nature of the geomagnetic depth sounding problem

The inducing field is usually of global dimensions but much interest lies in local variations of the magnetic field over a few tens of kilometers. The sphericity of the Earth can be neglected in such studies and the Earth treated as a plane-surfaced infinitely large conductor having some non-uniform distribution of conductivity.

Even if the inducing field can be taken as uniform over an area, the strength of the induced currents in that area is not completely determined by the inducing field and the ground conductivity in the immediate neighborhood. The strength of the induced currents depends on the distribution of the entire inducing field and the geometry and conductivity of a conductor over a region of similar dimensions as that of the inducing field (Dyck and Garland 1969). The geomagnetic depth sounding problem then is the determination of the redistribution of some extended system of induced currents by local differences in conductivity structure over that surface.

1.2 "Flat-Earth" model with uniform conductivity

Most of the induction theory presented here is

due to Price (1950, 1962).

For the "flat-earth" or infinite half-space model Maxwell's equations reduce to:

$\nabla \times E = -\frac{\partial B}{\partial t}$	outside the	$\nabla \times E = -\frac{\partial B}{\partial t}$	inside the
$\nabla \times H = 0$	conductor	$\nabla \times H = 4\pi J$	conductor
$\nabla \cdot B = 0$	($z < 0$)	$\nabla \cdot B = 0$	($z > 0$)
$\nabla \cdot D = 0$		$\nabla \cdot D = 0$	
		$J = \sigma E$	

E = electrical field intensity (volts/meter)

B = magnetic field induction (webers/m²)

D = dielectric displacement (coulombs/m²)

H = magnetic field intensity (amps/meter)

and ϵ , μ and σ are spatially dependent functions.

The surface of the conductor is represented by the $z = 0$ plane and z is taken positive downward. By taking the curl of Maxwell's equations and neglecting the displacement currents both inside and outside the conductor the resulting wave equations reduce to

$$\nabla^2 E = 0 \quad z < 0 \quad (\text{Laplace's Equation}) \quad (1.1)$$

$$\nabla^2 E = 4\pi\sigma(z)\mu^0 E \quad z > 0 \quad (\text{Diffusion or Induction Equation}) \quad (1.2)$$

It can be shown that since $\sigma = \sigma(z)$ only, all currents will flow parallel to the surface of the conductor

and $E_z = 0$ everywhere in the conductor. From $\nabla \cdot \mathbf{J} = 0$ for $(z > 0)$,

$$\sigma \left(\frac{\partial E_x}{\partial x} + \frac{\partial E_y}{\partial y} + \frac{\partial E_z}{\partial z} \right) = - E_z \frac{\partial \sigma}{\partial z}$$

and therefore

$$\frac{\partial E_x}{\partial x} + \frac{\partial E_y}{\partial y} = 0 \quad . \quad (1.3)$$

Let the electric field be of the form

$$\vec{E}(x, y, z, t) = \vec{Z}(z, t) \vec{F}(x, y) \quad (1.4)$$

where (1.3) becomes

$$\vec{F}(x, y) = \left(\frac{\partial P}{\partial y}, -\frac{\partial P}{\partial x}, 0 \right) \quad (1.5)$$

implying that the electric field is derivable from a scalar potential $P(x, y)$. Substituting (1.4) into (1.2) and separating the variables

$$\frac{1}{F} \left\{ \frac{\partial^2 F}{\partial x^2} + \frac{\partial^2 F}{\partial y^2} \right\} = \frac{1}{Z} \left\{ 4\pi\sigma\mu \frac{\partial Z}{\partial t} - \frac{\partial^2 Z}{\partial z^2} \right\} = -k^2$$

where k^2 is a constant of separation. The governing equations inside the conductor to be solved then are

$$\frac{\partial^2 P}{\partial x^2} + \frac{\partial^2 P}{\partial y^2} + k^2 P = 0 \quad (1.6)$$

for the horizontal field and

$$\frac{\partial^2 Z}{\partial z^2} = \{k^2 + 4\pi\mu\sigma \frac{\partial}{\partial t}\} Z \quad (1.7)$$

for the vertical field. Equation (1.6) also holds for $z < 0$. For $z < 0$ the Z equation is

$$\frac{\partial^2 Z}{\partial z^2} = k^2 Z$$

with the solution

$$\vec{Z}(z,t) = C(t)e^{-kz} + D(t)e^{kz} .$$

If the conductivity, σ , is a constant and the field is assumed to be harmonically varying with time dependence $e^{i\omega t}$, equation (1.7) reduces to

$$\frac{\partial^2 Z}{\partial z^2} = \theta^2 Z \quad (1.7a)$$

where

$$\theta^2 = k^2 + i4\pi\mu\omega\sigma$$

with the solution

$$Z = ae^{-\theta z} + be^{\theta z} . \quad (1.7b)$$

As $z \rightarrow \infty$ the electric field must go to zero, thus b must be equal to zero. Then

$$Z(z,t) = (Ce^{-(kz)} + De^{kz})e^{i\omega t} \quad z < 0$$

$$Z(z,t) = ae^{-\theta z}e^{i\omega t} \quad z > 0$$

are solutions to the vertical field.

Above the half-space ($z < 0$) the external field can be written as the gradient of a scalar potential Ω , which satisfies Laplace's equation. $H = -\nabla\Omega$ where

$$\Omega = \{A \exp(-kz) + B \exp(kz)\} P(x, y, t) e^{i\omega t}. \quad (1.8)$$

(Price, 1967).

Physically the term $A \exp(-kz)$ is the contribution to the potential due to electric currents in the ionosphere, and $B \exp(kz)$ is the contribution of the induced currents within the conductor to the field outside the conductor. The modulus of B/A is the ratio of the amplitude of the induced magnetic field to that of the inducing field, while $\arg(B/A)$ is the phase difference between the two fields.

Price (1967) computed the effect of the source field in the table below on a "flat-earth" model by use of an induction parameter $\beta = 4\pi\mu\sigma\omega/k^2$ where σ is the conductivity of the half-space, $\omega/2\pi$ the frequency of the inducing field and $k = 2\pi/\lambda$ where λ is the wave or scale length of the field.

TABLE 1.1

β	0.01	0.25	1.0	4.0	25	100	∞
Mod (B/A)	0.0025	0.065	0.22	0.48	0.75	0.87	1.00
Arg (B/A)	90°	77°	66°	39°	16°	8°	0°

It seems then that induction becomes important only when $\beta \gg 1$. $\beta \gg 100$ represents nearly complete control of the induced current by self-induction. The phase differences are seen to decrease as β increases; small phase differences imply that self-induction is the dominant mechanism, while large phase differences imply that Ohmic resistance is the dominant mechanism.

Combining (1.7) with $\nabla \times \mathbf{E} = - \frac{\partial \mathbf{B}}{\partial t} = - \mu \mathbf{H}$ and using the harmonic time dependence, the external field becomes

$$\mathbf{H} = - \frac{k}{i\mu\omega} [(C e^{-kz} + D e^{kz}) \left(\frac{\partial P}{\partial x}, \frac{\partial P}{\partial y} \right), kP(C e^{-kz} + D e^{kz})] e^{i\omega t} . \quad (1.9)$$

The boundary conditions are that the tangential component of \mathbf{H} and the normal component of \mathbf{B} be continuous across the interface. Applying them to the solution of (1.7) and comparing (1.8) to (1.9) produces the coefficients

$$C = - \frac{i\mu\omega A}{k} , \quad D = \frac{i\mu\omega B}{k} \quad (1.10)$$

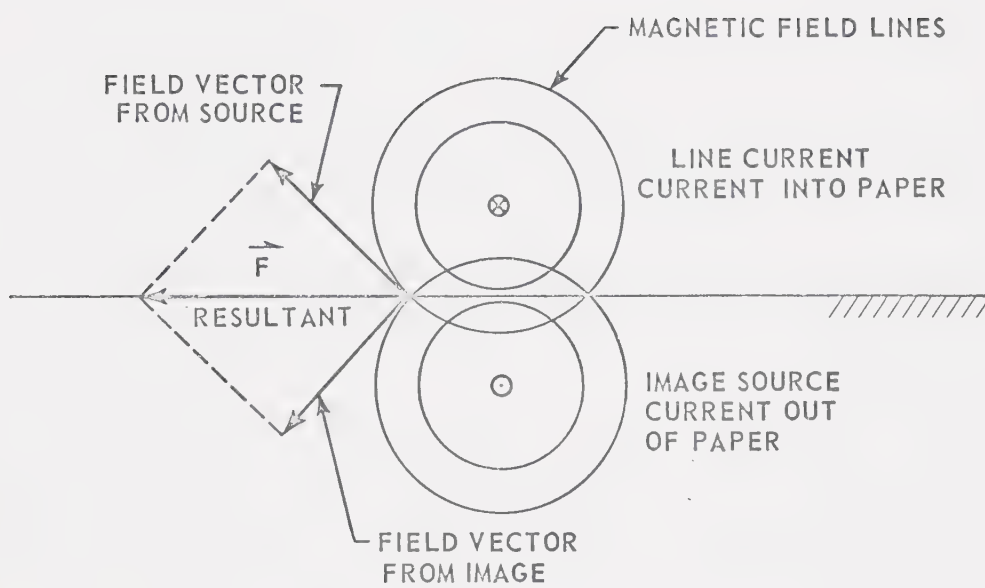
which when substituted into (1.9) give

$$\mathbf{H} = - [(A+B) \left(\frac{\partial P}{\partial x}, \frac{\partial P}{\partial y} \right), kP(-A+B)] e^{i\omega t} \quad (1.11)$$

on the $z=0$ plane. The inducing field was

$$\mathbf{H} = - [A \frac{\partial P}{\partial x}, A \frac{\partial P}{\partial y}, kAP] e^{i\omega t} . \quad (1.12)$$

Figure 1.1 Induction in a conductive half-space.



Comparison of the coefficients of (1.11) and (1.12) shows that the induced horizontal components add to the inducing field and the induced vertical component opposes the inducing vertical field. From Table 1.1 it can be seen that if $\beta \rightarrow \infty$, $B \rightarrow A$ so that in the limiting case of very high conductivity the magnetic field for any finite wavelength is

$$\mathbf{H} = - \left[2A \frac{\partial P}{\partial x}, 2A \frac{\partial P}{\partial y}, 0 \right] . \quad (1.13)$$

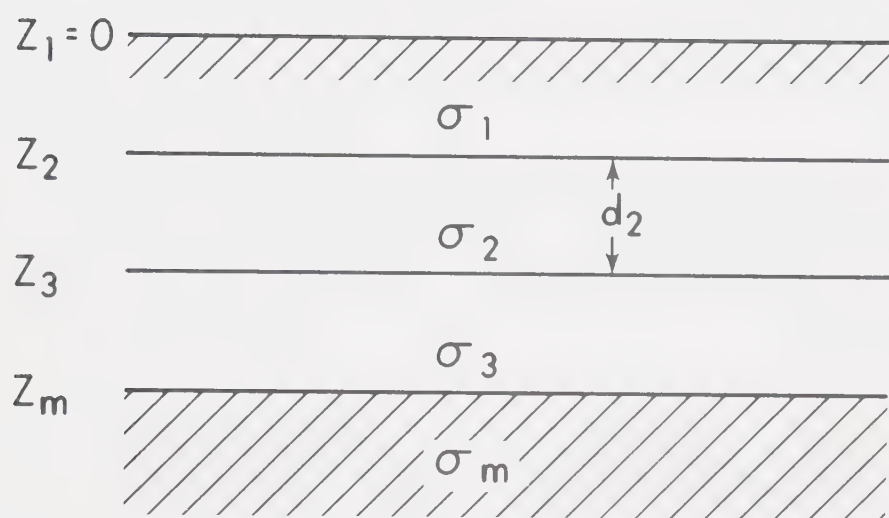
The horizontal components are then doubled while the vertical field components are cancelled.

The above result (1.13) can be illustrated graphically by the use of images. If an external line current source is taken above a "flat-earth" model (infinite half-space) it produces an image of itself the same distance below the boundary with an opposite direction of current flow (Fig. 1.1)

1.3 Plane-layered model with uniform conductivity

The spatial configuration of the surface field on the $z=0$ plane can be expressed as a spectrum of spatial wavelengths with a coefficient representing the amplitude of each. Let $S(k)$ be the ratio B/A (see section 1.2) of the internal to external tangential fields at the surface of the conductor for one particular frequency component.

Figure 1.2 Plane layered conductive model.



This ratio will vary from zero for an insulator to one for a perfect conductor. Let

$$T(k) = [1 - S(k)]/[1 + S(k)] . \quad (1.14)$$

The potential of a magnetic field at the boundary plane of a half-space filled by M plane layers of various conductivities with the last layer extending to infinity (fig. 1.2), can be expressed in a different form than equation (1.8) (Schmucker, 1969)

$$\begin{aligned} \Omega(x,y,z,t) = & \int_{-\infty}^{\infty} \int_{-\infty}^{\infty} \{E(\vec{k},t) \exp[i(\vec{k} \cdot \vec{r}) - kz] + \\ & + I(\vec{k},t) \exp[i(\vec{k} \cdot \vec{r} + kz)]\} dx dy \quad (1.15) \end{aligned}$$

with $\vec{k} \cdot \vec{r} = k_x x + k_y y$.

$$k = + \sqrt{k_x^2 + k_y^2}$$

The field is harmonic with time dependence $e^{i\omega t}$ and E and I are the external and internal coefficients.

The X , Y , Z field components at the surface of the substratum are:

$$\begin{aligned} X &= -ik_x (E + I) \\ Y &= -ik_y (E + I) \exp[i(\vec{k} \cdot \vec{r})] . \\ Z &= k (E - I) \end{aligned} \quad (1.16)$$

The field inside the m^{th} layer is

$$\left. \begin{aligned} X &= -i k_x f_m'(k, t, z) \\ Y &= -i k_y f_m'(k, t, z) \\ Z &= +k f_m(k, t, z) \end{aligned} \right\} i/\omega \exp[i(\vec{k} \cdot \vec{r})] \quad (1.17)$$

where $f_m' = -k^{-1} df_m/dz$, and f_m satisfies the diffusion equation (1.7a).

$$\theta_m = 4\sqrt{k^2 + i4\pi\omega\sigma_m} = \sqrt{\frac{J+k^2}{2}} + i\sqrt{\frac{J-k^2}{2}} \quad (1.18)$$

where $J^2 = k^4 + (4\pi\omega\sigma_m)^2$.

θ_m then is the propagation constant of the downward diffusing field in the m^{th} layer. By analogy with (1.7b) a general solution to (1.7a) for the m^{th} layer is:

$$f_m(k, t, z) = A_m(k, t)\exp(-k_m z) + B_m(k, t)\exp(k_m z)$$

with

$$f_m' = f_m \theta_m G_m(z)/k \quad (1.19)$$

where

$$G_m(z) = \frac{A_m e^{-\theta_m z} - B_m e^{\theta_m z}}{A_m e^{-\theta_m z} + B_m e^{\theta_m z}} \quad (1.20)$$

Two limiting cases of physical interest will now be considered. If the skin-depth value of the m^{th} layer is

large compared to the field wavelength i.e. $P_m k \gg 1$

where $P_m = (4\pi\mu\omega\sigma_m)^{-\frac{1}{2}}$, then (1.7a), with

$f_m = z$, $\theta_m = k$, reduces to

$$\frac{\partial^2 f_m}{\partial z^2} = k^2 f_m$$

and the incident field penetrates through this layer

as if it were non-conducting. The result at the other

limit, $P_m k \ll 1$, implies $\theta_m = (1+i)/P_m$ i.e. the attenuation is a skin-depth effect independent of k .

From the boundary conditions at the $z=0$ plane the ratio of internal to external parts

$$S(k) = I(k,t)/E(k,t) = \frac{\theta_1 G_1(0) - k}{\theta_1 G_1(0) + k} \quad (1.21)$$

which is the same for both the horizontal and vertical components of the field. X and Y then can be considered as components of a horizontal variation vector \vec{H} with

$$X = \frac{k_x}{k} H \quad Y = \frac{k_y}{k} H \quad . \quad (1.22)$$

From (1.17) it follows that

$$Z/H = i T(k) \quad (1.23)$$

where

$$T(k) = \frac{1 - S(k)}{1 + S(k)} = \frac{k}{\theta_1 G_1(0)} \quad .$$

The internal electric field vector

$$\vec{E} = i f_m(k, t, z) \exp[i(\vec{k} \cdot \vec{r})] \quad .$$

has components

$$E_x = \frac{k_y}{k} E \quad E_y = - \frac{k_x}{k} E \quad . \quad (1.24)$$

Since \vec{E} is orthogonal to \vec{H} , combined with (1.18) and (1.19)

$$X = - \frac{ik_x}{k} \frac{E}{\omega} \theta_m G_m(z)$$

$$Y = - \frac{ik_y}{k} \frac{E}{\omega} \theta_m G_m(z)$$

from (1.22), letting $m=1$,

$$\frac{E}{H} = \frac{i\omega}{\theta_1 G_1(0)} = \frac{i\omega T(k)}{k} \quad (1.25)$$

which is the surface impedance for $z=0$.

As seen from (1.17) and (1.22) the spatial gradients of the horizontal field at $z=0$ are

$$\frac{\partial X}{\partial x} + \frac{\partial Y}{\partial y} = ikH \quad , \quad \frac{\partial H}{\partial z} = - \frac{\theta_1}{G_1(0)} \cdot H$$

and when combined with (1.23) and (1.24) give relations which will be used in explaining the two-layer model

$$\frac{\partial X}{\partial x} + \frac{\partial Y}{\partial y} = \theta_1 G_1(0) z \quad , \quad \frac{\partial H}{\partial z} = - \frac{\theta_1^2 E}{i\omega} \quad . \quad (1.26)$$

To determine the vertical function, the continuity condition for the magnetic field vector at the interface $z=z_{m+1}$ is again used to give the relation

$$\theta_m G_m(z_{m+1}) \equiv \theta_{m+1} G_{m+1}(z_{m+1}) \quad .$$

With $z=z_{m+1}$, equation (1.20) when expressed in terms of hyperbolic functions yields the basic recurrence formula for plane conductors (Wait 1953), so that $G_m(z_{m+1})$ is now expressed in terms of $G_m(z_m)$. Writing $d_m = z_{m+1} - z_m$ for the thickness of the m^{th} layer with $C_{m+1} = \theta_{m+1} G_{m+1}(z_{m+1})$

$$G_m(z_m) = \frac{C_{m+1} + \theta_m \tanh(\theta_m d_m)}{\theta_m + C_{m+1} \tanh(\theta_m d_m)} \quad . \quad (1.27)$$

Equation (1.27) can be solved by applying the condition that no induced currents are produced in the layer extending to infinity, therefore for $d_m \rightarrow \infty$ equation (1.27) reduces to

$$G_m(z_m) = 1 \quad \text{for} \quad z \geq z_m \quad .$$

Now equation (1.27) can be solved by successive substitutions, starting at the m^{th} layer where $G_m(z_m) = 1$ to the surface where $G_1(0)$ is obtained from magnetic recordings.

Application of limiting cases of the skin-depth value of the m^{th} layer yields, after Schmucker (1964),

$$G_m(z_m) = 1 + 2\left\{\frac{C_{m+1} - \theta_m}{C_{m+1} + \theta_m}\right\} \exp(-2 \theta_m d_m) \quad (1.28)$$

for $|\theta_m d| \gg 1$ the case where the skin-depth value of the m^{th} layer is small compared to its thickness. The equation (1.28) indicates that there will be little penetration of this layer by the incident field.

For most magnetic events used in geomagnetic-depth sounding the relevant limiting case is

$$d \ll p(\text{skin-depth}) \ll k^{-1}$$

which implies that $(\theta_m d_m)$ is small and that the approximation $\tanh(x) \approx x$ may be used to obtain

$$G_m(z_m) = \frac{C_{m+1} + \theta_m^2 d_m}{\theta_m(1 + C_{m+1} d_m)} \quad (1.29)$$

which gives a good working approximation for G_m as a function of depth.

1.4 The two-layer model

The model used most frequently in the initial interpretation of depth sounding results is the two-layer model either with uniform conductivity or non-uniform conductivity. This section will treat the uniform conductivity case and show that depth sounding and magnetotellurics are theoretically comparable in this limit.

The model to be treated can be described as a uniform plane substratum of conductivity σ_c that is covered by a poorly conducting layer extending from $z_1 = 0$ to $z_2 = h$. The incident field penetrates through the top layer with little attenuation, while its depth of penetration into the substratum is small compared to its spatial wavelength $2\pi/k$. Use of the relations

$$\theta_1 = k(kh \ll 1) \quad , \quad \theta_2 = (1+i)/p_c$$

to substitute into equation (1.29) gives, with $c_2 = k_2$

$$G_1(0) = \theta_2/k(1 + \theta_2 h) = 1/k.c \quad . \quad (1.30)$$

The complex-valued parameter

$$c = h + \frac{1}{2} p_c + i \frac{1}{2} p_c \quad (1.31)$$

where p_c is the skin-depth, then determines the surface impedance and the relative magnitudes of the vertical fields as functions of frequency. The ratios

$$E/H = i\omega c$$

$$Z/H = -ikc \quad (1.32)$$

$$Z = c \left\{ \frac{\partial \lambda}{\partial x} + \frac{\partial Y}{\partial y} \right\}$$

are a result of combining equations (1.25) and (1.26) and recognizing that $T(k) = k.c$.

If the ratio E/H or Z/H is measured over a substratum then it is possible to compute its depth and conductivity uniquely; thus

$$h = \omega^{-1} [\text{Im} (E/H) - \text{Re} (E/H)] , \quad (1.33)$$

$$p_c = \omega^{-1} 2 \text{Re} (E/H)$$

for the two-layer case.

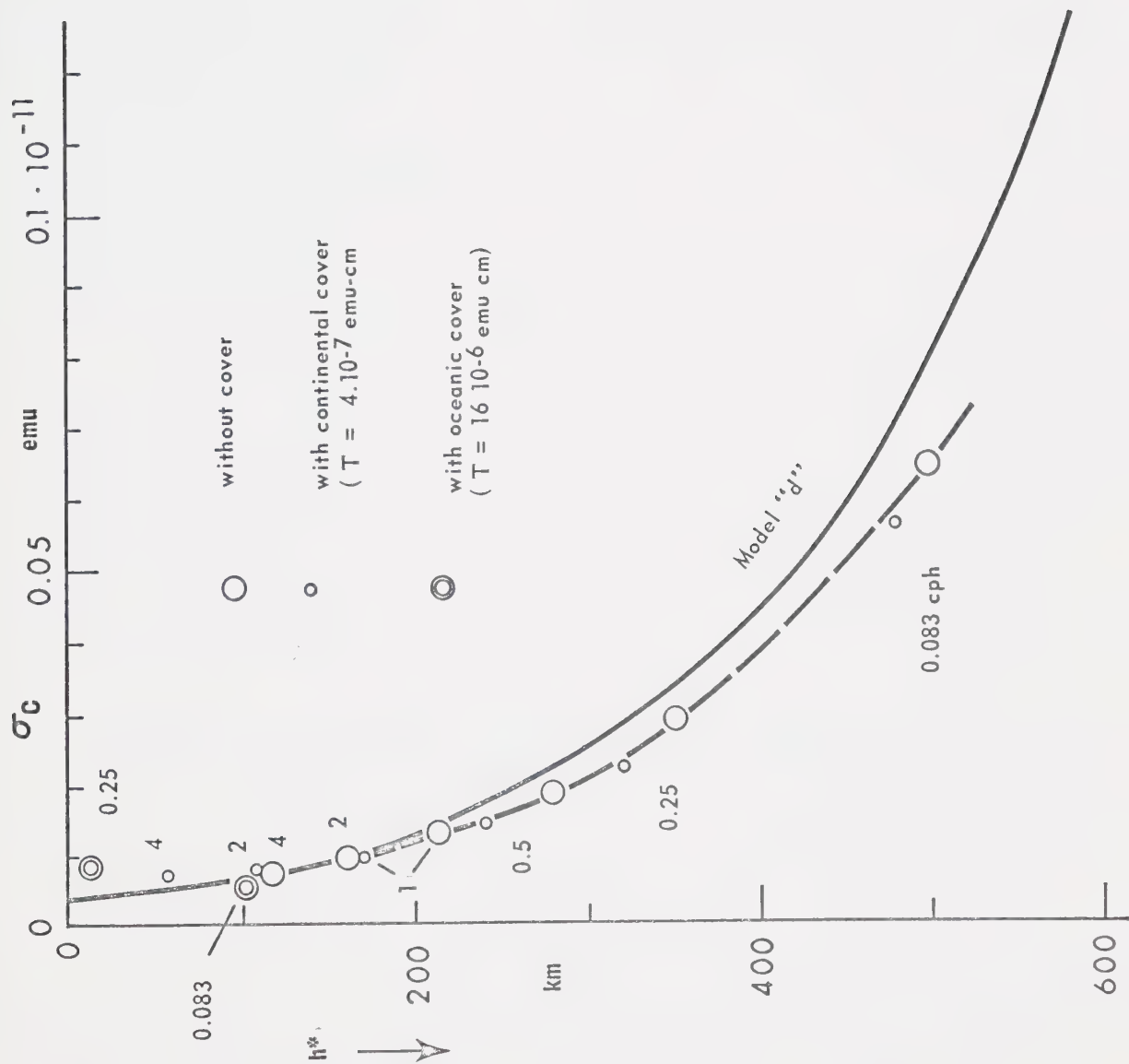
It is seen then that the real part of \underline{c} (out-of-phase E/H or Z/H) represents the mean depth of the internal eddy currents, while the imaginary part of \underline{c} (in-phase E/H or Z/H) yields with p_c the ambient conductivity at that depth. The height

$$h^* = h + \frac{1}{2} p_c \quad (1.34)$$

can be thought of as the "depth of a perfect substitute conductor". A multi-layered substratum is indistinguishable from, and therefore replaceable by, a uniform conductor at that depth h^* as far as its response to a single frequency component of the incident variation field is concerned. This equivalence makes the two-layer model very useful in the interpretation of deep sounding results in the frequency domain.

Since E/H and Z/H must always be positive or zero, h^* in (1.34) must also be positive or zero implying that

Figure 1.3 Depth, h^* , of a "perfect substitute conductor" at various frequencies for Lahiri and Price Model d of the Earth: after Schmucker (1969).



the out-of-phase component of E/H or Z/H will give the depth to a perfect substitute conductor

$$h^* = \omega^{-1} \operatorname{Im} (E/H) \quad (1.35)$$

while the in-phase component gives the apparent conductivity

$$\sigma_c = \omega \{8\pi [\operatorname{Re}(E/H)]^2\}^{-1} \quad (1.36)$$

at that depth. Fig. (1.3) from Schmucker (1969), shows h^* versus σ for a variety of frequencies for the Lahiri and Price model d conductivity distribution.

The magnetotelluric definition of the "apparent resistivity" (Cagniard (1953)) is based on the modulus of the impedance and would yield as the apparent skin-depth value the modulus of $c\sqrt{2}$.

1.5 Electromagnetic induction in non-uniform conductors

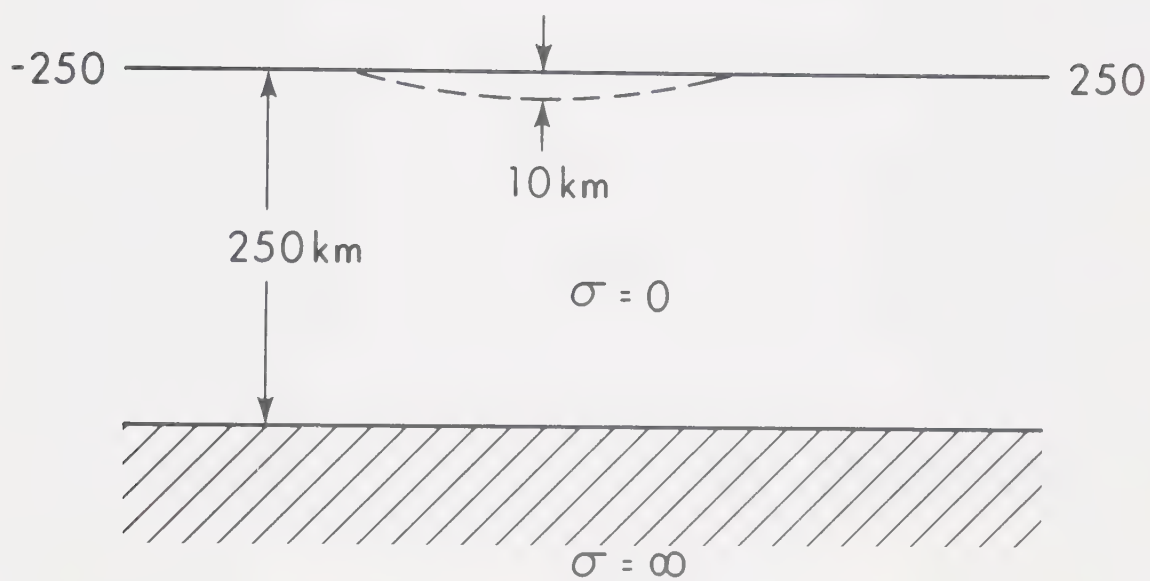
This section will deal with the effect of lateral conductivity inhomogeneities upon the surface magnetic field variations. This type of structure can be delineated very well by the G.D.S. method with respect to its strike and lateral extent, and to some degree to its depth.

The following treatment is restricted to essentially a theoretical representation of the first order effects of lateral conductivity inhomogeneities on the surface field.

Hence only the two-dimensional case need be treated. Since the anomalies will be considered in two dimensions, only one component of the horizontal field and the vertical field will be necessary to describe the induction process completely. For ease in going from theory to interpretation of results in later chapters, z will be taken as positive down and y is parallel to the change in conductivity, $\text{grad } \sigma$.

Two distinct types of anomalies will be treated even though other types of anomalies and combinations of anomalies exist. The surface anomaly is due to superficial conductivity variations in the crust. These anomalies are of interest in upper mantle investigations mainly because they can shield lateral conductivity changes in the upper mantle and cause misinterpretations of upper mantle conductivity structure. This shielding effect seems to have been in evidence along Caner's (1967) profile which was operated to map the northward extension of the Rio Grande anomaly. In the Uinta Basin in Utah deep conducting sediments cause phase anomalies without appreciably attenuating the effects of upper mantle structures below (Reitzel, Gough, Porath and Anderson (1970); Chapter 4 of this thesis). The North German anomaly is now known to arise from shallow sedimentary conductive structures (Vozoff and Swift 1968).

Figure 1.4 Conductive sheet, insulating crust and
conductive mantle.



The second anomaly to be treated is produced by lateral conductivity inhomogeneities in the upper mantle, which can be represented by a perfect or nearly perfect conductor with an undulating surface. This second type of anomaly is of direct importance to the upper mantle investigator.

Either type of anomaly following Schmucker (1969) can be thought of as the resultant of two different kinds of anomalous fields. The first kind arises from the induction of local currents, and production of associated anomalous internal fields, by the mainly horizontal "normal" field at the structure, and is represented by the transfer functions h_H , z_H , q_H (Schmucker 1969). The second kind results from normal induction in the horizontally layered parts of the structure by the inducing Z field and is represented by h_Z , z_Z , q_Z .

Surface Anomalies

The model considered (fig. 1.4) has a surface sheet and an underlying conductive half-space separated by an insulating layer. The surface can be represented by a non-uniform thin sheet with a variable total conductivity

$$J(y) = \bar{J} + J_a'(y)$$

where J is the integrated conductance in a sheet of thickness \underline{d} ,

$$J = \int_0^{\underline{d}} \sigma(z) dz$$

in the $z = 0$ plane. Price's (1967) boundary conditions for the anomalous part of the variation field above (+), and below (-) a thin sheet give

$$\frac{d}{dy} (H_a^+ + H_a^-) - (H^+ - H^-) - \frac{1}{\bar{J}} \frac{dJ}{dy} = 4\pi i\omega [\bar{J}Z_a + J_a Z] \quad (1.37)$$

in two dimensions ... \bar{J} is the x-component of the normally induced sheet current density for $J_a=0$ and can be denoted in normalized form

$$Q = 2\pi\bar{J}/\bar{H}^+ = \frac{1}{2} (\bar{H}^+ - \bar{H}^-) \quad (1.38)$$

Equation (1.38) can be replaced by the approximation

$$2Q = i\eta_s/(1 + i\eta_s)$$

where η_s is the pertinent induction parameter. η_s taken in the source field free limit is

$$\eta_s = 4\pi\omega\sigma c$$

and the complex-valued \underline{c} is given by equation (1.31).

The superimposed anomalous part of the induced sheet-current density is

$$j_a = (H_a^+ - H_a^-)/4\pi$$

where j_a is the result of both the first and second kinds of internal field

$$2\pi\bar{j}_a = q_H\bar{H} + q_Z\bar{Z} \quad . \quad (1.39)$$

Equation (1.39) can then be expressed as

$$\frac{d}{dy} [(Q + q_H)/J] = 2\pi i\omega z_H \quad (1.40)$$

$$\frac{d}{dy} (q_Z/J) = 2\pi i\omega (z_Z + J_a/J)$$

for the anomalous variations of the first and second kind respectively. The boundary conditions, equation (1.40), can be integrated in closed form to yield

$$q_H(y) = Q \cdot J_a(y)/(\bar{J}) + 2\pi i\omega J(y) \int_{y_0}^y z_H(\xi) d\xi \quad (1.41)$$

$$q_Z(y) = 2\pi i J(y) \int_{y_0}^y [z_Z(\xi) + J_a(\xi)] d\xi$$

where y_0 is some distant point on the negative y -axis and $Z_a(y)$ is zero for $y \leq y_0$.

A relaxation method suggested by Price (1949) when applied to equation (1.41) will give the induced field above an area where the conductivity distribution near the surface is well known. The stratified deep conductivity structure enters the problem as a free parameter to be adjusted to yield the best fit to the observed anomaly. Price suggested two approximation methods to solve the problem; 1) to neglect self-induction, 2) to neglect the Ohmic resistance. These approximations are complementary so that if the first does not lead to converging approximations, the second will do so.

Undulating Surfaces

The treatment presented is in the main that of Schmucker (1969) and Rikitake (1965).

Lateral conductivity inhomogeneities in the upper mantle cause a variable depth of penetration from place to place for a given frequency of a magnetic variation field. This variation could be the result of an undulatory depth

$$h'(y) = \bar{h}' + h_a(y)$$

of the "perfect substitute conductor". Since the transient magnetic vector above this conductor must be

tangential to its surface

$$\frac{dh'}{dy} = (\bar{Z} + Z_a)/(\bar{H} + H_a) . \quad (1.44)$$

The family of field lines that satisfy the boundary condition (1.44) and do not intersect the earth's surface, $z=0$, form the possible interfaces between non-conducting and perfectly conducting material. The field lines must also satisfy the condition that they merge with a pre-conceived normal level for the perfect substitute conductor, \bar{h}' , some distance from the anomaly. \bar{h}' can be computed from the equations developed in sections (1.3) and (1.4).

The downward extension of the variation field is carried out separately for its normal and anomalous parts. If the anomalous part really is of internal origin, then its downward extension is straightforward. The anomalous field can be expressed at $z=0$, by a series of spatial harmonics, if a sinusoidal field distribution, $H(y) = c \cdot \exp(iky)$, is assumed

$$\left. \begin{aligned} H_a &= \sum_n C_n \\ Z_a &= \sum_n -iC_n \end{aligned} \right\} \cdot \exp [n k_a (iy + z)] . \quad (1.45)$$

Also any attenuation by a surface conductivity layer is disregarded, that is the shielding effect upon H is small. The slope of the field line $Z(y) = h'(y)$ passing through the point (y, z) follows from equation (1.44) as

$$\frac{dh'}{dy} = \frac{Z_a(y, h') - h_a(y) \partial \bar{H} / \partial y}{H_a(y, h') + Q' \bar{H}} \quad (1.46)$$

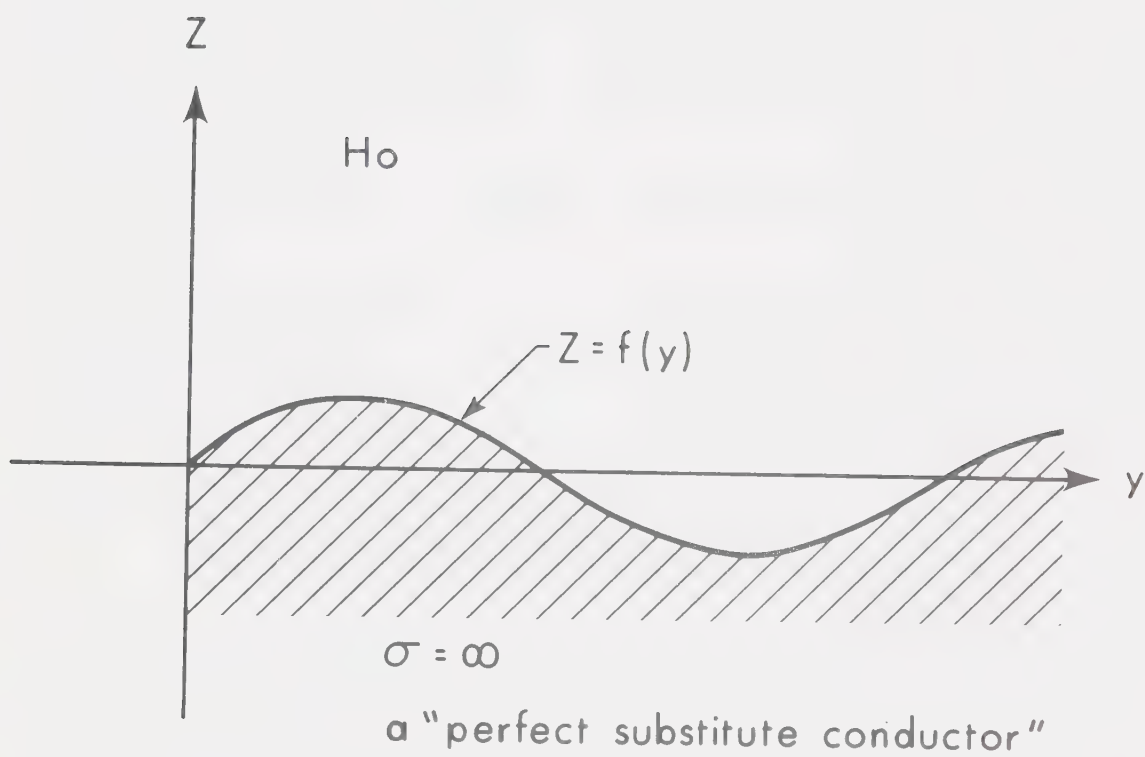
The entire set of field lines can be put together by graphical or numerical methods, starting with $h'(y) = \bar{h}'$ a point distant from the anomaly. The time functions of equation (1.46) must be roughly in phase, meaning that the attenuation in the surface layers is small as required initially. The argument of Q' , given by $\tan^{-1}(-\eta_s)$ is then small compared with unity. Therefore this type of interpretation applies to cases where self-induction is dominant, that is to deep conductors of large radius and high conductivity.

Schmucker (1969) considers a sinusoidal induction anomaly of the form

$$\begin{aligned} H_a(y, 0) &= C \sin(k_a y) \bar{H} \\ Z_a(y, 0) &= -C \cos(k_a y) \bar{H} \end{aligned} \quad (1.47)$$

with the conduction $\partial \bar{H} / \partial y \approx 0$.

Figure 1.5 Rikitake's model (1965).



Substituting equation (1.47) into (1.46) gives

$$\frac{dZ}{dy} = - \frac{C \cos(k_a y) \exp(k_a z)}{Q' + C \sin(k_a y) \exp(k_a z)} \quad (1.48)$$

$$\bar{H} = \exp(k_a z) .$$

The transformation $v = \exp(-k_a z)$ allows equation (1.48) to be solved analytically. The solution:

$$Z(y) = Z(0) - \frac{C}{Q' k_a} \sin(k_a y) \exp(k_a z) . \quad (1.49)$$

In the limit $k_a z \ll 1$ the sine term will predominate giving sinusoidal oscillations, while the limit $k_a z \gg 1$ produces oscillations in the form of square waves. The field lines oscillate asymmetrically about $Z(0)$.

Rikitake (1965) used a different method to study lateral conductivity inhomogeneities from the standpoint of sinusoidal undulations of a perfect substitute conductor. He assumed the surface of the conductor to have a sinusoidal dependence and then analysed the effect of an incident field on the undulations, whereas Schmucker assumed a sinusoidal anomalous field and continued this field downward to formulate the nature of the undulating conductor.

Rikitake (1965) let the surface of a conductor be represented by the function $z = f(y)$ on which the potential of the induced magnetic field can be defined as (see fig. 1.5),

$$W_i = \sum_n C_n e^{-nz} \sin ny \quad .$$

Since the normal component of the magnetic field at the boundary must go to zero,

$$-H_{iy} \sin \alpha + H_{iz} \cos \alpha + H_o \sin \alpha = 0$$

on $z = f(y)$

the cosine and sine terms are given by

$$\cos \alpha = (1 + f')^{-\frac{1}{2}}$$

$$\sin \alpha = f'(1 + f')^{-\frac{1}{2}}$$

$$f' = df/dy \quad .$$

The assumption of a surface $f(y) = h \cos y$ leads to a set of simultaneous equations which can be solved for C_n

$$\sum_n n C_n (h T_{n1} - S_{n1}) = H_o h \pi \quad \text{for } N = 1 \quad (1.50)$$

$$\sum_n n C_n (h T_{nN} - S_{nN}) = 0 \quad \text{for } N > 1$$

where

$$S_{nN} = \int_{-\pi}^{\pi} e^{nh \cos y} \sin ny \sin Ny \, dy$$

$$T_{nN} = \int_{-\pi}^{\pi} e^{-hn \cos y} \sin y \cos ny \sin Ny \, dy .$$

If $h \approx 0.1\pi$, the coefficients converge and give a field distribution similar to that of Schmucker within the prescribed limits of ratios of the field variation to the height of the undulations; $h = 0.1\pi$ and $k_a z \ll 1$ are equivalent limits that give the same sinusoidal oscillations. Rikitake's results for the undulation problem give a maximum of the horizontal inducing field above the undulation and a slightly asymmetric induced vertical field with a transition from positive to negative directly above the undulation.

1.6 Source fields

Perturbations of the magnetosphere by external sources produce currents in the ionosphere and magnetosphere that cause changes in the Earth's magnetic field. These magnetic variations can be characterized by the vector field, its time duration and its geographic extent.

Schmucker (1969) shows that polar magnetic substorms have frequency components and amplitudes such that the depth of penetration is limited to 600 km.

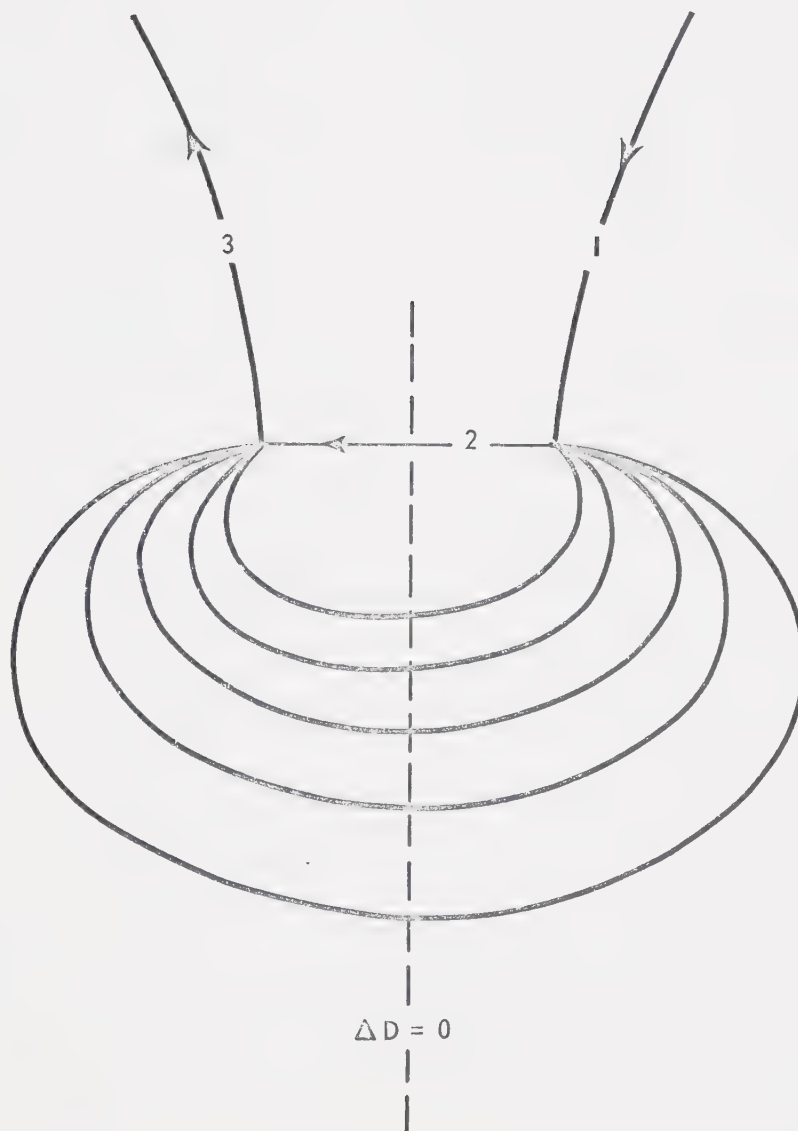
Currents above this limiting depth give magnetic field components which can be detected on the Earth's surface, making events of this type ideal for upper mantle studies. Substorm fields are of large extent and consequently suitable for study of structures across a continent. The morphology of substorms (Rostoker 1966) is known to such an extent as to permit one to make rough theoretical estimates of the character of the external field of a particular event.

Bonnevier et.al. (1969) suggest that the parts of the currents, associated with polar magnetic substorms, whose fields are important at the Earth's surface, can be represented by a three-dimensional current model (fig. 1.6). The currents are: 1) a current flowing downward along a geomagnetic field line into the ionosphere, 2) an intense westward electrojet, 3) a return field-aligned current. The closed loops extending outward from the westward electrojet can be taken as parallel to the Earth's surface and roughly along a geomagnetic equipotential. The gradient across these equipotentials represents the external horizontal magnetic variation observed on the Earth's surface.

The line labelled $\Delta D = 0$, fig. 1.6, is the demarcation line of a substorm (Rostoker, 1966). That

Figure 1.6 Possible currents in a polar magnetic
substorm. After Oldenburg (1969).

POSSIBLE CURRENTS ASSOCIATED
WITH POLAR MAGNETIC SUBSTORM



is, stations east of this line will observe a negative D bay and stations west of this line will observe a positive D bay. Rostoker (1966) has shown that if the current system itself moves, some stations will observe a transitional bay, i.e. the demarcation line moves from east to west across the stations.

The current model predicts that the characteristics of a substorm can be expected to vary with geomagnetic latitude, as has been observed for many years. In the auroral zone where the electrojet is dominant, large negative-H bays will occur with positive Z components to the north and negative Z to the south of the auroral electrojet.

In mid-latitudes positive-H bays and negative-Z bays are to be expected if the perturbations are caused only by the auroral electrojet. Also the intensity of the substorm should decrease as we proceed south of the current system. The horizontal field should also become more uniform. Exceptions to this general situation occur during particularly intense storm activity, when it is possible for the current system to move southward and broaden itself to such an extent that observations at mid-latitudes show a southward increase of H (fig.4.12).

In a storm southward increases of H may arise from the field of the ring-current in the magnetosphere, but in mid-latitudes this increase will amount to only about five gammas.

Rostoker (1968) has stated that the onset of a polar magnetic substorm is always accompanied by at least two distinct Pi2 micropulsations which occur almost simultaneously at stations hundreds of kilometers apart. Thus the onset times to within 30 seconds for a substorm can be obtained from magnetograms which clearly show these micropulsations.

1.7 Two basic geomagnetic depth sounding methods

The two main methods of GDS investigation are the "Base station" and the "Array" methods. The high cost of magnetometers and field programs limited most of the early work in GDS to the "Base station" method. Schmucker (1964) and Caner et al. (1967) carried out extensive programs in the western United States with this method.

The design and construction of a low-cost three component magnetometer by Gough and Reitzel (1967) permitted the "array" method to be employed in the western United States. The writer was a collaborator

in the first field program employing this method. Forty-two magnetometers were used in the western United States during the summer of 1967 (Reitzel, Gough, Porath and Anderson 1970). The array method allows simultaneous recording of the same variation event over an area, with concentrations of magnetometers over suspected anomalous zones. A further advantage of the array method is that it makes possible a formal separation of three components of a variation field into internal and external parts by the use of surface integral methods developed by Vestine (1941), by Price and Wilkins (1963) and by Weaver (1963) and applied by Oldenburg (1969), Porath, Oldenburg and Gough (1970) and the writer.

Base station method

Geomagnetic depth sounding investigation by the "Base station" method proceeds by recording different magnetic events of the same type, such as bays and substorms, at different locations in a specified area where a permanent observatory is located or where a portable magnetometer remains fixed during several events. The analysis of the magnetograms is then directed toward a statistical correlation between the anomalous and normal

parts of these events. At each survey station a 3×3 matrix of transfer functions is obtained, connecting the components of the anomalous and the normal magnetic variation vectors at that site in the frequency domain. Schmucker (1969) states that these transfer functions will give the proper statistical basis for the subsequent interpretation of the induction anomaly in terms of internal conductivity structures.

The spatial configuration of the primary inducing field is essentially ignored by this method, which is thus limited to mid-latitude and equatorial areas where the external field can be assumed to be more or less uniform. Porath et al. (1970) have shown that even in mid-latitudes the external field can be far from uniform. The "Base station" method is definitely limited in determining the anomalous and normal fields, since this analysis is a function of the detailed knowledge of the large scale variation field which may have scale length of order 7,000 km.

Array method

The "array" method proceeds by locating many magnetometers in a specified area (in our case 42 magnetometers in a 700 km. by 1,300 km. area) which

remain fixed at their sites for several magnetic disturbances. The investigator may allow his station spacing to vary as he wishes, but the location of the station with respect to anomalous structures cannot be as arbitrary. Other geophysical and geological data can be used to determine zones of possible anomalous substructure, thereby allowing concentrations of stations in these zones to obtain as much information as possible about the suspected anomaly. The ideal method is to operate an exploratory array first to determine the location of the anomaly, then to use a more concentrated array in the anomalous zone in a second investigation.

If separation is to be attempted control stations at large distances from the anomaly, preferably in normal areas, should be operated to give a good representation of the external field with respect to its scale length. Scale lengths of magnetic variations in mid-latitudes are typically of the order 7,000 km. (Schmucker 1964, Porath et al. 1970).

The first order result of the "array" method is a two-dimensional picture of a single magnetic disturbance over an area of large extent. The disturbance can be Fourier analysed at each station to give its spectral components. The amplitudes and phases of spectral components when plotted on maps give a two-dimensional

picture of their variation across the array at a particular frequency. Section 1.8 will go into more detail about such Fourier transform maps. The "array" method also shows that much additional information can be obtained from the anomalous horizontal fields induced by the normal external horizontal fields over local internal conductors, with the strike of the conductor along the locus of the change of gradient of the anomalous horizontal field. Both the horizontal and vertical components map boundaries of the lateral conductivity inhomogeneities with greater accuracy than most methods of upper mantle investigation.

1.8 Fourier transform maps

The diffusion of the external magnetic field into the Earth, the diffusion of the fields of the internal eddy currents and the induction process in a conductive structure are all dependent on the frequency of the external magnetic variation field. The relation between the external and internal fields, whose vector sum forms the variation field observed at the surface, is also a function of frequency. Therefore more information can be obtained from the amplitude and phase relations at particular frequencies than can be extracted from the original data in the time domain. Thus the concept of

a two-dimensional representation of these spectral components at a particular frequency, ω , can be thought of as a direct consequence of the "array" concept toward better determinations of the Earth's conductivity structure. This use of Fourier transform maps was developed by Reitzel, Gough, Porath and Anderson (1970).

A limited area of the Earth's surface can be represented by a plane, $z=0$, upon which observations of the magnetic variation field at many stations are to be made. Spectral estimates of a component, $X(t)$, of the variation field can be determined at each of these stations in accordance with the equations

$$X_j = \frac{1}{\sqrt{2\pi}} \int_{-\infty}^{\infty} X(t) e^{-i\omega t} dt \quad (1.51)$$

or replacing the integral with a sum of finite terms,

$$\begin{aligned} X_j = \frac{1}{2} a_0 + \sum_{k=1}^{N-1} (a_k \cos(\frac{\pi j k}{N}) + b_k \sin(\frac{\pi j k}{N})) \\ + \frac{1}{2} a_N (-1)^j \end{aligned} \quad (1.52)$$

where $j = 0, 1, 2, \dots, 2N-1$ give $2N$ real numbers

$X_0, X_1, X_2, \dots, X_{2N-1}$, which computes the Fourier sine and cosine series coefficients $a_0, a_1, b_1, a_2, b_2, \dots, a_{N-1}, b_{N-1}, a_N$. The relations

$$A_k = \sqrt{a_k^2 + b_k^2} \quad (1.53)$$

$$\text{Arctan} \left(\frac{b_k}{a_k} \right) = \theta_k$$

give the amplitude and phase of the magnetic variation $X(t)$ at a particular frequency component k , respectively.

For a particular frequency component k , the values A_k and θ_k at each station can be plotted on a map and contoured using linear interpolation as an approximation.

If one dimension of an anomaly is no greater than the corresponding dimension of the array, then this anomaly will produce gradients in the amplitude maps that can be interpreted qualitatively in terms of conductivity structure. These gradients would be due to internal currents rather than external sources because the external sources vary fairly smoothly across a mid-latitude array (section 1.6). Although the smoothness of the fields decreases toward the auroral electrojet, the gradients produced by major conductivity changes may still be distinguishable in maps of unseparated Fourier transform parameters.

The phase is complementary to the amplitude in the same manner as the sine and cosine transforms are complementary. Thus an anomalous field gradient may be observed in the phase maps while little or no anomalous

behaviour is detected in the amplitude maps. The phase maps can contain information that may confirm interpretations made from the amplitude maps. An example of such a confirmation follows. Lateral conductivity inhomogeneities can often be modelled by a step structure that should produce an asymmetry in the Z amplitude maps across the step structure. If an additional hump is placed on the edge of this step then a reversal should occur in the Z component. Since the phase maps contain information about the sign of the anomalous field, the reversal of Z should appear as steep gradients in the Z phase maps. This was exactly the case when the Wasatch Front anomaly was being interpreted from amplitude and phase unseparated maps (Chapter 4).

The amplitude and phase unseparated maps allow a good first interpretation of anomalous fields in terms of conductivity structure on a qualitative basis.

The numerical magnitudes of the sine and cosine transforms (sine and cosine Fourier coefficients) have physical meaning only in relation to the sign and magnitude of the spectral component concerned at the start of the time interval, T , transformed. A change in the starting time will change the relative magnitudes and signs of the cosine and sine transforms, and the

distribution of a given spectral term of the time series between the cosine and sine coefficients.

In order to separate the total field into its external and internal parts in the frequency domain, the sine and cosine transform maps of each must be separated independently because the surface integrals used for separation can only be applied to fields in constant phase across the map. The separated components can be later recombined by the relations

$$F_e = (\cos^2 F_e + \sin^2 F_e)^{\frac{1}{2}} ; \quad \text{Arctan}\left(\frac{\sin F_e}{\cos F_e}\right) = \phi_e \quad (1.54)$$

$$F_i = (\cos^2 F_i + \sin^2 F_i)^{\frac{1}{2}} ; \quad \text{Arctan}\left(\frac{\sin F_i}{\cos F_i}\right) = \phi_i$$

where F_e and F_i are the external and internal amplitudes and ϕ_e and ϕ_i are the external and internal phases, respectively. The variation of F_e across the map should in general represent the external variation field on the $z=0$ plane due to currents flowing in the ionosphere plus the fields due to normal internal currents in the highly-conducting mantle. The variation of F_i across the map should represent in the main the magnetic field on the $z=0$ plane due to internal currents flowing in the Earth. Non-uniformities in these eddy currents reflect non-uniformities in the conducting substrata. Quantitative

estimates of the depth and conductivity of these non-uniform conductors can be made by use of the equations presented in sections (1.4) and (1.5).

1.9 Separation of the magnetic fields

Separation of a magnetic field into its internal and external parts was first accomplished on a global basis for the main geomagnetic field by Gauss (1839) and later for time-varying fields by Chapman and Whitehead (1923), Lahiri and Price (1939) and others. Separations of local magnetic fields on a plane have been carried out by Siebert and Kertz (1957) and by Porath et al. (1970).

Global separation

Global separation requires the fitting of a magnetic field known or assumed over the Earth's surface to a number of spherical harmonics and the estimation of contributions to each harmonic from external and internal sources. The most general spherical harmonic representation of a scalar potential from which surface magnetic fields on a sphere can be derived is of the form (Chapman and Bartels 1940)

$$\begin{aligned}
 V = a \sum_{n=0}^{\infty} \sum_{m=0}^n P_n^m(\cos\theta) [& c_n^m (r/a)^n + (1-c_n^m)(a/r)^{n+1}] \\
 \times A_n^m \cos m\phi + & [s_n^m (r/a)^n + (1-s_n^m)(a/r)^{n+1}] B_n^m \sin m\phi]
 \end{aligned}
 \tag{1.55}$$

a = the radius of the Earth

r = distance from the center of the Earth

c_n^m and s_n^m represent fractions of the harmonics of $\cos m\phi$ and $\sin m\phi$ between zero and one which are due to sources outside the sphere. If the radial gradient $Z = \frac{\partial V}{\partial r}$ (the vertical field measured at the surface) is known it can be expanded in spherical harmonics

$$\left. \frac{\partial V}{\partial r} \right|_{r=a} = \sum_{n=0}^{\infty} \sum_{m=0}^n P_n^m(\cos\theta) (\alpha_n^m \cos m\phi + \beta_n^m \sin m\phi). \quad (1.56)$$

Equation (1.55) can be differentiated with respect to r , with r set equal to a . Comparison of this result with that of equation (1.56) will give the values of the coefficients c_n^m and s_n^m . The coefficients A_n^m and B_n^m are found from the northward, X , and eastward, Y , field components, since these and not the potential constitute the observed data:

$$Y_{r=a} = \left(-\frac{1}{r \sin\theta} \frac{\partial V}{\partial \phi} \right)_{r=a} = \frac{1}{\sin\theta} \sum_{n=0}^{\infty} \sum_{m=0}^n P_n^m (mA_n^m \sin m\phi - mB_n^m \cos m\phi)$$

$$X_{r=a} = \left(\frac{1}{r} \frac{\partial V}{\partial \theta} \right)_{r=a} = \sum_{n=0}^{\infty} \sum_{m=0}^n \frac{dP_n^m}{d\theta} \{A_n^m \cos m\phi + B_n^m \sin m\phi\}$$

Y gives the coefficients most easily but a comparison of those derived from X provides a check of the analysis.

This method is not applicable to analysis of local fields mainly because it would require too many harmonics to determine the potential accurately enough over a limited area.

Price and Wilkins (1963) made a three-dimensional separation of a surface magnetic field by use of surface integrals. The event analysed was the Sq field of 1932-1933. The horizontal components of the Sq field were interpolated using a necessary condition for a potential field, that the line integral of magnetic force around any closed contour on the surface was equal to zero. This relation can be found by applying Stokes' theorem to the curl-free condition $\nabla \times H = 0$, where H is the horizontal field. A grid was then drawn with 10° latitude and 15° longitude intersections and values of the field were found at the grid points. Once a potential was given an arbitrary value at one point, the potential at all other points could be evaluated.

The separation is based on the relation

$$(V_e - V_i)_A = V_o + \frac{1}{2\pi} \int_S \left\{ \frac{1}{r} \frac{\partial}{\partial n}(V-V_o) - (V-V_o) \frac{\partial}{\partial n} \left(\frac{1}{r} \right) \right\} dS$$

(1.57)

V_0 = arbitrary constant

\vec{n} = normal to the surface at dS

r = distance from point A to the surface
element dS

S = any closed surface

$V = V_e + V_i$ = the total potential

due to Vestine (1941). This integral was used by Price and Wilkins to compute the difference between internal and external parts of the potential at any point A on the surface. If the surface S is a sphere equation (1.57) reduces to

$$(V_e - V_i)_A = \int_S \frac{V + 2aZ}{4\pi aR} dS .$$

Z = inward normal component of force

a = radius of the sphere

Separation on a plane

The use of magnetic variations to determine upper mantle conductivity structure requires analysis of local fields. Methods of analysis of these fields have been and are being developed.

Siebert and Kertz (1957) attempted a separation in two dimensions of the local field vector recorded at fifteen stations across the North German anomaly. By

finding certain profiles along which one component of the horizontal field had no gradient, they were able to transform the three-dimensional problem into a two-dimensional one. The separation into internal and external parts was completed by means of an integral operator. In many cases this condition is much too strict to allow a valid interpretation of the separated fields. What is required then are integral formulae appropriate for separation on a plane in the general case.

Hartmann (1963) obtained suitable separation formulae by treating the separation of fields as a problem in potential theory and using Green's functions of the first and second kind. Weaver (1963) developed two and three dimensional formulae by taking the two-dimensional Fourier transform of Laplace's equation for the potential and applying the Faltung theorem.

Oldenburg (1969) and Porath et al. (1970) have used the approach of Price and Wilkins (1963) to effect a three-dimensional separation analysis of local magnetic fields. The starting point for this separation is Vestine's formula,

$$2\pi(V_e - V_i)_A = \int_S \left(\frac{1}{r} \frac{\partial V}{\partial n} - \frac{V}{r^2} \frac{\partial r}{\partial n} \right) dS \quad . \quad (1.58)$$

For local fields over a few hundred kilometers the sphericity of the Earth can be neglected, implying that the surface S is to be regarded as a hemisphere with an infinite radius. If $(X_A, Y_A, 0)$ is a point at which the fields are to be separated then

$$r^2 = (X_A - X)^2 + (Y_A - Y)^2, \quad \frac{\partial}{\partial n} = - \frac{\partial}{\partial Z}$$

Z taken as positive downward. On the surface S , $\frac{\partial r}{\partial n} = 0$ and equation (1.58) reduces to

$$2\pi (V_e - V_i) = \int_S \frac{1}{r} \frac{\partial V}{\partial r} dS. \quad (1.59)$$

Differentiation of the above equation will give the expression for the separated magnetic field, X, Y, Z to give

$$\begin{aligned} (X_e - X_i)_o &= - \frac{1}{2\pi} \int_S \frac{xZ}{r^3} dS \\ (Y_e - Y_i)_o &= - \frac{1}{2\pi} \int_S \frac{yZ}{r^3} dS \\ (Z_e - Z_i)_o &= \frac{1}{2\pi} \int_S \frac{xX + yY}{r^3} dS. \end{aligned} \quad (1.60)$$

When the equations (1.60) are combined with the observed components $X = X_e + X_i$, $Y = Y_e + Y_i$ and $Z = Z_e + Z_i$ a complete separation of each of the magnetic components is obtained.

Geomagnetic depth sounding is concerned with four types of magnetic variations:

1. Normal external field
2. Anomalous external field
3. Normal internal field
4. Anomalous internal field

At mid-latitudes the inducing field is taken as the sum of the normal external and normal internal fields. The normal internal field exhibits the induction properties of the "flat-earth" models discussed in sections 1.2 and 1.3, while the anomalous internal field arises from lateral inhomogeneities in an internal conductor as discussed in section 1.5.

It should be pointed out that fields having spatial wavelengths much larger than the dimensions of the array cannot be separated by the formulae above. Thus it is the dimensions of the array that dictate which fields are "anomalous" and which are inseparable "normal" parts.

1.10 Limitations of geomagnetic depth sounding

As was pointed out in section 1.9 a complete separation of the internal and external parts of a transient magnetic field is not possible because the area in which observations are made is small compared

to the spatial extent of the primary inducing field. Therefore the anomalies must be interpreted to some extent on the basis of a preconceived mean conductivity distribution estimated from other sources. The most commonly used source outside GDS is magnetotellurics. But conductivity estimates from magnetotellurics are greatly distorted in areas of deep seated conductivity anomalies (Peeples 1969). This is due to the distortion of the horizontal magnetic and electric components over areas of extensive lateral conductivity inhomogeneities; the plane layered approximation is no longer valid.

Porath et al. (1970) have shown that if the area of investigation is large enough good estimates can be made of the conductivity at depth from separation results. Such estimates can be shown to correlate with geophysical models of the upper mantle from other methods, mainly geothermal studies and measurements of conductivities of ultrabasic silicates at high pressures and temperatures.

In the real physical situation observations of the magnetic field are made over surface layers that form a thin conducting sheet of great complexity representing a second limitation to GDS. The flow of shallow eddy currents may be irregular, becoming most severe in

the ocean effect near coastlines and in areas of thick sedimentary basins. The relevant calculations to determine these effects are generally intractable; a start has been made by Price (1949) in a study of induction in thin sheets.

Figure (1.7) illustrates the method of Schmucker (1969) for a three layer model with a top layer of thickness d , a poorly conducting intermediate layer of thickness h and a highly conducting half-space, which represents the Earth's surface layers, highly resistive zones of the crust and the uppermost mantle, and the highly conducting mantle respectively. The approximation $\theta_1 \approx (1 + i)/p_1$ (skin depth effect), $\theta_2 \approx k$ (dependence on the dimensions of the source field), $k_3 \approx (1 + i)/p_3$ will be used in layers 1,2,3 respectively. h is to be taken small compared to the wavelength of the source field but large with respect to the skin-depth value p_3 , thus the wave number \underline{k} of the incident field can be ignored in the following relations. The recurrence formula equation (1.27) gives

$$G_{\alpha}(d) = (k h^{-1})$$

$$G_1(0) = \frac{1 + \theta_1 h \tanh(\theta_1 d)}{\theta_1 h + \tanh(\theta_1 d)}$$

with the resulting approximation to the attenuated electric field at the bottom of the top layer

Figure 1.7 Penetration of electric variation
fields. After Schmucker (1969).

$$\frac{E(d)}{E(0)}$$

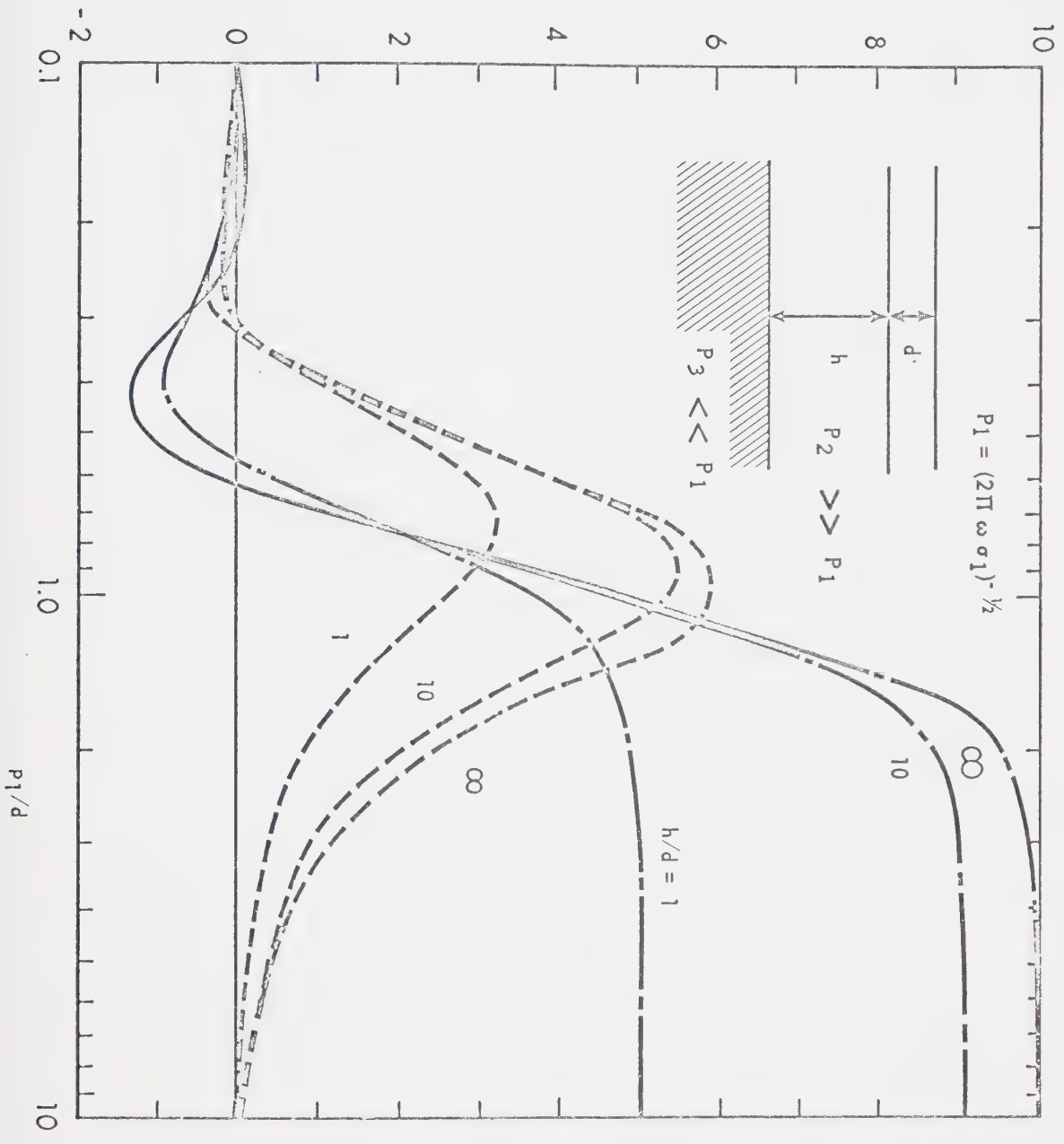
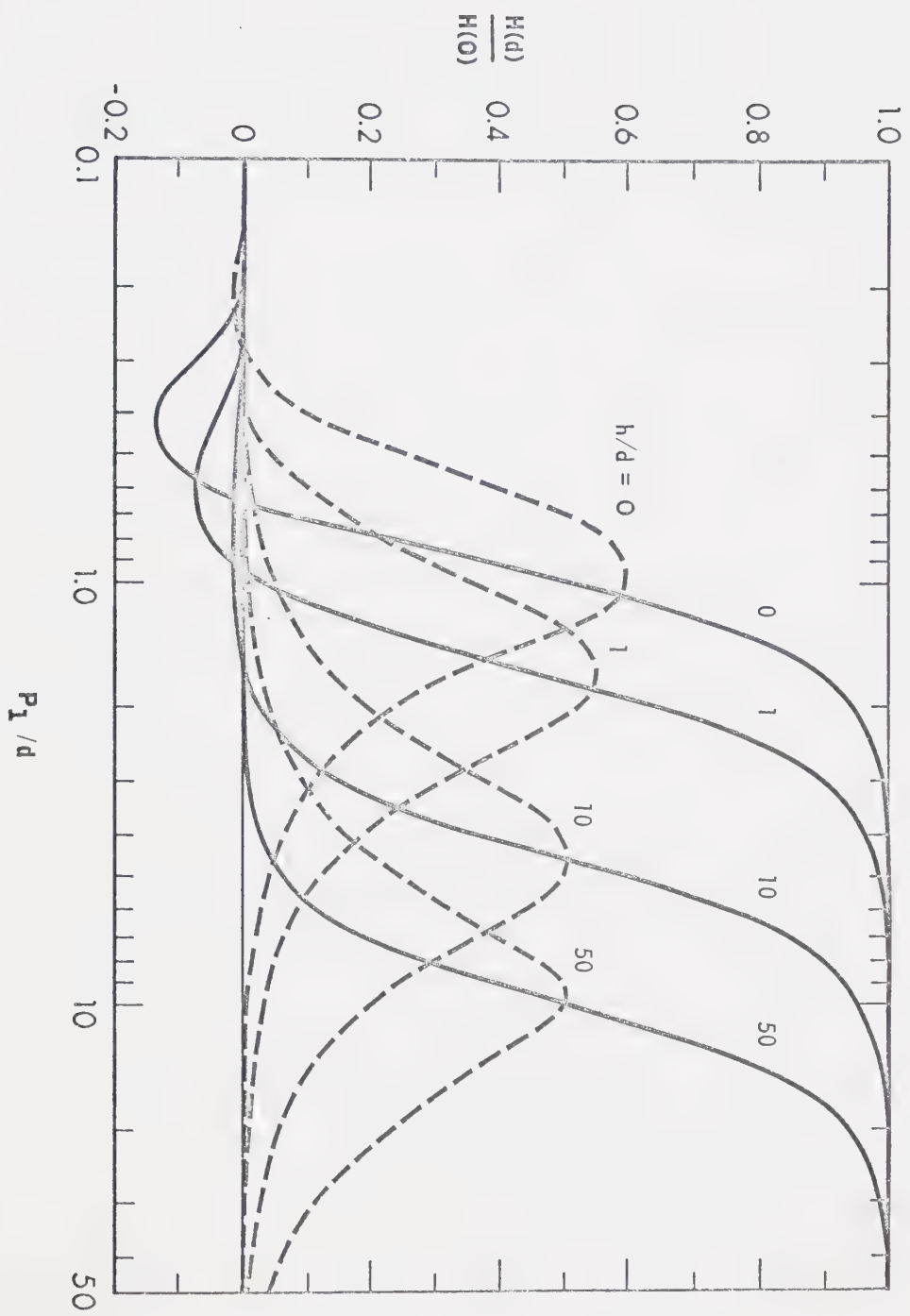


Figure 1.8 Penetration of magnetic variation
fields. After Schmucker (1969).



$$\frac{\varepsilon(d)}{\varepsilon(0)} \approx 1 - \frac{d}{n+d} \quad . \quad (1.61)$$

The asymptotic behaviour of the curves in figure 1.7 shows that p_1 should be at least three times the thickness d for the approximation in equation (1.61) to hold. The curves plotted for differing values of d/h show that even though $p_1 \gg d$ the ratio d/h limits the uniformity of E in the top layer.

A numerical example given by Schmucker (1964) helps to illustrate the above argument. Given a 4 km. ocean ($\sigma_1 = 4 \times 10^{-11}$ e.m.u.) above a highly conductive mantle at depth 100 km., then $d = 4$ km., $h = 100$ km., $d/h = 1/25$. Therefore the attenuation of E in the ocean will be less than 4% if $p_1 > 12$ km. giving source fields of about 38 minutes period as the lowest permissible period for Price's method to hold.

The phase lead of the induced field to the inducing field can reveal roughly where most of the internal eddy currents are with respect to their depth. Inspection of figures (1.7) and (1.8) shows that if $h/d = 1$ a substantial part of $E(0)$ and $H(0)$ are attenuated for values of $p_1/d < 1$ for the out-of-phase (dashed) curves. This means that strong eddy currents are flowing in the highly conducting shallow top layer and that these currents will have a phase lead to $H(0)$. As the value

h/d and p_1/d become larger the eddy currents will flow on the average at greater depths than $d+h$, in the half-space. It is seen that these currents will produce fields that are in the main in phase with $H(0)$. It is then possible for the investigator to distinguish roughly between shallow and deep highly-conducting structures simply by determining the phase differences between the internal and external fields.

CHAPTER 2

PREVIOUS GEOMAGNETIC DEPTH SOUNDING IN THE WESTERN UNITED STATES

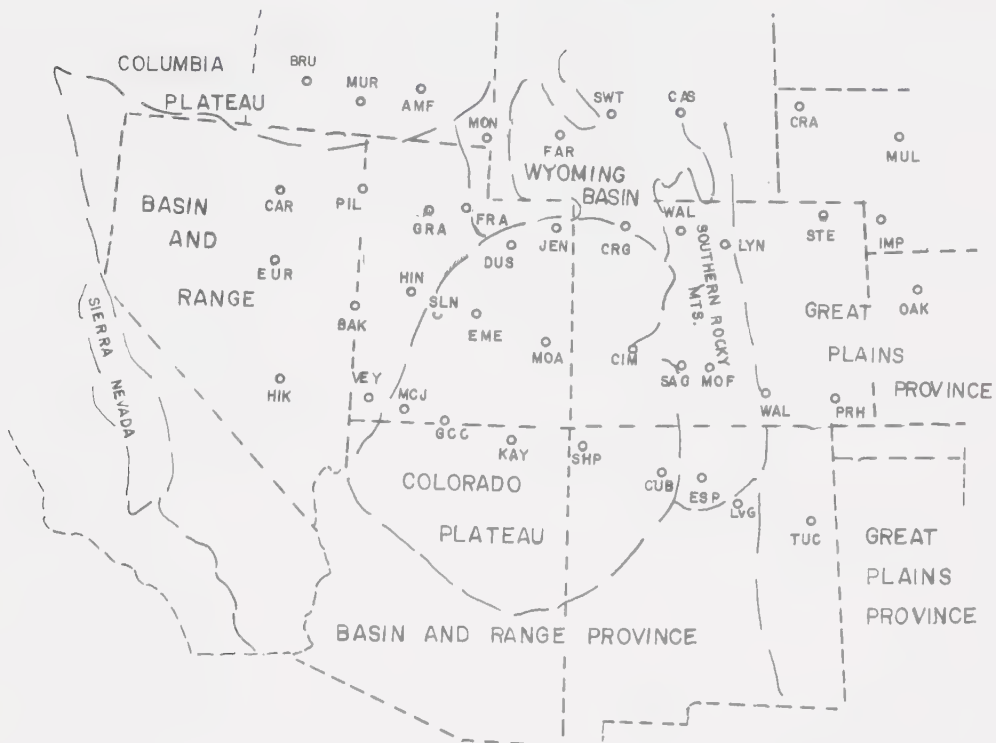
Schmucker (1964), Caner et al. (1967) and Reitzel and Gough (1969) used Geomagnetic Depth Sounding (GDS) in investigations of the upper mantle conductivity structure in the Cordillera prior to 1967. Figure 2.1 locates the stations used by these investigators.

During the International Geophysical Year (IGY) 1957/1958 the Coast and Geodetic Survey of the United States operated a net of seven temporary geomagnetic observatories in the western United States. Schmucker (1964) reported that significant and consistent anomalies of the Z (vertical) variations were encountered, especially at Price, Utah. No detailed study of the internal conductivity anomalies could be carried out due to the great distance between the stations. The average station spacing was about 400 km.

During the years 1959/62 Schmucker carried out extensive observations at many stations in the southwestern United States. The line of stations of most importance to the study of the Cordillera, shown in figure 2.2, consists of six stations across southern Arizona, New Mexico and west Texas.

Figure 2.1 Geomagnetic deep sounding in the
western United States: locations
of observation.

LOCATION OF 1967 ARRAY



LOCATION OF PREVIOUS STUDIES

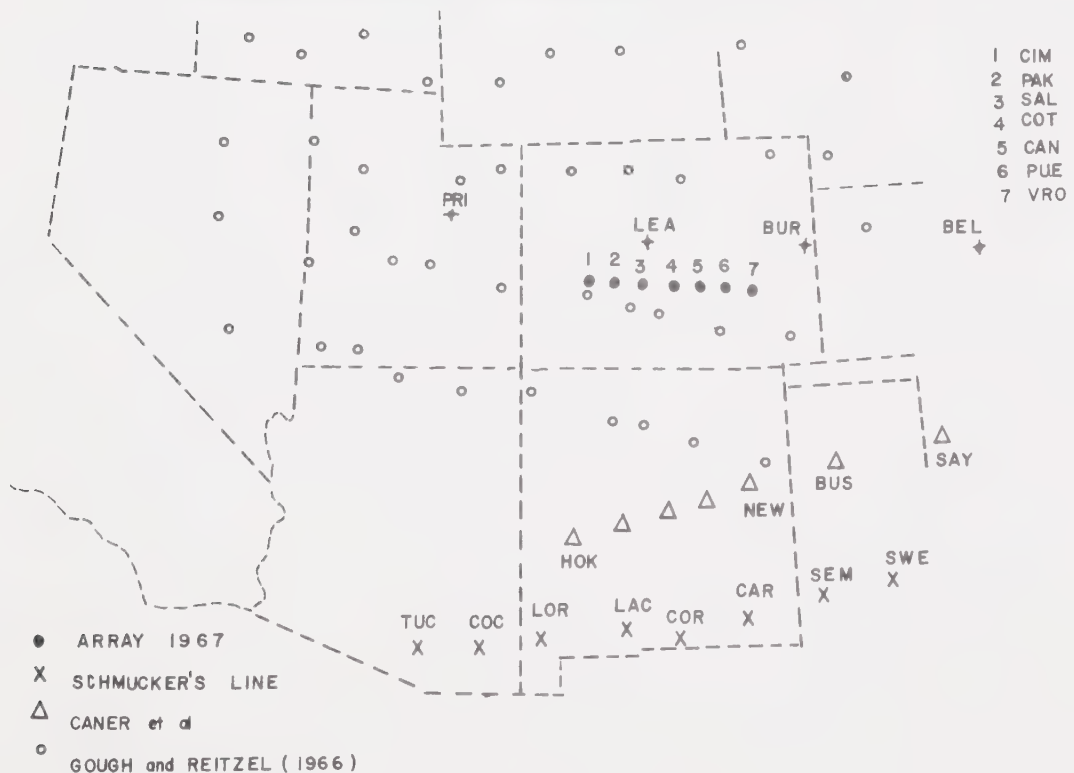
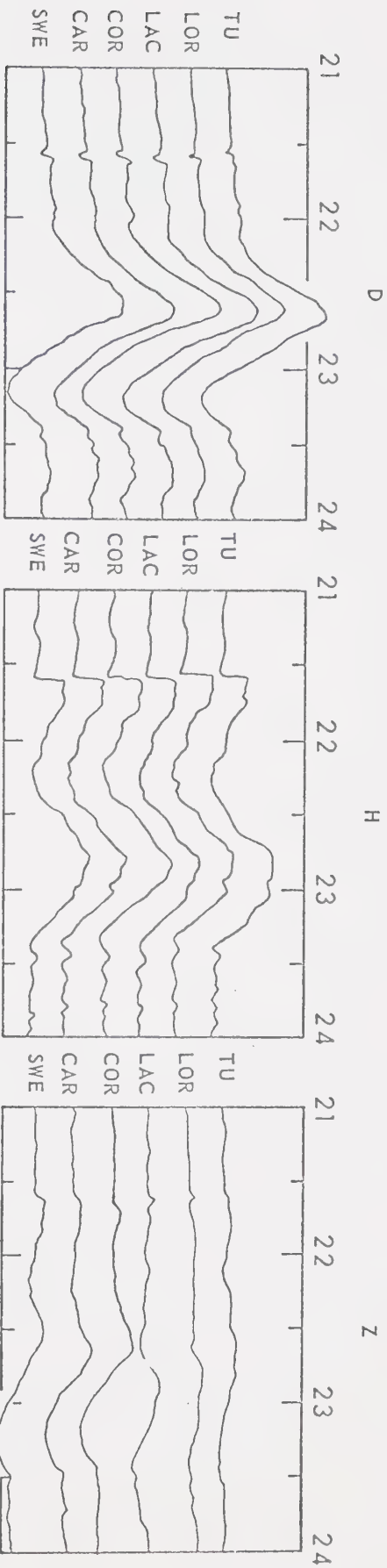
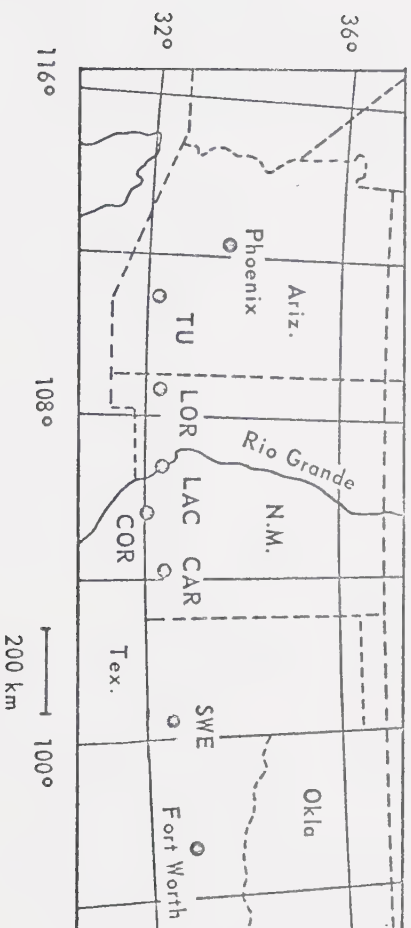


Figure 2.2 Schmucker's observations of a bay variation of May 10, 1960, and locations of his stations. After Schmucker (1964).



May 10, 1960



100 gammas
 A A A
 D H Z

Schmucker used the "base station" GDS method, with the permanent magnetic observatory at Tucson, Arizona as his base or fixed station, in his investigation of the Rio Grande anomaly (see section 1.7). He distinguished between the normal and anomalous parts of the observed variation fields, defining the normal part as the sum of the smoothed external and internal parts of variations for the case of a rather uniform external source field and a horizontally stratified conductivity distribution. The normal variations were taken to be uniform in mid-latitudes. Since there is a linear correlation between the normal and anomalous parts, Schmucker sought to derive at each station a characteristic and frequency-dependent linear transformation matrix, $f(P, \omega)$, which would express at each station the anomalous part of the observed variations in terms of the normal part over the whole area. He defined the following functions to express the correlation between normal and anomalous variations. $F(P, t)$ is the time varying disturbance vector of the observed variation at the station, P , and $F_0(t)$ and $F_a(P, t)$ represent its normal and anomalous parts:

$$F(P, t) = F_0(t) + F_a(P, t) = F_0(t) + f(P, \omega)F_0(t) .$$

(2.1)

It is assumed that a frequency analysis has been performed on the observed variations and that D, H, Z are harmonic time functions of form $\exp(i\omega t)$. If it is assumed that a time function $Z(t)$ is linearly related to a second time function $H(t)$, with both being normalized to zero mean value for a given interval $-\frac{1}{2} T_0 \leq t \leq \frac{1}{2} T_0$, their relation will be independent of time within this interval and expressible by a linear transfer function $Z_H(t)$ in the frequency domain, assuming $T_0 \rightarrow \infty$. The Fourier transform of $X(t)$ can be expressed by

$$C_X(f) = \int_{-\infty}^{\infty} H(t) e^{-2\pi i f t} dt$$

and thus it may be said that

$$C_Z(f) = (Z_H(f) \cdot C_H(f))$$

Let S_H be the power spectrum of $H(t)$ and S_Z the power spectrum of $Z(t)$ then following relations hold.

$$S_H = (C_H C_H^*) / T_0$$

$$S_{ZH} = S_{HZ}^* = (C_Z \cdot C_H^*) / T_0$$

$$Z_H = S_{ZH} / S_H$$

where the product of C_H with its complex conjugate C_H^* is real and positive and the product C_Z with C_H^* gives

the cross-spectrum between $Z(t)$ and $H(t)$. The transfer function Z_H is now expressed in terms of power and cross-spectra. Thus

$$Z = Z_o + Z_a = Z_o + z(D)D_o + z(H)H_o + z(Z)Z_o \quad (2.2)$$

where the coefficients in equation (2.2) are complex and of the form

$$Z(D) = Z_u(D) + iZ_v(D) .$$

The subscripts u and v are respectively in-phase and out-of-phase with the associated inducing component of the normal field. For small differences in phase or in two-dimensional field distributions equation (2.2) reduces to

$$Z = Z_o + z(B)B_o + z(Z)Z_o$$

$$\text{with } Z(B) = Z(D) \cos\alpha + Z(H) \sin\alpha \quad (2.3)$$

$$\text{and } B_o = D_o \cos\alpha + H_o \sin\alpha$$

where B_o is the projection of the horizontal disturbance vector on a direction given by angle α . For the case of zero phase all quantities of equation (2.3) are real, $\tan\alpha = Z_u(H)/Z_u(D)$ and for a 2-dimensional anomaly $\tan\alpha = Z(H)/Z(D)$.

Schmucker found that the $Z(t)$ variation across the Rio Grande anomaly resembled $D(t)$ and was nearly in phase with it. Therefore the angle, α , can be set to zero and equation (2.3) gives

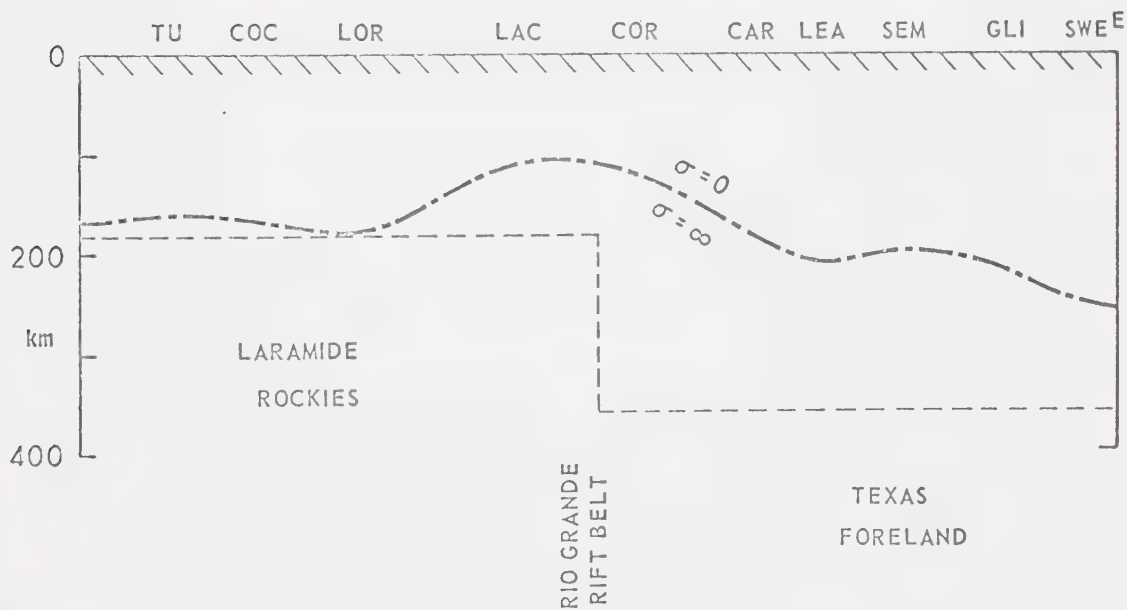
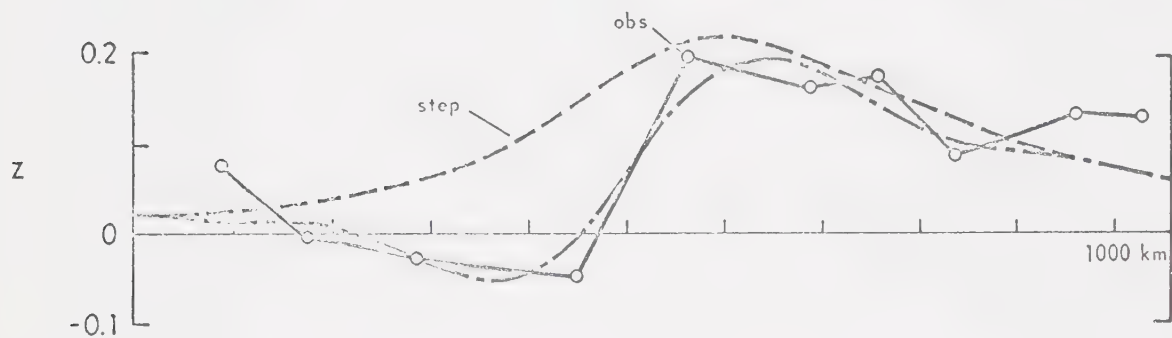
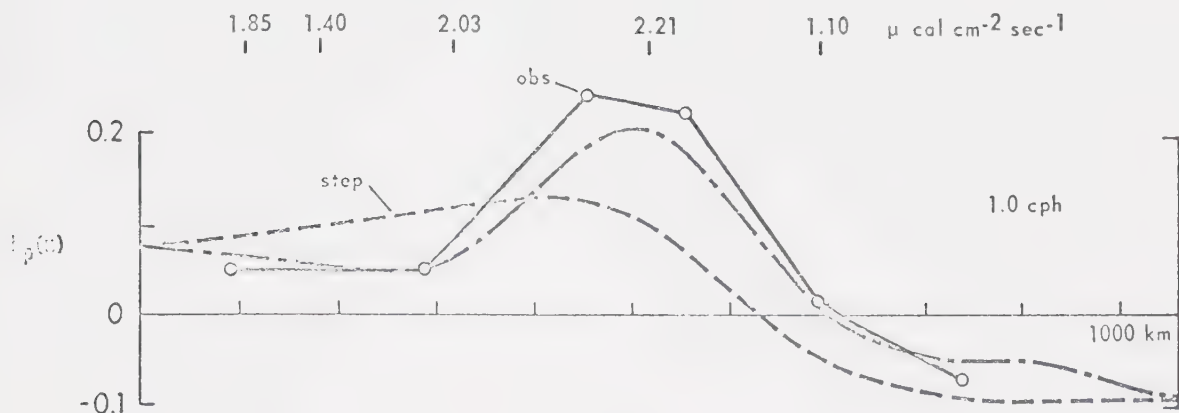
$$Z = Z_o + z(D)D_o + z(Z)Z_o .$$

The implication is that the trend of the conductor is north-south.

In records of geomagnetic substorm fields or bays Schmucker found an increase in the Z/D ratio east of COR and an anomalous Z at COR (figure 2.2). The increased Z/D ratio at Sweetwater as well as the reduced Z/D ratio at Tucson are both to be considered "normal" in the sense that both stations are assumed to lie within large areas of horizontally stratified, but different conductivity structures. The above Z/D ratios suggest that either the total conductivity of the surface layers is consistently lower in southern Texas than in southern Arizona or that the depth of the highly conducting part of the upper mantle is greater under Texas than under Arizona.

Schmucker interpreted the Rio Grande anomaly as a systematic change of the internal part of the Z variations which is caused by a large scale change in

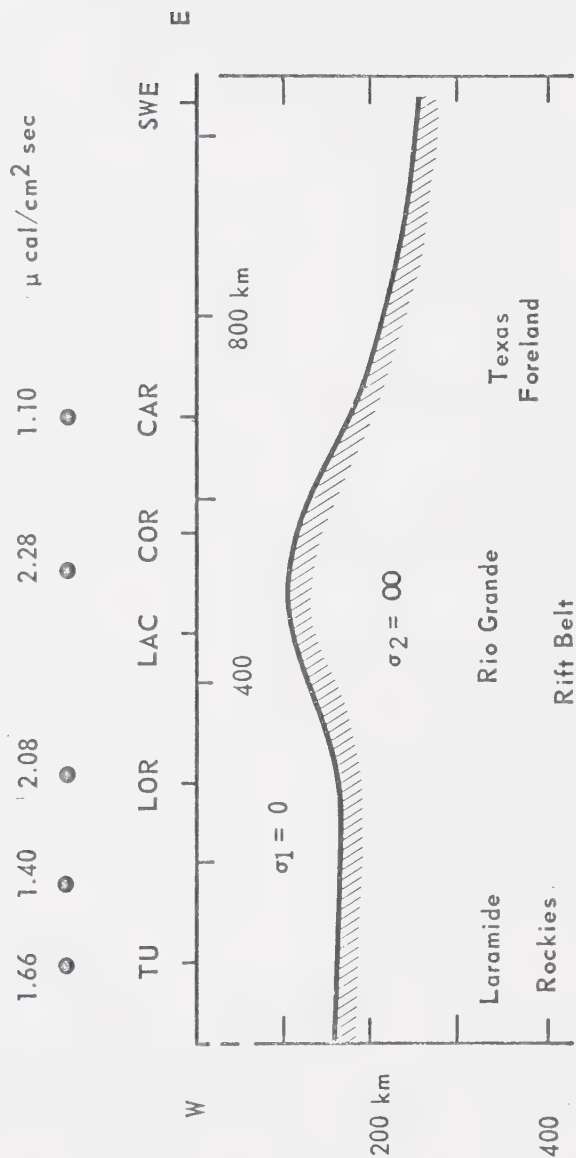
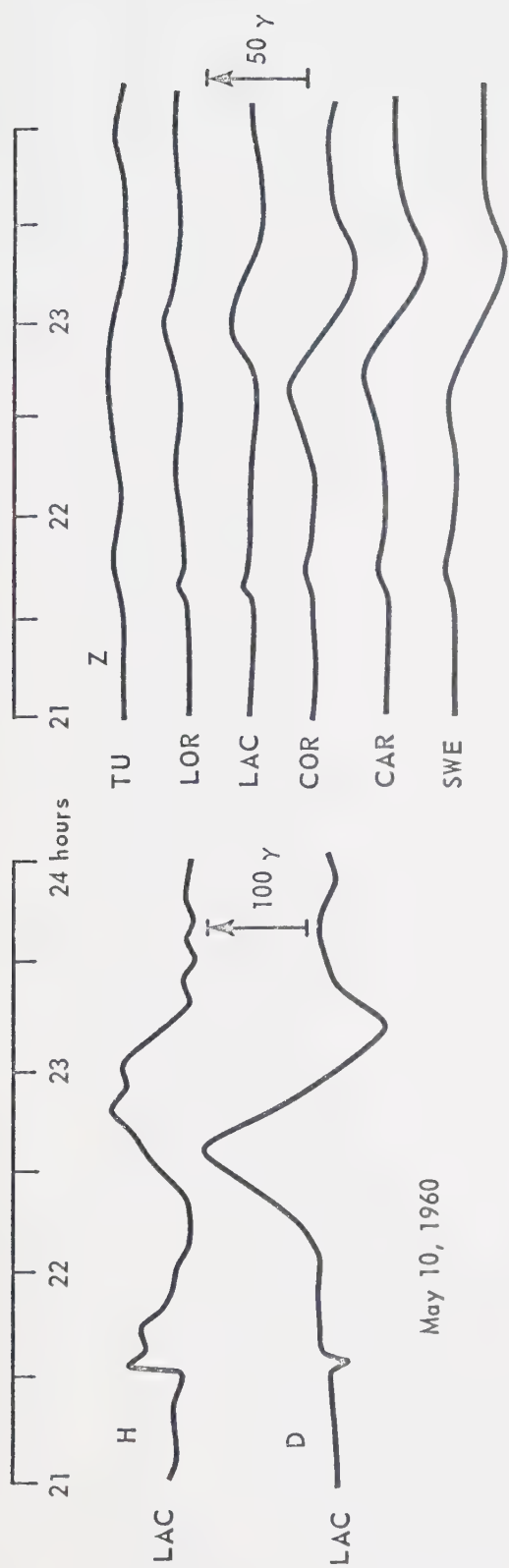
Figure 2.3 Schmucker's second model for the
Rio Grande anomaly (after Schmucker,
1969).



the internal conductivity structure, since inspection of figure 2.2 shows that the higher Z variations are not restricted to a limited area; the Z variations do not return to normal as defined by the small Tuscon-type Z variation. Anomalous variations as defined in equation (2.2) occur mainly between LAC and COR.

Schmucker modeled the Rio Grande anomaly by employing the methods presented in section 1.5 together with conformal mapping techniques applied to conductors of infinite conductivity and of various shapes and sizes. His first model (Schmucker, 1964) consisted of a north-south aligned step structure with the depth to the "perfect substitute conductor" 160 km. west of LAC and 320 km. east of LAC (figure 2.3) It can be seen from figure 2.3 that the step model does not explain the sharp increase of the anomalous Z variations between LAC and COR, which becomes greater for short period variations with a more pronounced negative anomaly between COR and LAC. The alternative model of figure 2.3 gives much better fit to the observations by placing the surface of the perfect conductor higher between LAC and COR. Schmucker at first attributed the local anomaly at LAC to a highly conductive, 100 km. wide shallow layer that might include surface layers, extending north-

Figure 2.4 Schmucker's third model for the
Rio Grande anomaly (Schmucker,
1969).



south between LAC and COR. A closer inspection of figure 2.3 shows that it is in fact the in-phase component of Z_n which experiences the reversal between LAC and COR, which means that the reversal is associated with currents in a large conductor in which self-induction is more important than resistive induction. Schmucker (1969) has since revised his model to concur somewhat with the above argument. Figure 2.4 shows his new interpretation of the Rio Grande anomaly along with corroborating heat flow results along the same line as his magnetic stations. Schmucker's anomaly demonstrates the presence of structure in upper mantle conductivity at the boundary between the Basin and Range and the Great Plains provinces. The general form of the conductive structure of figure 2.4 resembles the structure (step plus superposed ridge) suggested by Porath, Oldenburg and Gough (1970) to account for the Wasatch Front anomaly in Utah at the boundary between the Basin and Range Province and the Colorado Plateau (Chapter 4).

Caner, Cannon and Livingstone (1967) set out an east-west profile of stations 750 km. long near latitude 35° N from Horse Springs (HOR), New Mexico to Sayre (SAY), Oklahoma (figure 2.1). This profile was extended another 250 km. eastward by use of the permanent observatory at the University of Oklahoma, Norman. The

observations were made in an attempt to map the northward extension of the Rio Grande anomaly (after Schmucker 1964).

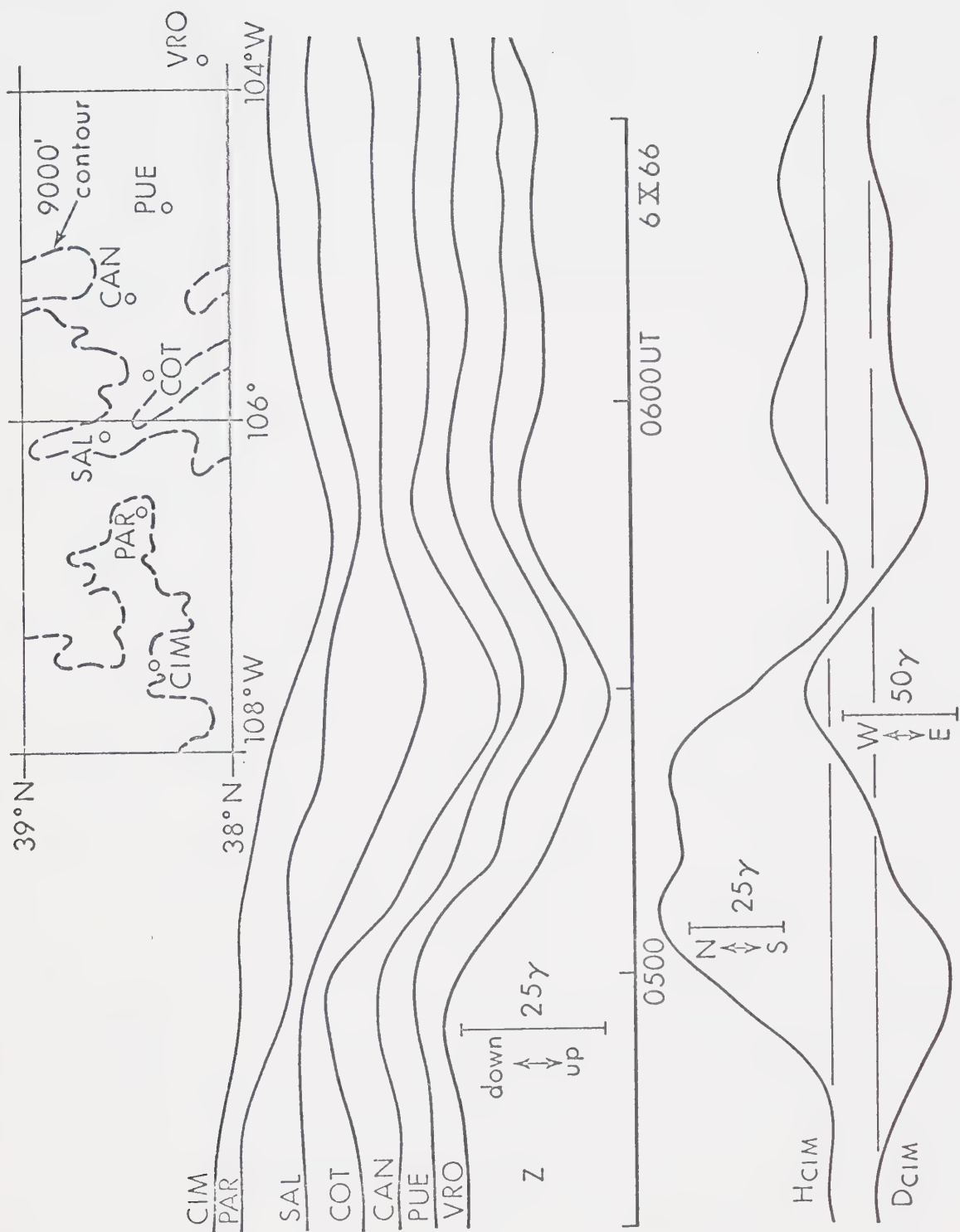
Caner et al. (1967) used the "base station" method of GDS. Peak to peak amplitudes of recorded magnetic variations in the range of periods 10 to 60 minutes were measured in three components to determine whether a station was in a "low Z" or "high Z" zone. The classification of the stations in this manner was aided by the introduction of the parameter I,

$$I = \Delta Z / [(\Delta H)^2 + (\Delta D)^2]^{\frac{1}{2}}$$

which is the ratio of the measured vertical to horizontal amplitudes. The I-ratios at various stations differed by factors of two or three and were thus easily separated into categories "low I" and "high I". The approximate locations of the "low I" to "high I" transition zones then can be readily determined.

Caner et al. (1967) used the polar plot method of Parkinson (1959, 1962) to define correlations between the amplitude of the vertical component and the direction of a horizontal change vector. At a normal station the I-ratio is uncorrelated with the azimuth of the horizontal change

Figure 2.5 East Front anomaly of Colorado
(Gough and Reitzel, 1969).



vector, $\bar{\alpha} = \arctan \Delta D / \Delta H$, and at an anomalous station the I-ratio is a maximum for certain values of $\bar{\alpha}$ thus defining a preferred direction. Caner et al. (1967) found that the transition station Sayre showed I-ratios intermediate between those obtained at the western stations of Newkirk and Bushland and those at the eastern stations of Norman and Dallas. The station Sayre was devoid of any definite correlation between the horizontal change vector and the vertical change vector. A transition zone was located well to the east of the Rockies at the Texas-Oklahoma border. Caner interpreted these results as a swing to the east of the Rio Grande anomaly. Results of the 1967 array do not support this conclusion. Later studies (Porath 1969) suggest that Permian sediments, which are up to 10,000 feet thick in the area may have masked the effect of the deep conductivity structure.

Gough and Reitzel (1969) set out an east-west profile north of that of Caner et al. (1967) at about $38^{\circ} 30' N$ between $108^{\circ} W$ and $104^{\circ} W$, using variometers of their own design. This profile was operated to search for a northward extension of the Rio Grande anomaly and was placed with reference to IGY stations at Leadville (low-Z) and Burlington (high-Z). Figure 2.5 illustrates results from a bay variation recorded

Figure 2.6 Magnetotelluric measurement sites
of Swift (1967).

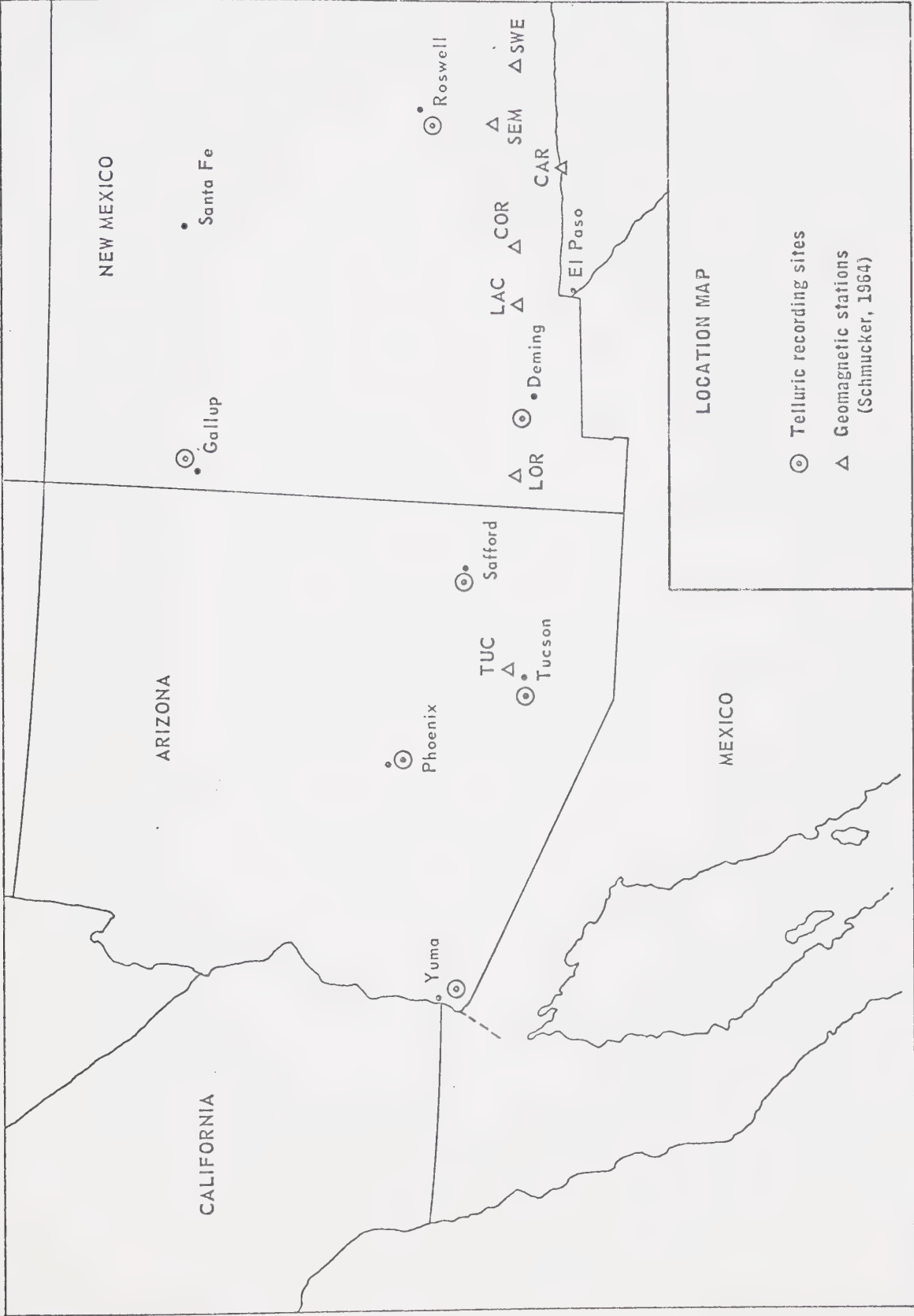
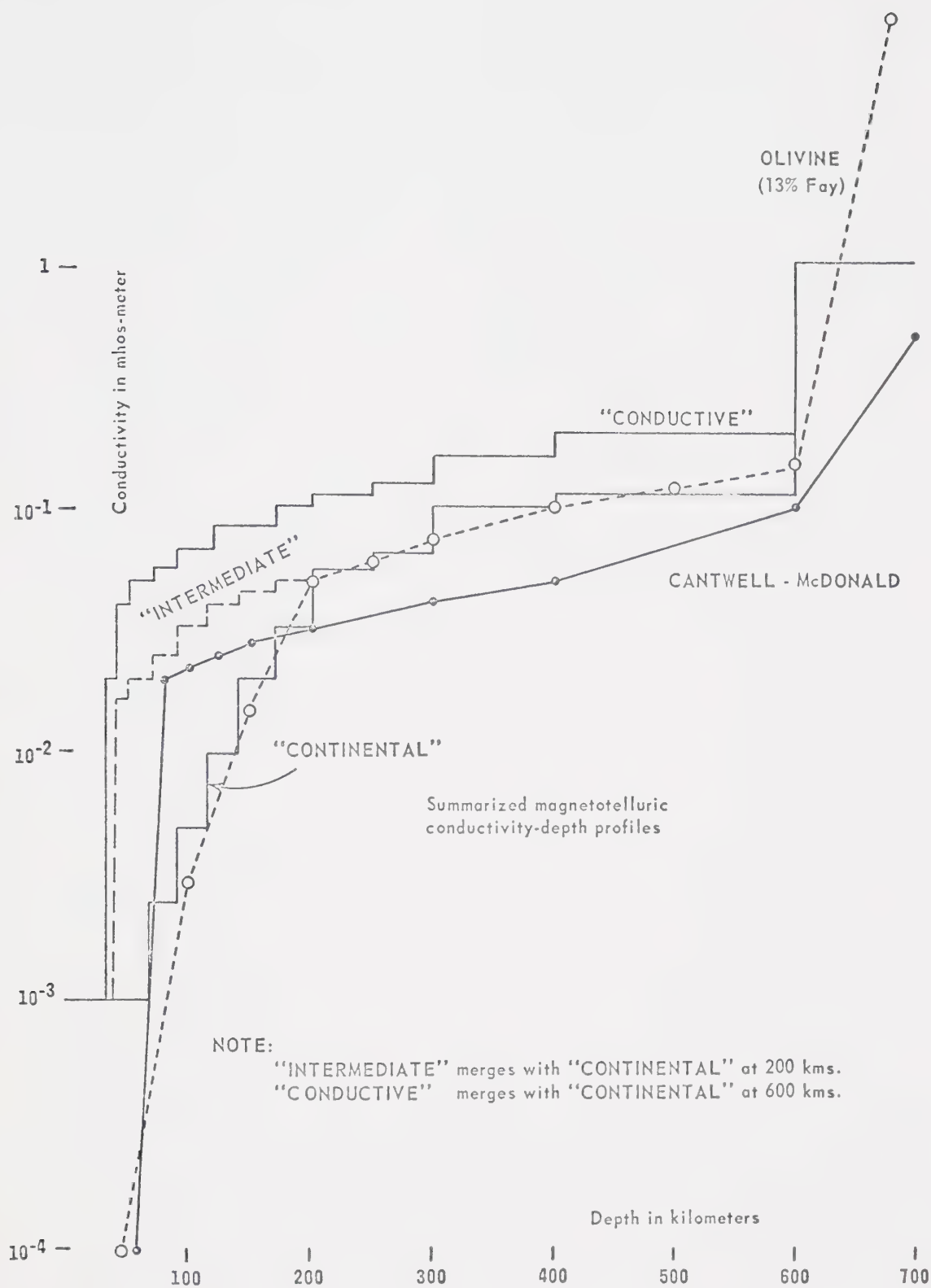


Figure 2.7 Conductivity profiles (after
Swift, 1967).



(from Swift, 1967)

along this profile. The H,D,Z components of the disturbance are shown for CIM with the Z variation for seven stations. D is recorded in the opposite sense from that used by Schmucker (1964). Z as a function of time resembles D much more than H. The transition occurs at Salida which is about 100 km. west of the Front Range of the Southern Rockies.

The anomaly at Salida was thought at the time to be the northward extension of the Rio Grande anomaly. However the results of the 1967 array (Reitzel et al. 1970, Porath et al. 1970, this thesis) suggest that the Rio Grande anomaly is continuous with the Wasatch Front anomaly rather than that underlying the Southern Rockies.

Swift (1967) in the summers of 1965 and 1966 carried out large scale magnetotelluric measurements in the south-western United States by combining telluric data from seven stations with Tucson geomagnetic observatory data. Figure 2.6 gives the locations of the stations. The magnetotelluric data were analysed for tensor apparent resistivities, principal directions and two dimensionality measures. The measured apparent resistivities were interpreted in terms of inhomogeneous resistivity structure by employing theoretical values for two-dimensional models obtained with the aid of a

transmission line analogy due to T.R. Madden. The theoretical values took into account the known surface geology.

The anisotropy of the measured apparent resistivities was primarily due to inhomogeneities in surface conductivity and was corrected to give an areal pattern that suggested an anomalously conductive upper mantle beneath southern Arizona and New Mexico.

The conductivity profiles interpreted from the magnetotelluric results were classified by Swift as:

"Continental" for Roswell

"Intermediate" for Phoenix, Gallup, Deming

"Conductive" for Safford

and can be seen in figure 2.7 along with the Cantwell-McDonald profile. The Cantwell-McDonald conductivity vs depth profile is the result of Cantwell (1960) fitting his long period magnetotelluric result of conductivity vs depth to those of McDonald (1957), obtained also from long period magnetotelluric investigations, and Lahiri and Price (1939), obtained from the internal parts of semi-diurnal Sq-variations and smoothed storm-time D_{st} variations. It seems that the magnetotelluric evidence generally supports Schmucker's results in indicating increased conductivities in the upper mantle under the Basin and Range Province.

Swift has interpreted low frequency magnetotelluric data in terms of a petrologically valid upper mantle conductivity structure in a geologically anomalous region.

CHAPTER 3

TECHNIQUES OF OBSERVATION AND INTERPRETATION

3.1 The array

In the summer of 1967, a program of study of the conductivity distribution in the upper mantle under the Western United States was begun in the hope of defining boundaries of regions of different mantle conductivity structure more accurately than had before been possible. To accomplish this, 42 magnetic variometers had been designed and constructed at the Southwest Center in Dallas and at the University of Alberta in Edmonton. The instruments were arranged along four east-west lines about 1300 km. in length, crossing the Southern Rockies and the Colorado Plateau, and extending well into the Great Plains and Basin and Range provinces (figure 3.1). Though covering an area 700 by 1300 km. between 36° and 40° north latitude and 102° and 116° west longitude, the variometers were concentrated across the Southern Rockies and the Wasatch Fault zone. The evidence of vertical displacements at the Wasatch Front and the abundant volcanics to the west of it had suggested the possibility of structure in the isotherms there. Schmucker (1964) had earlier reported anomalous or high Z (vertical) magnetic

Figure 3.1 The 1967 variometer array.



displacements at the IGY magnetic observatory at Price, Utah in the Wasatch fault zone area.

The spacing between lines was about 150 km. and that between stations averaged 120 km. Small conductivity anomalies at depths less than 100 km. may be missed by such an array. This risk was accepted in order to search a maximum area for upper mantle conductivity structure.

3.2 Variometers and field procedures

The variometers (Gough and Reitzel, 1967) are classical in type, with magnets (H,D,Z components) suspended on torsion wires. Variations in the magnetic field will produce variable torques on the magnets which cause them to move through small angles and the angular positions of these magnets are recorded photographically in analog form at ten second intervals. The magnetic variations will then appear as traces of rectangular spots on 35 mm. film. Two base lines were recorded by means of light spots reflected from fixed mirrors.

The most serious problem of a classical type of variometer is that of thermal response. This was solved by encasing the variometer in a five foot aluminum tube and burying this in a vertical hole. Calculations have shown that a weekly variation of 30°C at the surface results in a temperature change of only 0.1°C at the

suspended magnets. A first order compensation for the consequent small changes of moment in the H and Z magnets was accomplished by use of auxiliary permanent magnets which were adjusted at some temperature to cancel half the Earth's field at the suspended magnet.

The instruments were leveled with a Brunton compass to within 0.1° in order to prevent contamination of one component by another. The sensitivity of the instrument is better than one gamma and with a sampling rate of ten seconds, reliable records of magnetic events with periods greater than one or two minutes were obtained.

Because the energy of magnetic variations decreases greatly at periods below 20 seconds, the problem of aliasing is negligible with a sampling interval of ten seconds. The timing was controlled by an Accutron timer made by Bulova, which gave contact closures every ten seconds, every hour and every 24 hours. Small coils near the magnets were used to deflect the traces at hourly and daily contact closures.

At periodic servicing visits (usually at 10 day intervals) to each variometer standardizing fields known to within one percent were applied by means of permanent magnets (two southern lines) or by means of coils and

magnets (two northern lines). This procedure served to determine the sensitivities of the three suspended magnets and to give absolute time (WWV radio signals) which could later be transferred to an hour mark produced by the Accutron timer on the film record. From two such visits the rate of drift of the Accutron could be determined with the assumption that the drift was linear. The Accutrons were found to have reasonably constant rates of order 10 seconds per day or less and time was generally reliable within one minute. With good field operation better than two percent precision of calibration can be secured by these methods, although the precision attained at some stations was less in 1967.

An independent check of the relative time between the instruments of the array and also a check on the assumption that the rate of drift of the Accutron was approximately linear was obtained by correlation of geomagnetic micropulsations which should occur simultaneously (within a minute) over the entire array (Rostoker, 1968). These micropulsations, known as $Pi2$'s, have periods 40 to 150 seconds and are clearly visible at the beginning of each magnetic event at all stations on the horizontal traces. Thus the maximum

error in timing was no more than one minute and in most cases considerably less.

3.3 Magnetic variation records

This thesis includes analyses of two magnetic variation events: 1) a magnetic substorm occurring from 0500 to 0830 UT on September 1, 1967 and 2) a moderate storm occurring from 2300 to 1230 UT on September 20-21, 1967. The substorm was selected because of the large amplitudes of magnetic variation and because it was recorded with nearly 95% efficiency. The storm was selected because of its length and varied frequency content, both of which are desirable to permit the use of long period variation fields in studying structures. The efficiency of recording for the storm varied from east to west. The western half of the array, that covering the Wasatch fault zone, recorded with 91% or greater efficiency and the eastern half, that covering the Southern Rockies, with 63% or greater efficiency. Greater efficiency was achieved in the horizontal components, mainly because the Z component was metastable at several stations. Results have shown that the horizontal components yield as much information about the structure of the anomalies as the vertical component, particularly after separation.

Enlarged Xerox prints of the film records containing the magnetic event were commercially digitized at one minute intervals. Before digitizing the Xerox traces were smoothed by underlining them in pencil so as to avoid aliasing from micropulsations of periods less than about two minutes. The initial value of each component was subtracted from each succeeding value. Physically this means that the field is thought to be quiet before the variation and the initial value can be set to zero. The components of the variation fields were normalized by means of factors calculated from the field standardization data.

3.4 Spectral analysis

Geomagnetic depth sounding is concerned with variations in conductivity at depth. Consequently the skin-depth, $p = 1/(4\pi\mu\sigma\omega)^{1/2}$, becomes an important parameter to estimate. The penetration of the external field into the Earth, the induction process in a conductive structure and the escape of the field of the internal currents depend on the frequency, ω . The relation between the external and internal fields, whose vector sum forms the recorded variation field,

is likewise a function of frequency. More information can thus be extracted from amplitude and phase relations at definite frequencies than can be obtained from the original data in the time domain. For these reasons it is desirable to represent the total magnetic variation field as a Fourier series in the frequency domain and to use the sine and cosine coefficients of the series, or the amplitude and phase, to display spatial variations in the magnetic variation field across the array.

The equation

$$X_j = \frac{1}{\sqrt{2\pi}} \int_{-\infty}^{\infty} X(t) e^{-i\omega t} dt \quad (3.1)$$

is the general formulation of Fourier transform of a time series $X(t)$. The Fourier analysis used throughout this thesis was that given by the RHARM program in the IBM SSR package employing the Cooley-Tukey algorithm. Given $2N$ real numbers $X_0, X_1, X_2 \dots X_{2N-1}$ this subroutine computes Fourier sine and cosine coefficients $a_0, a_1, b_1, a_2, b_2, \dots a_{n-1}, b_{n-1}, a_n$ in the equation

$$X_j = \frac{1}{2} a_0 + \sum_{k=1}^{N-1} \left(a_k \cos\left(\frac{\pi j k}{N}\right) + b_k \sin\left(\frac{\pi j k}{N}\right) + \frac{1}{2} a_N (-1)^j \right) \quad (3.2)$$

where $j = 0, 1, 2, \dots, 2N-1$.

Each magnetic variation, which can be treated as a time series, had a linear trend removed before Fourier analysis. The first and last ten minutes of each time series were smoothed by multiplying them by coefficients of a sine function evaluated from 0 to $\pi/2$. This smoothing is necessary to prevent the introduction of fictitious high frequency components that would be caused by sudden changes at the beginning and end of a finite time series.

The Fast Fourier algorithm demands that the number of points in the time series be an integral power of two. Thus it was necessary to add zeros to the end of the time series representing the substorm and the storm. Further zeros, beyond the next integral power of two above the number of data points, were added to increase the number of spectral estimates. Physically this is reasonable since the substorm and storm can be regarded as transients in an otherwise steady magnetic field, so that the steady magnetic field is represented by a zero amplitude time series.

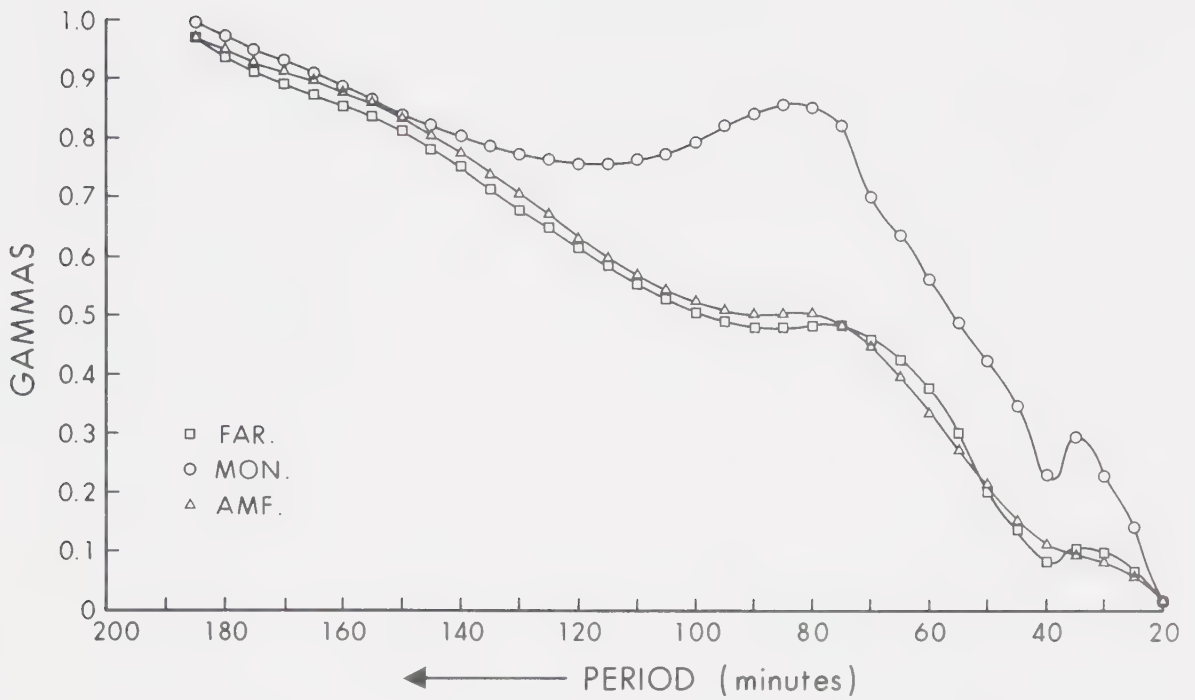
To find the effect of adding zeros, an analysis was undertaken by Mr. D.W. Oldenburg and the writer in which the length of the work vector M (the number of real data points N , plus the number of zeros added) took values 256, 512, 1024 and 2048. N was 211 for the

substorm. All frequencies found in the Fourier analysis when $N=256$ were found for each succeeding value of M . It was found that the sine and cosine coefficients of the Fourier series were attenuated by different (for each different value of M) but constant factors. For the coefficients to approximate field values in gammas, each coefficient must be multiplied by a factor N/M . If this is done the sine and cosine coefficients will be the same at a particular frequency for all values of M . While additional estimates secured by increasing M must be less reliable, the spectra for values of M from 256 to the maximum value 2048 remained smooth. For the present analysis $M=2048$ was used for the substorm and $M=4096$ was used for the storm which is represented by a time series $N=811$.

As an additional check on the validity of the use of the Cooley-Tukey Fast Fourier algorithm with numerous zeros added after the real data, data from the substorm of September 1, 1967 recorded at several stations were Fourier analysed using both the Cooley-Tukey algorithm and a slow Fourier program which did not place special restrictions on the number of data points analysed; 211 points were used for the substorm without zeros. The two methods yielded identical spectra in both the

Figure 3.2 Fourier spectral amplitude and phase
for vertical component of substorm
of September 1, 1967, for stations
across the Wasatch Front on Line 1.

AMPLITUDE Z COMPONENT



PHASE

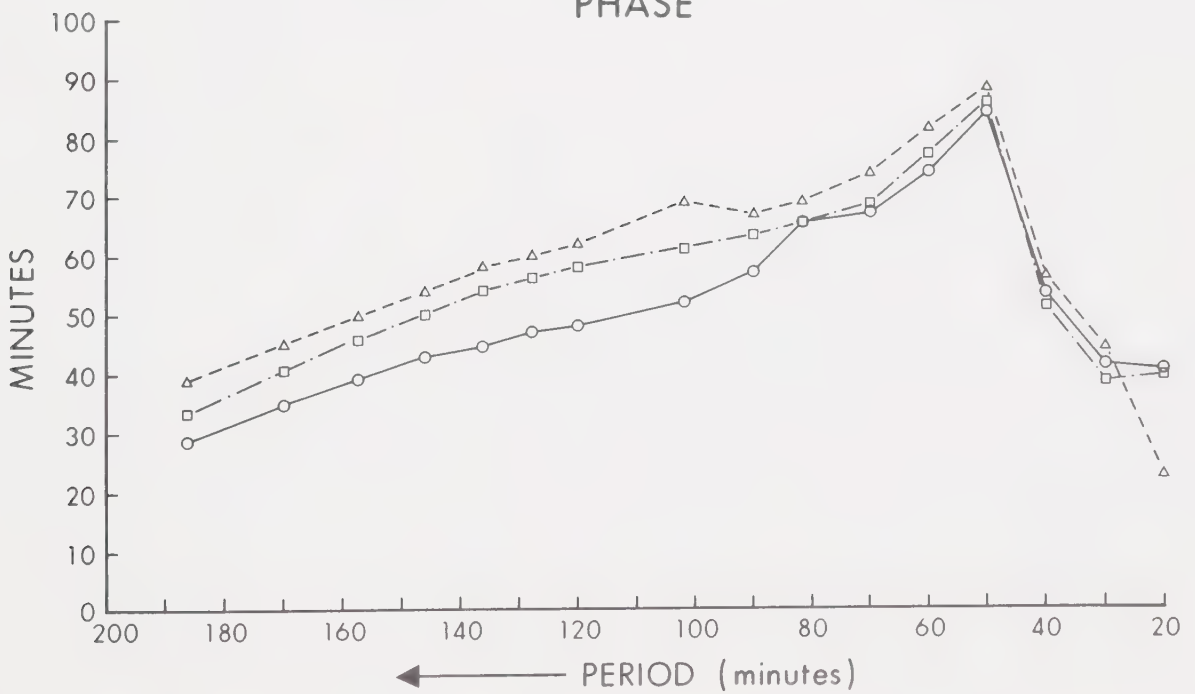
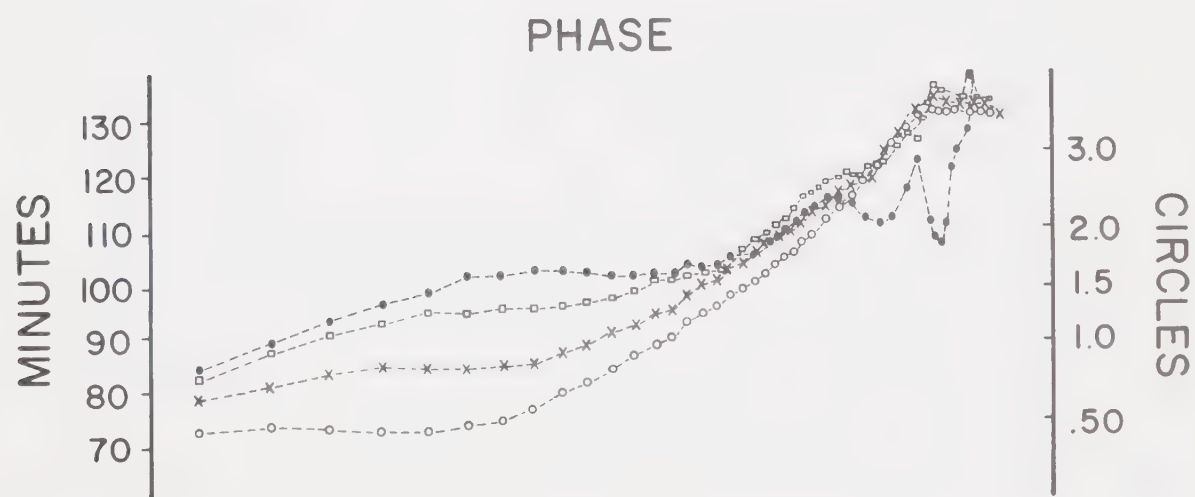
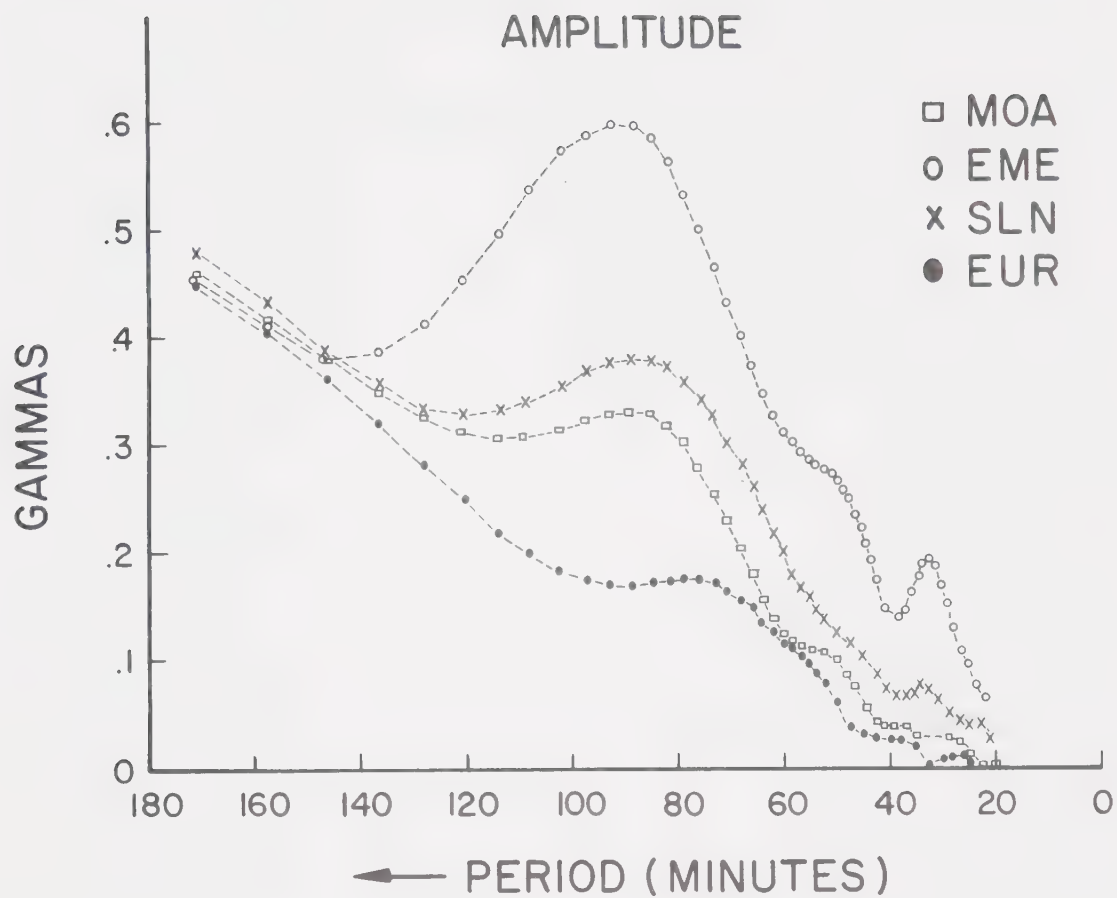


Figure 3.3 Fourier spectral amplitude and phase
for vertical component of substorm
of September 1, 1967, for stations
across the Wasatch Front on Line 3.



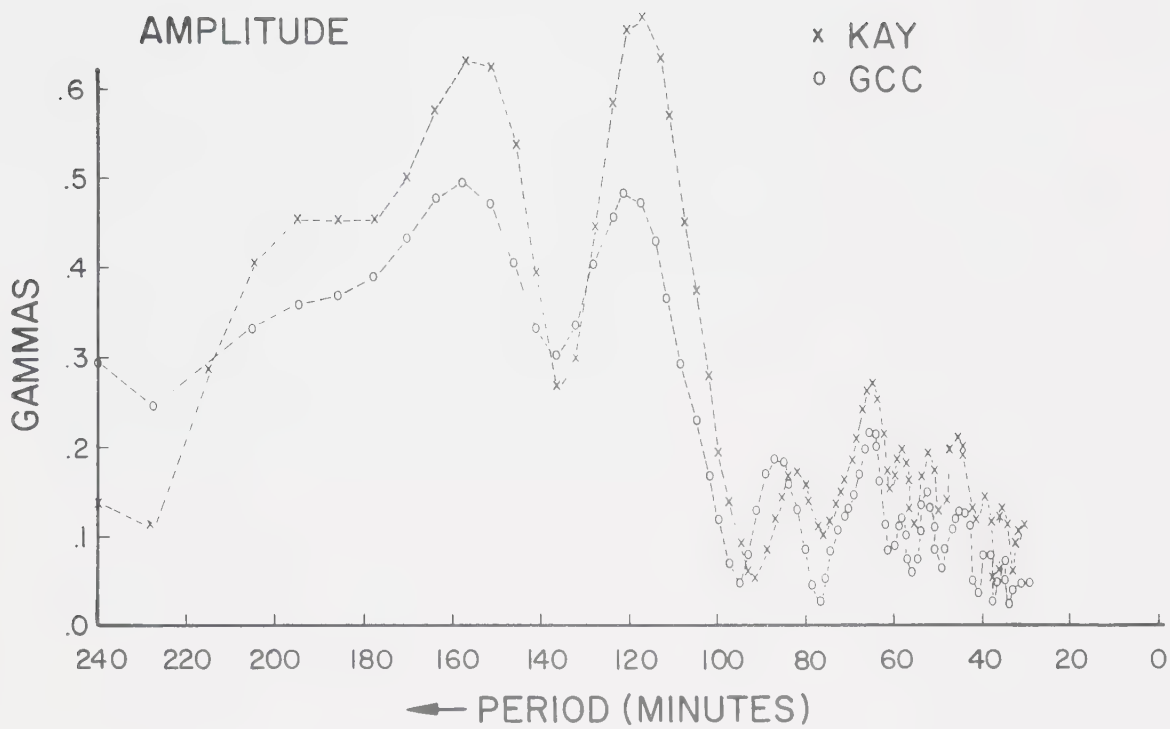
amplitude and phase. This check was carried out by Dr. H. Porath at the Southwest Center for Advanced Studies.

At some stations where the amplitudes were very large, mainly on lines 1 and 2 for the D component, fictitious values were interpolated in the gaps seen in the Calcomp plots in figure 4.2 to permit some attempt at spectral analysis. The results for these stations at which the gaps are numerous should be treated with reserve.

Figures 3.2, 3.3 and 3.4 are examples of the Fourier transforms of the vertical components of the substorm and the storm for some stations over the Wasatch Front. The substorm has a smooth amplitude spectrum and very marked differences are observed between stations for periods from 20 minutes to 2 hours. Most spectra contain very little energy at periods less than 20 minutes. Substantial phase differences are observed between stations, especially where anomalous induction occurs. But for periods exceeding 90 minutes, these phase differences may be partially due to variations in the long period trend removed before Fourier analysis.

A line spectrum (figure 3.4) is obtained for the storm with peaks at periods of 155,120,85,65 minutes and

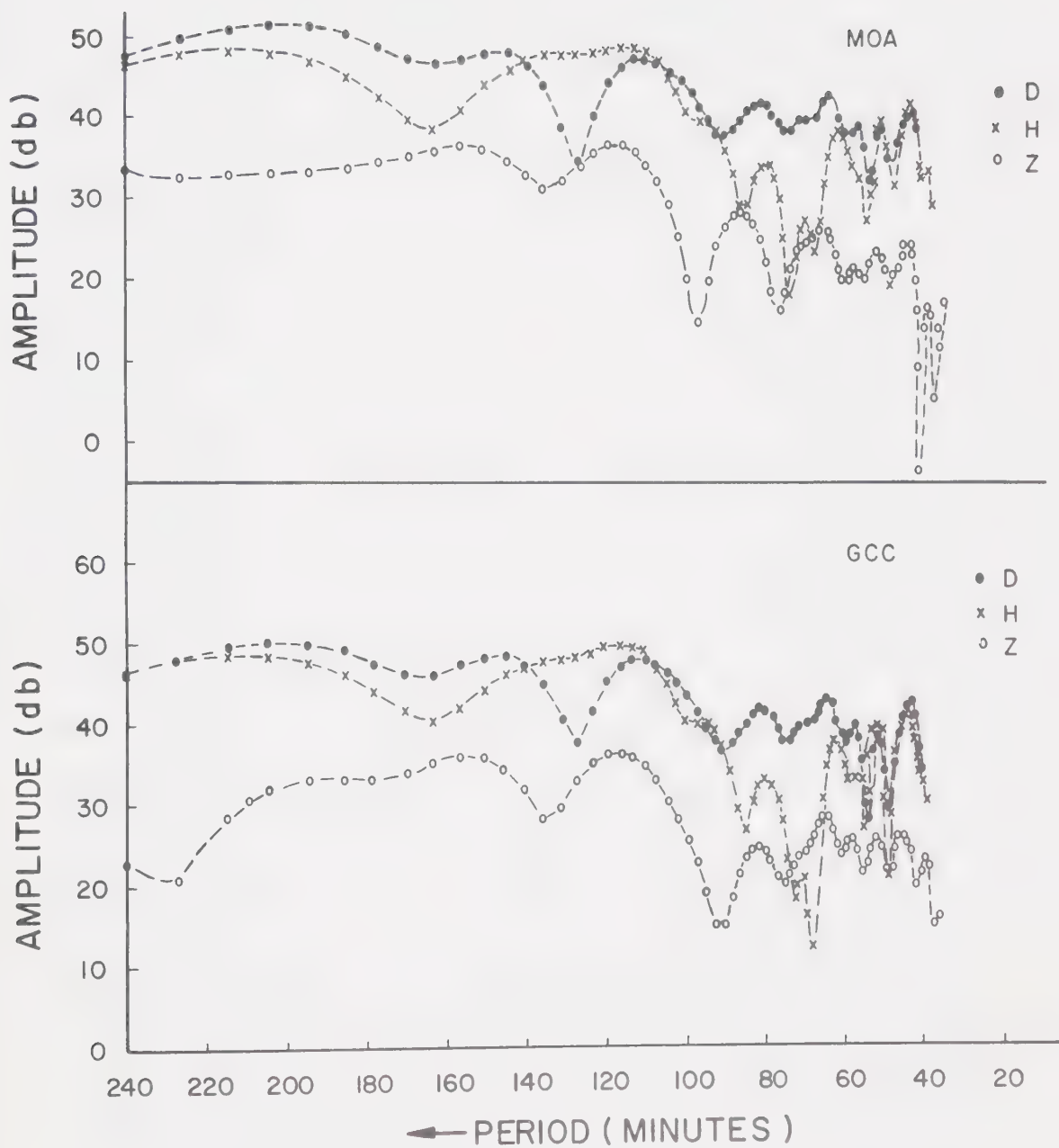
Figure 3.4 Fourier spectral amplitude and phase
for vertical component of storm of
September 20-21, 1967, at stations
of Line 3 on either side of the
Wasatch Front.



several peaks below 60 minutes. The spectrum again contains very little energy for periods under 20 minutes. A differential shift between the energy maxima of the horizontal and vertical components is observed in the storm spectra for periods longer than 50 minutes (figure 3.5). This is probably related to the fields induced by internal currents. The internal field becomes relatively smaller for longer periods due to the lower efficiency of the induction process at the longer periods. Above a conductive half-space in which the conductivity varies with depth alone, the horizontal fields of internal currents increase the external horizontal fields, whereas for the vertical component the internal field is opposed to the external field and the resultant component is the difference (section 1.2). The net effect is a shift of the peaks of the horizontal components toward the shorter periods and conversely the vertical peaks shift toward the longer periods.

Regular variations in amplitude and phase of the Z spectra at neighbouring stations suggest that these spatial variations may reflect large scale conductivity changes across the array. Results of

Figure 3.5 Spectra of three components of
field of storm of September
20-21, 1967.



mapping these spatial variations for several periods are shown and interpreted in chapter 4.

3.5 Separation of the variation fields

To evaluate the surface integrals of equation (1.55) quoted in chapter 1, the magnetic components must be plotted on a rectangular grid. The stations were transferred from a sphere to a plane by plotting them on an equal area map. The Z-direction is taken normal to any point on the plane and the X and Y directions are those of the longitude and latitude at that point. As the meridians are not parallel, a transformation to a rectangular grid is required. The separation of the total magnetic field variation into its internal and external parts is then carried out on the new plane. A north-south reference line was drawn through the center of the array, and at each station the angle η , between a line parallel to the reference line, and the meridian indicating true geographic north, was found. Z is invariant for this transformation. Let XP and YP denote northward and eastward field values on a rectangular grid parallel to the reference line. The transformations to convert X to XP and Y to YP are

$$\begin{aligned}
 XP &= X \cos \eta - Y \sin \eta \\
 YP &= X \sin \eta - Y \cos \eta
 \end{aligned}
 \tag{3.3}$$

The transformation (3.3) is applied with appropriate η to the time series at each station. The transformed time series are then Fourier analysed and mapped. For the remainder of this section to avoid confusion X will denote XP and Y , YP .

To draw contour maps of the sine and cosine transforms of the X, Y, Z components, the values between stations must be interpolated. As a first approximation the fields are contoured using linear interpolation between stations. A second constraint can be applied to the interpolation process if it is required that the fields be derivable from a scalar potential.

If the field is indeed derivable from a scalar potential function, then the magnetic field $\vec{H} = \vec{H}(\vec{X}, \vec{Y}, \vec{Z})$ measured on the Earth's surface must be curl-free i.e.

$$\nabla \times H = 0 .$$

Therefore

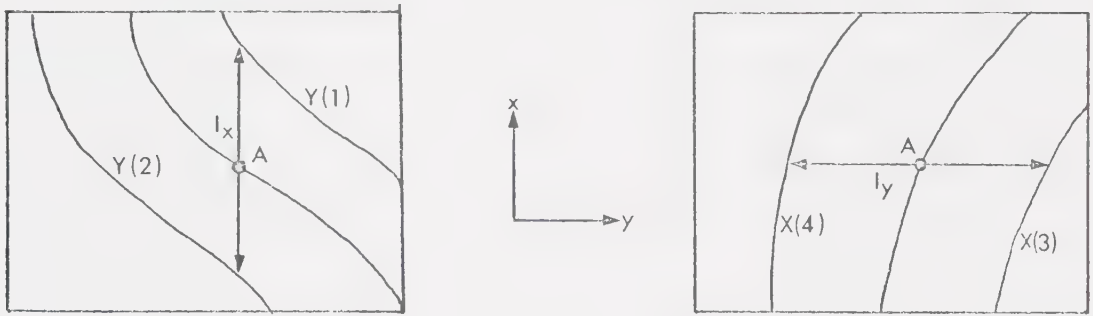
$$\hat{i} \left(\frac{\partial Z}{\partial Y} - \frac{\partial Y}{\partial Z} \right) + \hat{j} \left(\frac{\partial X}{\partial Z} - \frac{\partial Z}{\partial X} \right) + \hat{k} \left(\frac{\partial Y}{\partial X} - \frac{\partial X}{\partial Y} \right) = 0 . \tag{3.4}$$

Each term in equation (3.4) must be equal to zero. Because observations were made on a plane, only the relation

$$\frac{\partial Y}{\partial x} = \frac{\partial X}{\partial y} \quad (3.5)$$

will provide a usable constraint. Therefore after the maps of the XP and YP components have been contoured by linear interpolation, the contours can be adjusted to meet the curl-free condition in equation (3.5).

For example for Y



$$\frac{\partial Y}{\partial x} = \lim_{\delta \rightarrow 0} \frac{Y(x+\delta) - Y(x-\delta)}{\partial \delta} \approx \frac{Y(1) - Y(2)}{l_x}$$

and for X

$$\frac{\partial X}{\partial y} \approx \frac{X(4) - X(3)}{l_y}$$

where

l_x = distance in the x direction between Y(1) and Y(2),

l_y = distance in the y direction between X(1) and X(2),

then (3.5) implies

$$\frac{Y(1) - Y(2)}{l_x} = \frac{X(4) - X(3)}{l_y} .$$

Practice has shown that when superposing the X and Y maps the condition (3.5) was satisfied best when the gradient of Y in the x direction was large (of course this means that the gradient of X in the y direction must also be large). If the gradients were small, the curl-free condition gave little in the way of improvement to the linearly interpolated contours. Interpolation on a contoured map using the curl-free condition was first suggested by Reitzel (Gough and Reitzel, 1969).

Since the contouring was carried out on an x-y plane, $\frac{\partial X}{\partial z}$ and $\frac{\partial Y}{\partial z}$ are not known and no similar constraint to equation (3.5) can be employed in the contouring of Z. Z maps prepared for separation were contoured by linear interpolation and modified by avoiding sharp changes in gradient.

The magnetic field component maps were extrapolated beyond the limits of the array to give better estimates of the values of the surface integrals at points within the array. The curl-free constraint was used on the extrapolated horizontal fields. Such an extrapolated field will clearly contain errors and is certainly not unique, but should give a better approximation to the real field than, for instance,

the assumption that the field was zero or constant outside the array. The extrapolation was carried to 300 km. outside the array. The farther one extrapolates the more unreliable the field but the effect of errors in distant elements of area falls as $1/r^2$ (r is the distance from the point of separation to the surface element, equation (1.55)). The Z field was extrapolated by smoothly extending the contours outward from the original array.

The surface integrals may be determined if the average values of $X, Y, Z, \partial X/\partial x, \partial Y/\partial y, \partial Z/\partial x$ and $\partial Z/\partial y$ are known for each square on a symmetric grid, centered at the point of separation and used as a "summation window". Oldenburg (1969) evaluated the effects of square windows of sides 700, 900 and 1100 km., and found that the results even near the edges of the array varied only by 1 or 2 gammas. Oldenburg (1969) also wrote a program to compute the surface integrals by moving a square grid about the maps. The value of the difference between the internal and external parts of each magnetic component was then found for the center of this "window". Near the edge of the array the separation is dependent on the less reliable extrapolated field and some values inside the array are excluded. In this way considerable errors arise near the edges of the array.

When separating in the frequency domain the cosine and sine transform maps must be plotted, contoured and separated independently since the surface integrals can be applied only to fields in constant phase across the map. After separation they may be combined according to the relations

$$F_e = (\cos^2 F_e + \sin^2 F_e)^{\frac{1}{2}} ; \quad \tan \phi_e = \frac{\sin F_e}{\cos F_e} \quad (3.6)$$

$$F_i = (\cos^2 F_i + \sin^2 F_i)^{\frac{1}{2}} ; \quad \tan \phi_i = \frac{\sin F_i}{\cos F_i}$$

where F can represent any magnetic component (X, Y, Z) and the subscripts e and i refer to the external and internal parts respectively. It should be mentioned that the numerical magnitudes of the cosine and sine transforms have physical meaning only in relation to the sign and magnitude of the spectral component concerned at the start of the time interval, ΔT , transformed. A change in the starting time will introduce changes in the relative magnitudes and signs of the cosine and sine transforms, thus determining whether a given term in the time series appears in the cosine and/or sine transform or in both.

CHAPTER 4

ANOMALIES IN THE VARIATION FIELDS AND CONDUCTIVE STRUCTURES

4.1 Interpretation procedures

Three components of the magnetic variation fields, plotted by the Calcomp as standard type variograms, were first examined for amplitude and phase changes along each east-west line, especially in Z. Next, maps of three types were plotted for different purposes:

- (a) The amplitude and phase of the Fourier transforms at selected periods were plotted and contoured. These maps of the unseparated variation fields have been found very convenient for location and semi-quantitative interpretation of internal conductive structures.
- (b) The sine and cosine coefficients of the Fourier transforms at selected frequencies were mapped and contoured for separation of the fields into external and internal parts in the period domain.
- (c) Instantaneous field components at selected times were mapped and contoured by D.W. Oldenburg (1969) for separation in the time domain.

The procedure developed and used by Oldenburg (1969) has been used to separate the magnetic fields into internal and external parts; the integral expressions used are quoted in Chapter 1 (equations 1.60). For separation in

the time domain the procedure is very sensitive to discrepancies between stations in time and the times must be chosen when all three components have reasonable amplitudes. At least four different times have to be separated to give any picture of the internal and external variations of a substorm; Oldenburg (1969) separated the substorm of September 1, 1967 at the times 0630, 0645, 0700, 0715 UT. The substorm was four and one-half hours long and it would be desirable to separate at more times. For a storm which is approximately three times as long and of variable frequency content a prohibitive number of instantaneous fields would have to be separated. As each separation of instantaneous fields involves the hand contouring of six maps, separation at many times is not practicable by our present methods. Separation in the time domain gives a very good picture of the time variations in the separated parts across the array. The external field components provide estimates of the scale length, λ , of the external field. Results also illuminate the morphology of the auroral magnetic event which from our viewpoint is the source function of the input signal to the array (Oldenburg 1969).

The above separation procedure is also valid in the frequency or period domain. The advantages of a frequency domain separation are:

- (1) Time discrepancies between stations are less critical than in the time domain.
- (2) Phase and amplitude representation of the external and internal fields are obtained at the chosen periods. This is important because magnetic induction and diffusion processes are frequency dependent.
- (3) The Fourier transform maps of type (b) show the conductive structures more strongly than the time domain maps (c), because in effect the energy of the whole event at each selected frequency is gathered in the Fourier transformation. For this reason the discussion of models of conductive structures makes use of separated fields in the period domain.

The use of the various types of anomaly maps, separation of fields and modelling of conductive structures have been discussed by Reitzel, Gough, Porath and Anderson (1970) and by Porath, Oldenburg and Gough (1970).

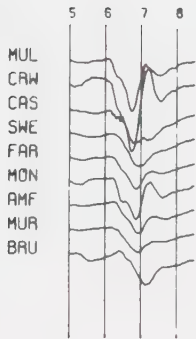
4.2 Variograms

Variograms of a substorm of September 1, 1967 and a storm on September 20-21, 1967 are shown in figures 4.1, 4.2a and 4.2b. The east-west lines of variometers are numbered 1 to 4 from north to south (figure 3.1). The variation anomaly associated with the eastern front of the Cordillera, formed in the area of the array by the

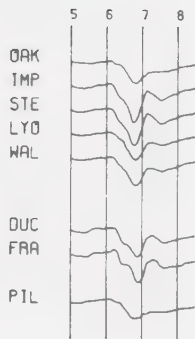
Figure 4.1 Variograms for substorm of September
1, 1967.

SEPTEMBER 1, 1967

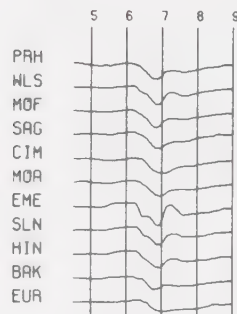
LINE 1



LINE 2



LINE 3



LINE 4

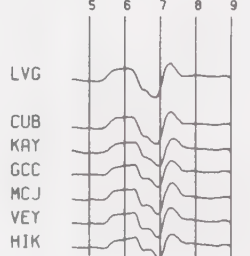
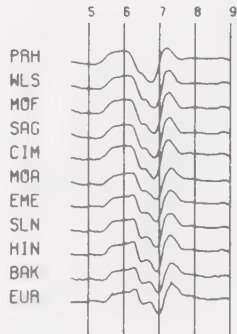
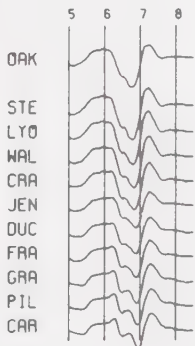
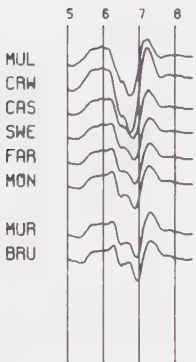
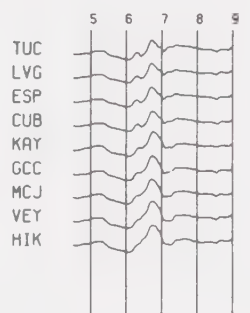
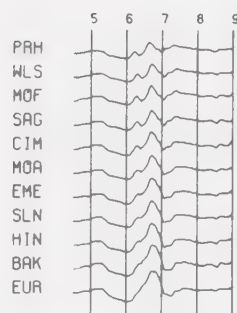
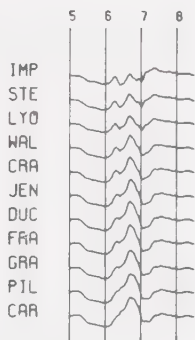
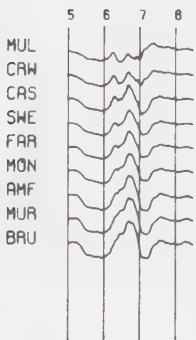
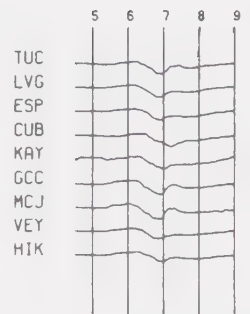
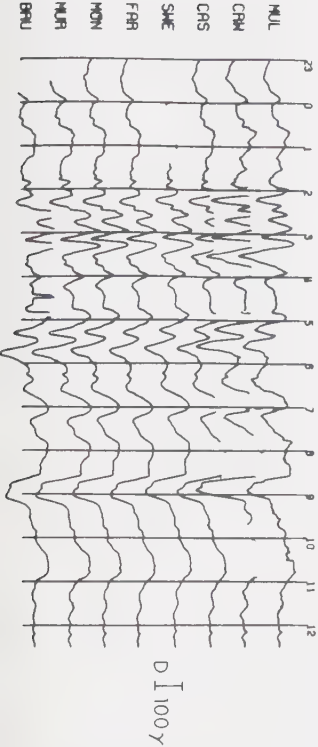
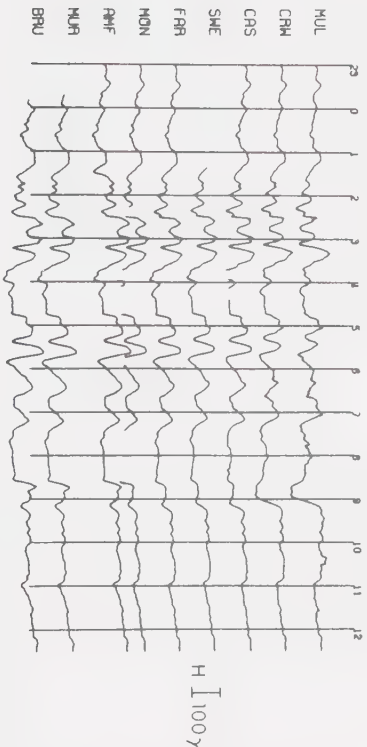
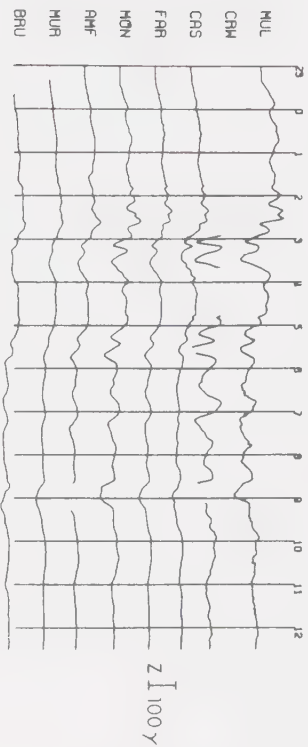


Figure 4.2a Variograms for storm of September
20-21, 1967. Two northern lines
of array.

SEPTEMBER 20, 1967

LINE 1



LINE 2

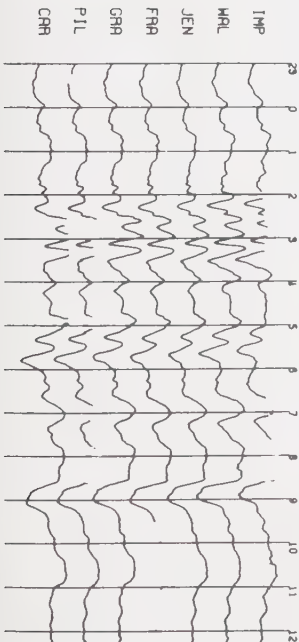
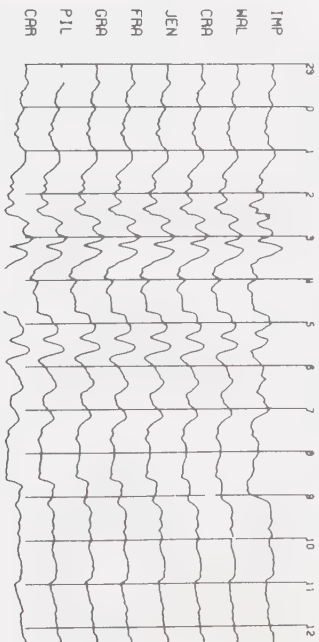
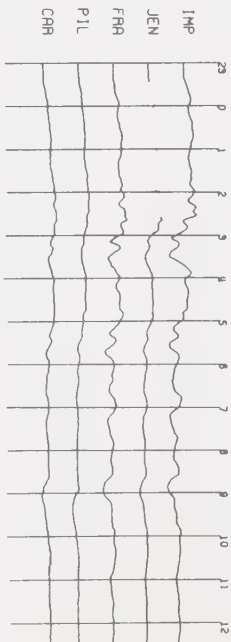
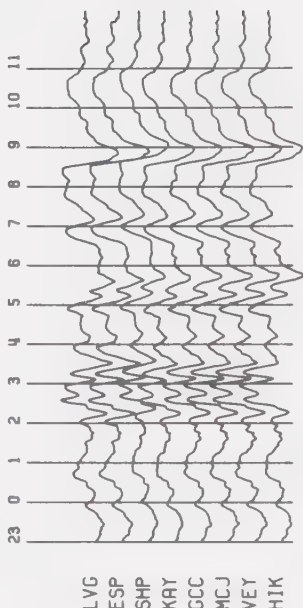
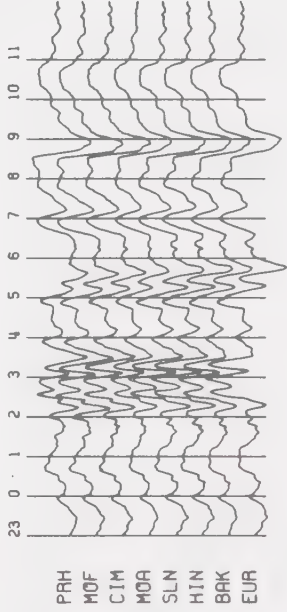
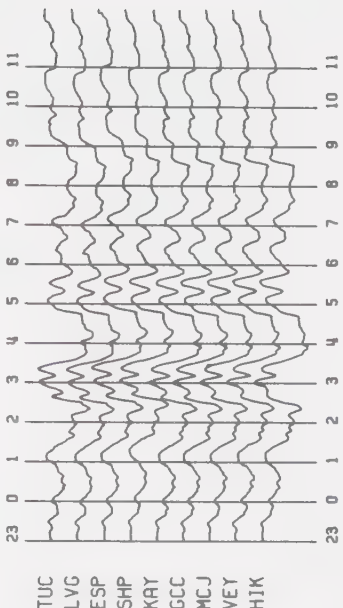
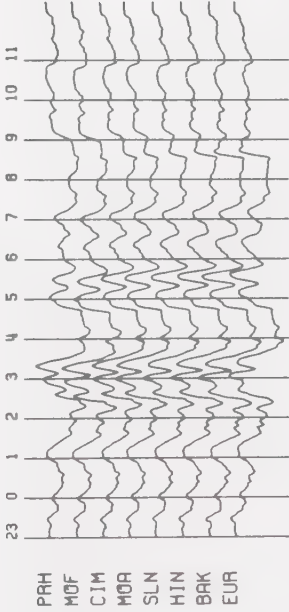
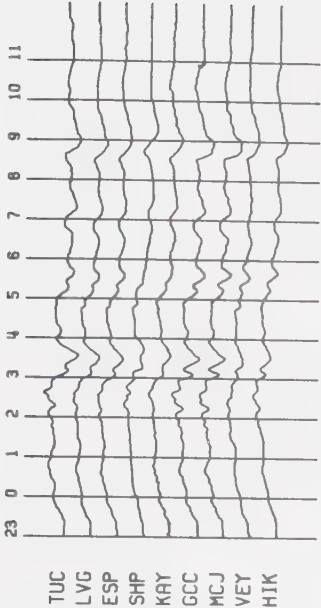
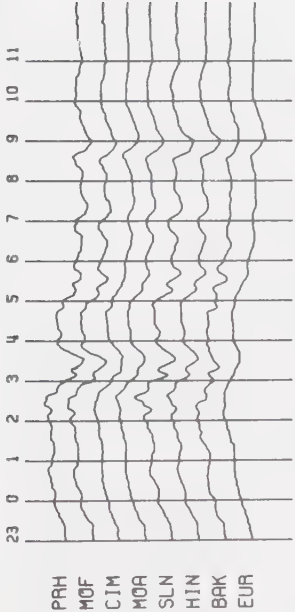


Figure 4.2b Variograms for storm of September
20-21, 1967. Two southern lines
of array.

SEPTEMBER 20, 1967

LINE 3

LINE 4



Southern Rockies, can be seen in the vertical component of the substorm in the increase of Z between CAS and CRW (line 1), between LYO and STE (line 2) and between SAG and WLS (line 3). Only a small increase is observed for the substorm at the eastern most station, TUC, in line 4. The presence of the East Front anomaly is more obvious for the storm. This difference in the response of the vertical field for the storm is most likely due to the different azimuth of the external fields; the dominant azimuths are NW-SE for the substorm and NE-SW for the storm. A further bay event on September 28, 1967 also shows the presence of the East Front anomaly in northern New Mexico by a substantial increase in Z between LVG and TUC (Porath, private communication).

The variograms strongly indicate the existence of another variation anomaly with roughly a north-south trend over the Wasatch fault zone in Utah. This will be called the Wasatch Front anomaly. The increase in the Z component can be seen between the stations MUR and MON (line 1), PIL and FRA (line 2), SLN and EME (line 3) and VEY and MCJ (line 4) for the substorm. The Z component of the storm was not recorded at EME, but increases in Z can be seen between the other pairs of stations. The similarity in the traces of $Z(t)$ and $D(t)$, especially in Figure 4.1, indicates the presence of anomalous internal Z at these

stations. Upward (negative) Z variations are seen to be approximately in phase with westerly (negative D) horizontal variations. This and the fact that stations west of the Wasatch Front (PIL, EUR, HIK) have very low Z amplitudes suggest that the Basin and Range province is a region of high mantle conductivity. The Calcomp plot of the storm shows reversals just west of the Wasatch front. The phase reversals in the Z component for periods of about 30 minutes at BAK and PIL, suggest that a ridge in the conductivity structure lies along the edge of the Basin and Range province at the Wasatch Front.

BRU at the west end of line 1 shows $Z(t)$ resembling a horizontal component with contributions from both $H(t)$ and $D(t)$. The variograms suggest upward Z following southward H . This may indicate the presence of a highly conducting body south of this station, which could be interpreted as the northern edge of the Basin and Range province.

4.3 Maps of unseparated spectral components

Figures 4.3 to 4.6 represent maps of the spectral components of the substorm. Figures 4.7 and 4.8 represent similar maps of the storm.

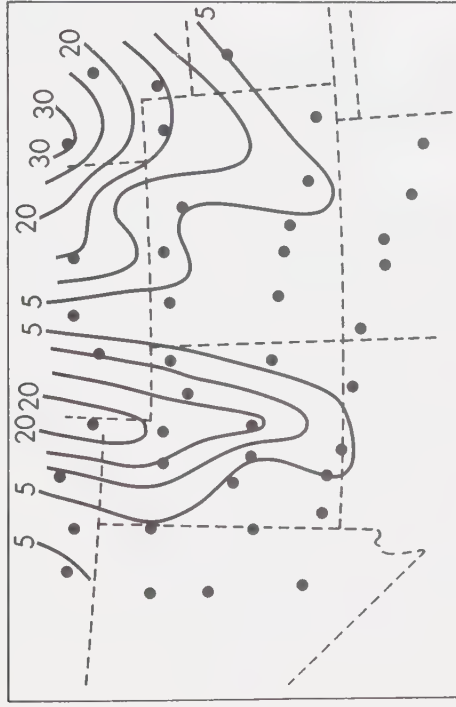
The vertical field amplitude maps of figure 4.3 show two prominent north-south striking maxima, one along

Figure 4.3 Fourier spectral amplitudes of the
vertical component substorm field.

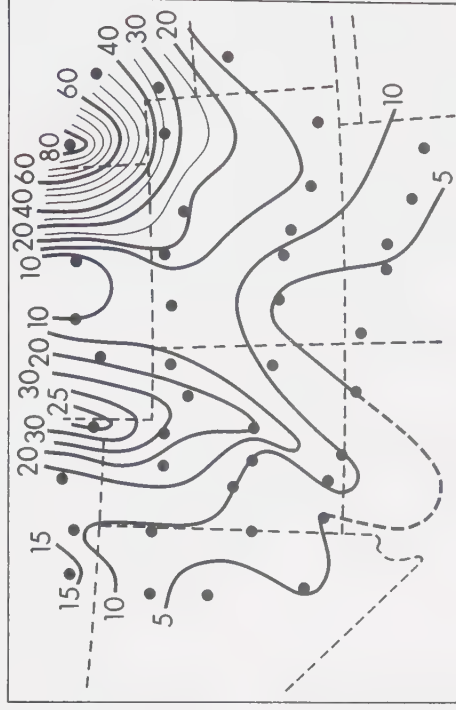
SUBSTORM SEPT. 1, 1967.

VERTICAL COMPONENT FOURIER SPECTRAL AMPLITUDES

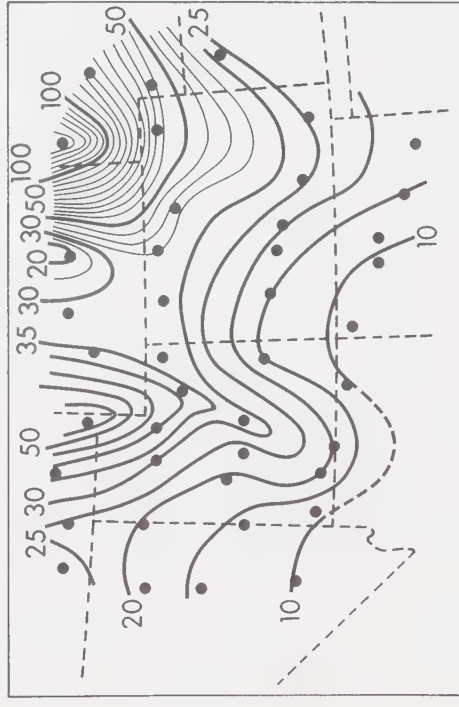
CONTOUR INTERVAL: 0.5 GAMMA



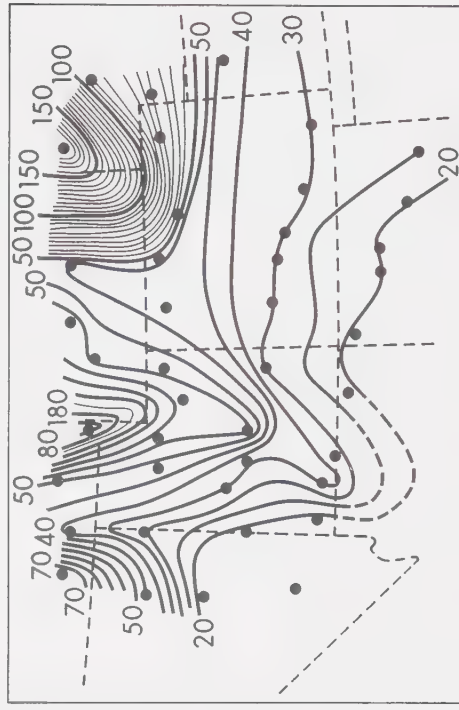
T = 30 MINUTES



T = 45



T = 60



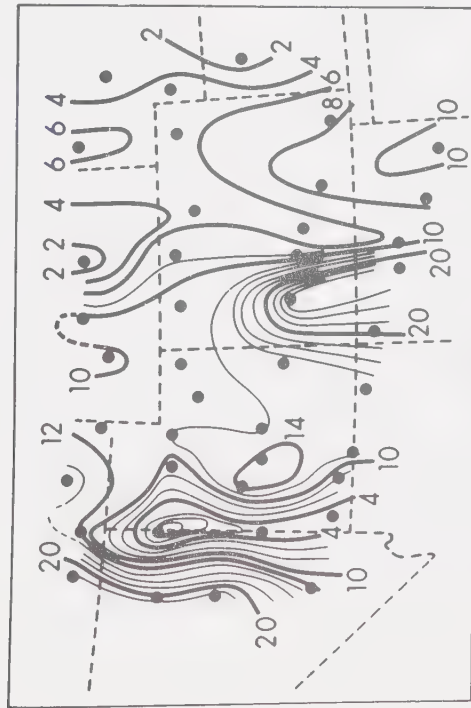
T = 89

Figure 4.4 Fourier spectral phases of the
vertical component substorm
field.

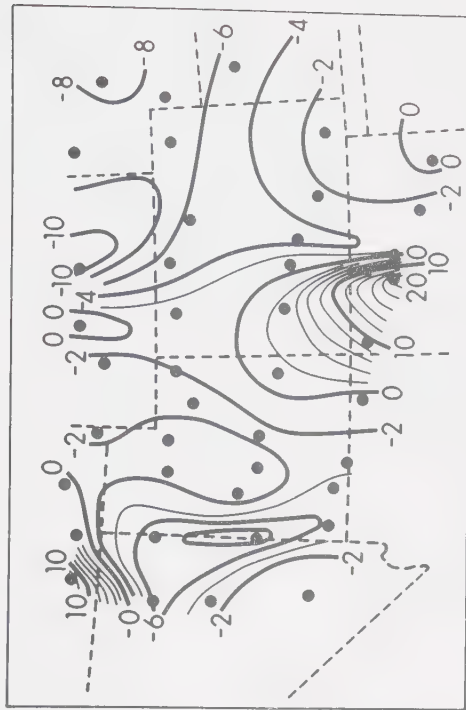
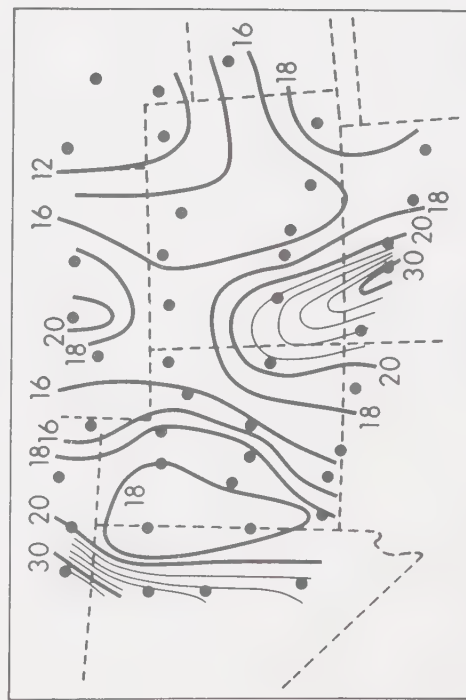
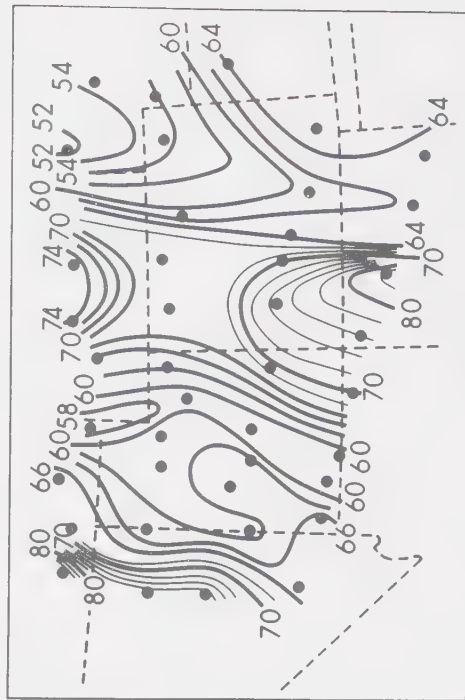
SUBSTORM SEPT. 1, 1967.

VERTICAL COMPONENT:FOURIER SPECTRAL PHASES.

CONTOUR INTERVAL : 2 MINUTES



T = 30 MINUTES

 $T = 45$ 
$$T = 60$$


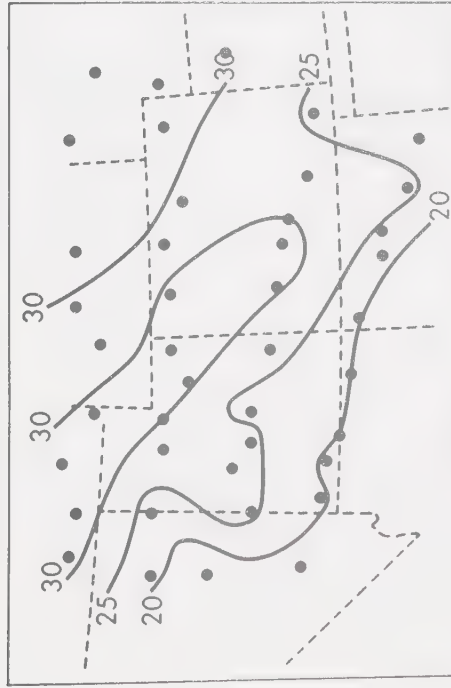
$T = 89$

Figure 4.5 Fourier spectral amplitudes of
horizontal components of the
substorm field.

SUBSTORM SEPT. 1, 1967.

HORIZONTAL COMPONENTS : FOURIER SPECTRAL AMPLITUDES

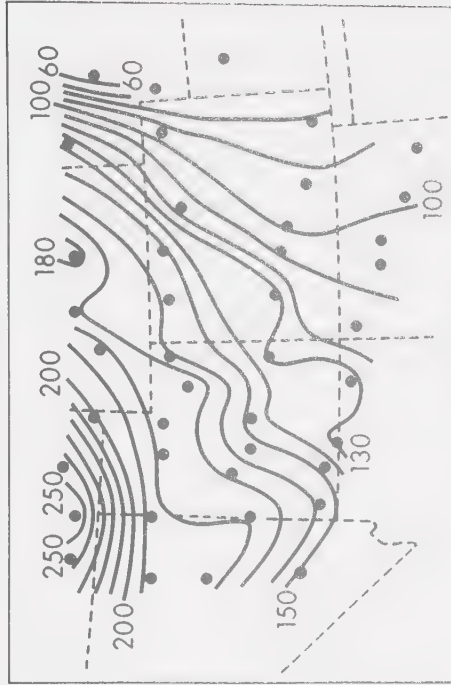
CONTOUR INTERVAL : 0.5 GAMMA



X (T = 30 MIN.)

Y (T = 30)

CONTOUR INTERVAL : 1.0 GAMMA



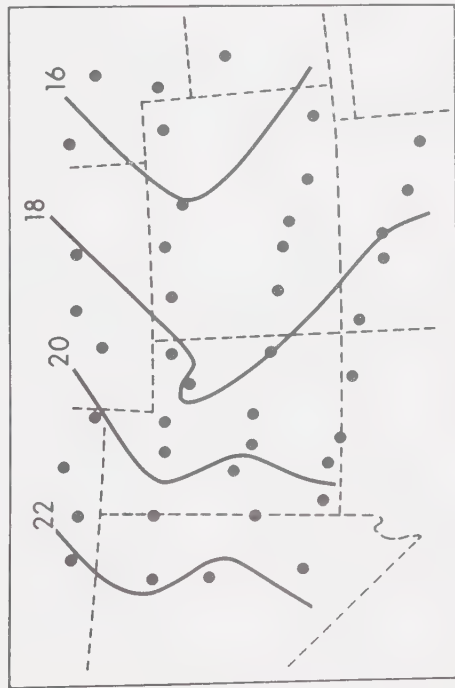
X (T = 89)

Y (T = 89)

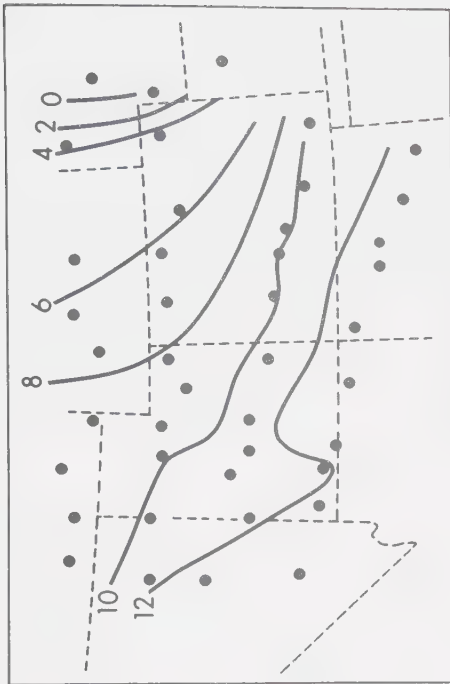
Figure 4.6 Fourier spectral phases of horizontal
components of the substorm fields.

SUBSTORM SEPT. 1, 1967.

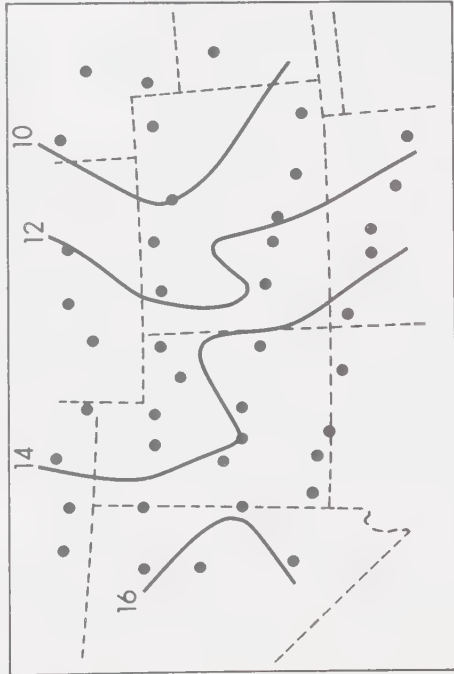
HORIZONTAL COMPONENTS : FOURIER SPECTRAL PHASES
CONTOUR INTERVAL: 2 MINUTES



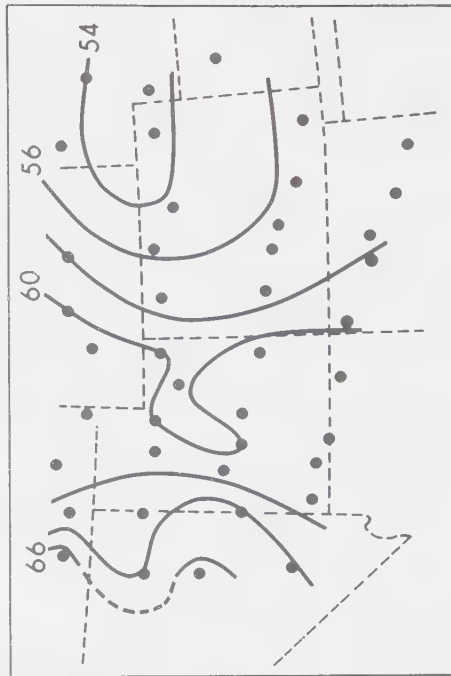
X (T = 30 MIN.)



Y (T = 89)



X (T = 30)

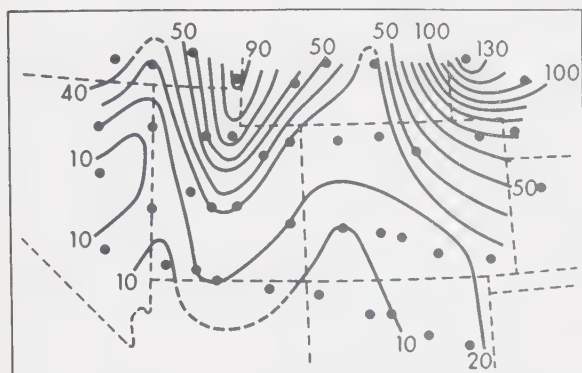


Y (T = 89)

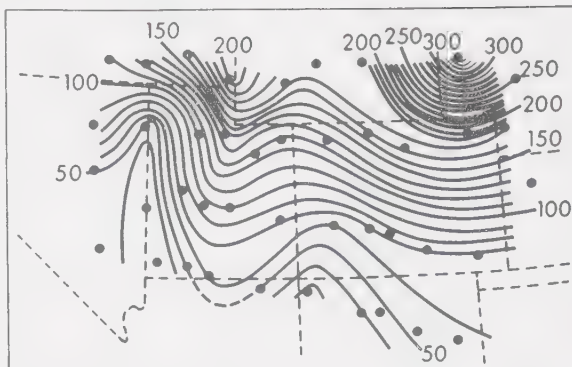
Figure 4.7 Fourier spectral amplitudes for three
 components of the storm field.

STORM SEPT. 20-21, 1967.

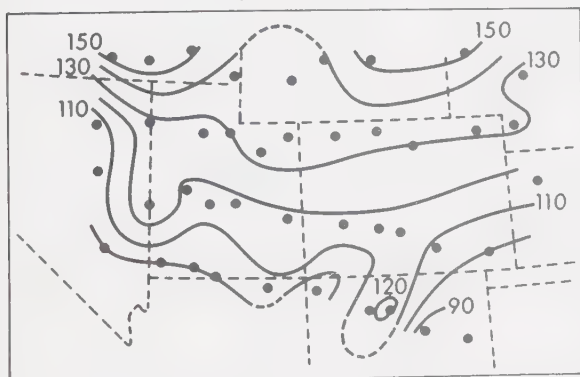
FOURIER SPECTRAL AMPLITUDES
CONTOUR INTERVAL 1.0 GAMMA



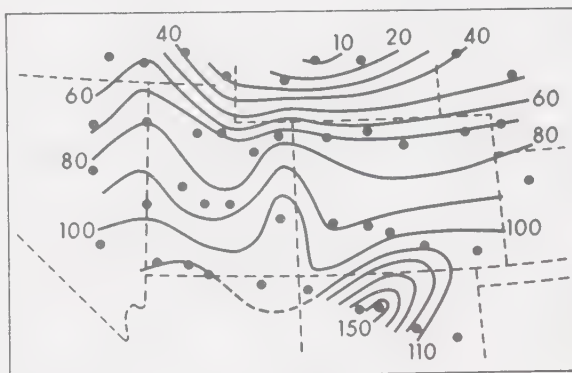
Z (T = 45 MINUTES)



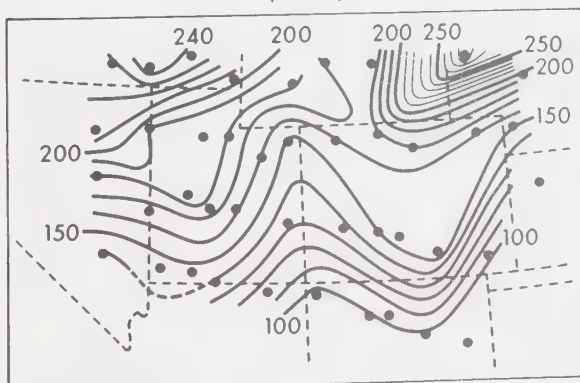
Z (T = 150)



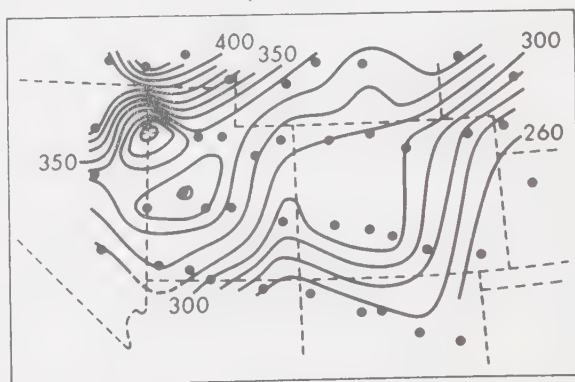
X (T = 45)



X (T = 150)



Y (T = 45)



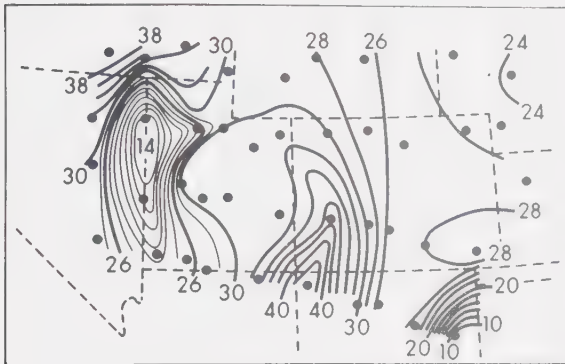
Y (T = 150)

Figure 4.8 Fourier spectral phases for three
 components of the storm field.

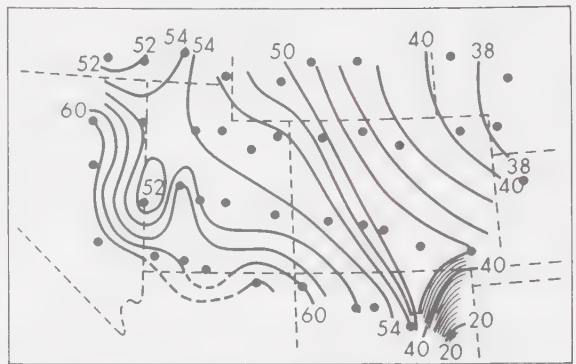
STORM SEPT 20, 1967

FOURIER SPECTRAL PHASES

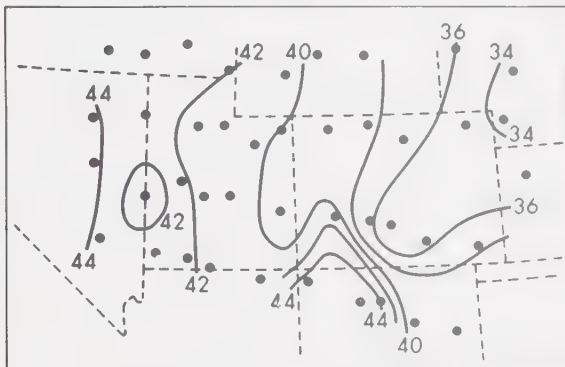
CONTOUR INTERVALS AS INDICATED (C/I)



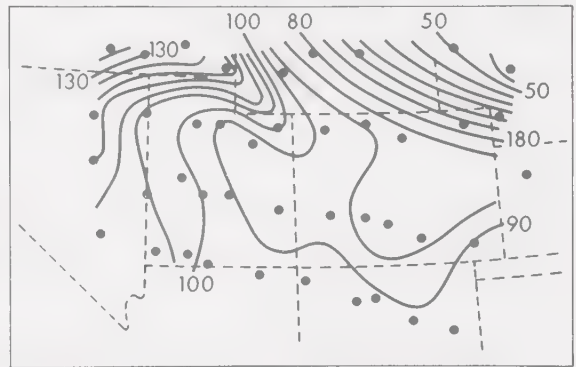
Z (T = 45) C/I 2 MINUTES



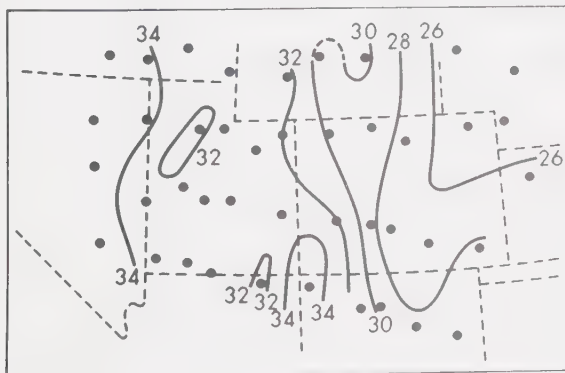
Z (T = 150) C/I 2 MINUTES



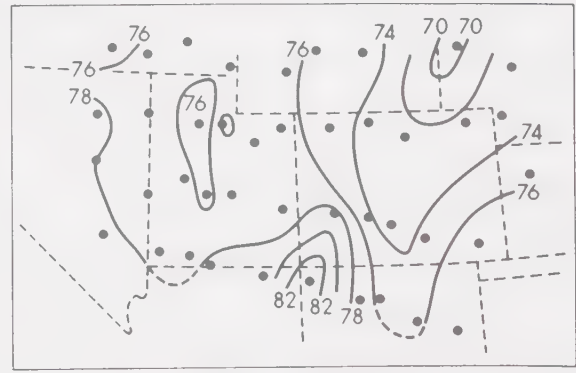
X (T = 45) C/I 2 MINUTES



X (T = 150) C/I 5 MINUTES



Y (T = 45) C/I 2 MINUTES



Y (T = 150) C/I 2 MINUTES

the east side of the Southern Rockies and the other east of the Wasatch Front in Utah (see figure 4.9). These anomalies show more strongly at the longer periods partly because of the greater penetration of the long-period fields, but partly also because the magnetic events have more energy at the longer periods. That the second effect is more important in the present case is suggested by the virtual disappearance of the anomalies from a map of Z amplitude at period 120 minutes for the substorm (figure 4.10). The storm has high energy in the Z spectrum near period 150 minutes (figure 3.4), and the anomalies show well in the Z amplitude map at this period (figure 4.7). It is important to select periods at which the energy is high, for the separation of fields and model calculations.

Care must be taken in the use of the storm maps to remember an inequality in the amount of information available for contouring the eastern and western halves of the array. About ninety percent efficiency in recording was attained for the west and only sixty percent in the east. Also at several of the stations in the N-E sector of the array the Z and D traces were driven off scale by the large storm fields. The gaps in the discontinuous traces of figure 4.2a were filled with fictitious interpolated data to give some attempt at spectral estimates. The north-eastern parts of the maps of Z and Y in figures

Figure 4.9 Simplified map of two local internal currents and relationships between external and internal field components.

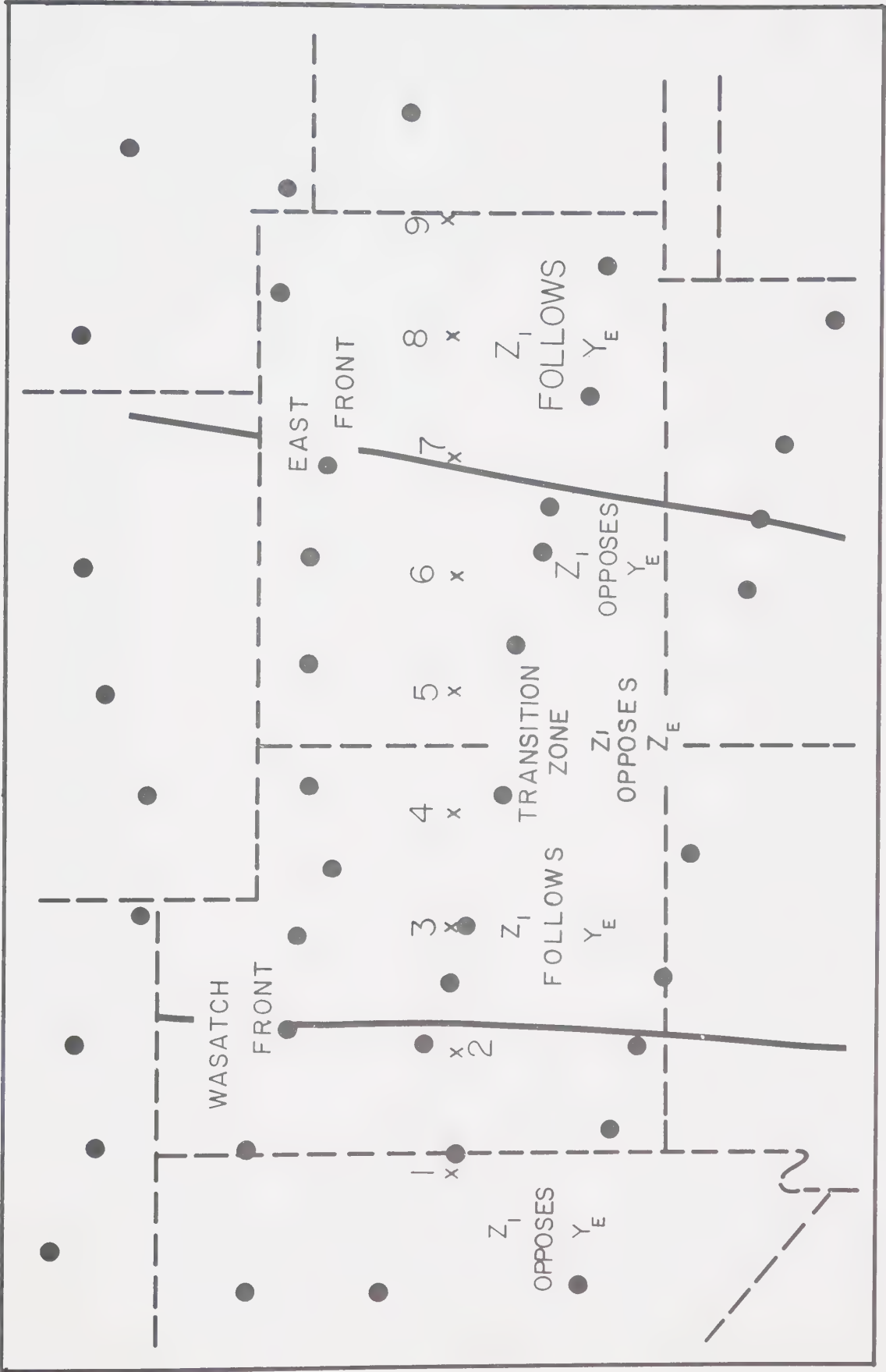
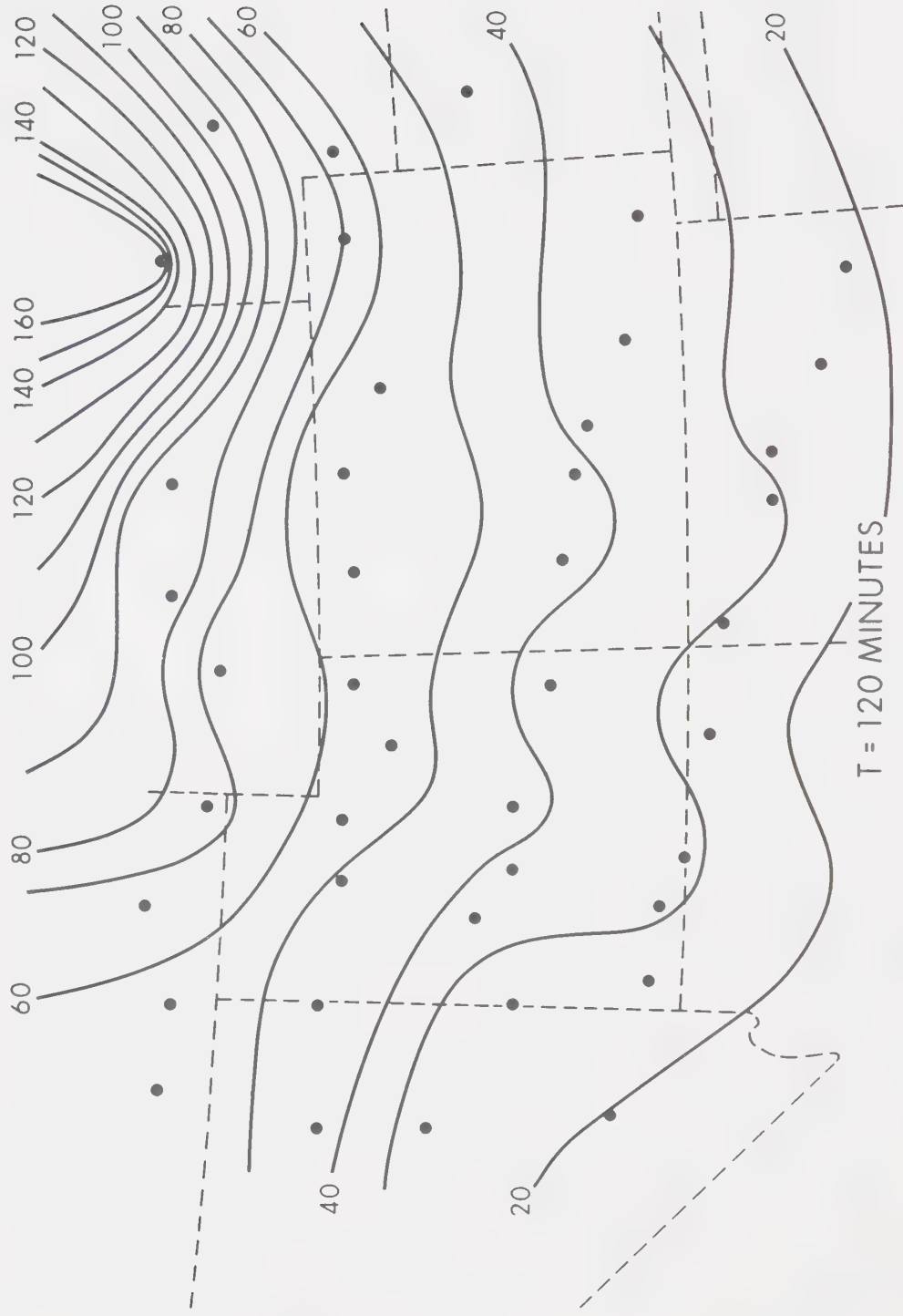


Figure 4.10 Fourier spectral amplitude for vertical
component of substorm at $T=120$ minutes.

SUB-STORM SEPT. 1st 1967

VERTICAL COMPONENT : FOURIER SPECTRAL AMPLITUDE
CONTOUR INTERVAL : 1.0 GAMMA



4.7 and 4.8 are therefore to be treated with caution. Greater importance is to be attributed to the results obtained from the western half. Since this is an area 700 km by 650 km the results remain important with respect to determining underlying conductivity structure. The maps of figures 4.3 and 4.7 for Z at T=45 minutes for the substorm and storm are strongly alike, suggesting that the contouring was reasonably accurate.

The eastward horizontal component Y shows strong evidence of both the East Front and the Wasatch Front current systems in the amplitude maps for the substorm (figure 4.5). The maximum of Y is west of that of Z in both cases. In each case Y falls again to the west of its maximum, indicating a linear current. At the Wasatch Front this is believed to represent a local upwelling in the conductive mantle in a ridge superimposed on a step which leaves the conductive medium higher under the Basin and Range province than under the Colorado Plateau. Schmucker (1969) reached similar conclusions with respect to the conductivity at the edge of the Basin and Range province in southern New Mexico (figure 2.4). Later sections will show that similar depths to the upwelling were also found, suggesting that the Wasatch Front structure is a northward extension of the Rio Grande structure. The Y amplitude maps at the East Front suggest a strip of current under

the Southern Rockies between the East Front and the Colorado Plateau. A comparison of the Wasatch Front and East Front Y anomalies at $T=30$ and 89 minutes shows that the width of the strip would have to be wider under the East Front than under the Wasatch Front (figure 4.5).

The amplitude maps of the X component of the substorm (figure 4.5) are relatively featureless, as would be expected where the major conductive structures strike north-south. A small anomaly in X, associated either with the Uinta uplift or with the deep sedimentary Uinta Basin (20,000 ft.) in northern Utah, is seen in a sine transform map at period 50 minutes (Reitzel et al. 1970). As Schmucker (1964) points out, deep basins of conducting sediments can cause anomalous variations at periods up to one hour or more. Superficial anomalies usually show a conspicuous phase lead of the induced to inducing field (Schmucker, 1964) and early arrival times of X for the substorm in this region may be an expression of the Uinta Basin anomaly.

The X component maps for the storm show a reversal in north-south gradient of the amplitude between $T=45$ and 150 minutes. Whereas X diminishes southward at period 45 minutes it increases southward over the entire array at $T=150$ minutes (figure 4.7). Other maps, not shown, indicate that the reversal occurs close to $T=90$ minutes.

By way of analogy with the substorm it would appear that the external field should decrease southward. It must be pointed out clearly though that the analogy may not be valid in the absence of a model of the storm current system. Discussion on this feature of the storm transform maps will be continued in the next section, that dealing with the separated storm fields.

The phase maps not only contain information with regard to anomalous conductivity structure, but also enable the significance of the amplitude maps to be assessed. The phases of X and Y vary smoothly across each map. A strong Z phase anomaly just west of the Wasatch Front is most pronounced at periods 30 and 45 minutes in the substorm maps (figure 4.4) and at 45 minutes for the storm (figure 4.8). At the shortest periods the phase relationship would be impossible for induction by external Z fields, but when it is remembered that anomalous internal Z is induced by Y the phase anomalies are seen to be consistent with local linear currents along the Wasatch Front. These linear currents have already been proposed to account for the amplitude anomalies in the Z and Y components across the Wasatch Front. Similar Z phase anomalies can be seen near CUB in figures 4.4 and 4.8 for the substorm and storm fields respectively; this

anomaly is located just west of the Southern Rockies. These Z phase anomalies can be explained in the manner of the Z phase anomalies across the Wasatch Front as representing the effect of anomalous internal Z fields associated with linear currents flowing along a ridge under the Southern Rockies, and induced by the normal Y field. Further discussion of phase maps will be deferred to the section covering separated phase maps.

4.4 Separated fields in the period domain

As was stated before, two variation events were recorded by our 1967 array in the western United States. The fields of the substorm of September 1 have been separated at four times in the time domain and at T=30 and 60 minutes in the period domain by Oldenburg (1969), and at T=50 and 89 minutes by Porath (Porath, Oldenburg and Gough 1970).

The author has separated the storm fields of September 20-21, 1967 at the three periods 89, 150 and 256 minutes. As has been explained, the storm was poorly recorded in the north-east corner of the array and it is in the western half of the array that the results of the separation are most meaningful. The eastern stations give adequate control of the fringe field of the Wasatch Front. Unfortunately the East Front

is close enough to the Wasatch Front that the currents under the Southern Rockies contribute considerably to the internal field at the Wasatch Front (Porath et.al. 1970) so that the modelling of the Wasatch Front from storm separation results is necessarily of a qualitative nature. However, quantitative depth estimates for a line current model of the Wasatch Front agree with those of Oldenburg (1969) and Porath et al. (1970). The agreement of the results from the storm with those from the substorm means that the models put forward for conductive structures in the upper mantle are not derived from a single event. The work of Reitzel et al. (1970), Porath et al. (1970), Oldenburg (1969) and the present author has established the presence of two-dimensional conductive structures striking approximately north-south under the Southern Rockies and Wasatch Front, and has placed limits on the depths, dimensions and conductivities of these structures.

4.5 Separated storm fields

Normal fields

It is known (section 1.9) that fields with scale lengths greater than the dimensions of the array cannot be separated. To remove the inseparable field a "normal" horizontal field H_n is assumed. H_n is defined as the vector sum of the normal external field H_{en} and a normal

internal field H_{in} due to currents flowing at depth in the highly conducting mantle. The removal of H_n leaves an anomalous internal field, H_{ia} , to be separated from an inhomogeneous residual external field H_{ea} . Porath et al. (1970) attempted a removal of the normal field by fitting a polynomial in x and y by least squares to the horizontal components X and Y with the boundary condition

$$\frac{\partial X}{\partial y} = \frac{\partial Y}{\partial x} .$$

This attempt was unsuccessful since the matrix for calculating the coefficients became ill-conditioned for surfaces of higher order than a plane. When possible H_n would be removed before separation. However since only a plane approximation can be made to the external field, the fields must be separated first to see if the plane approximation is appropriate. The complicated external parts of the separated storm field for periods 89, 150 and 256 minutes could not be represented by a constant or even by a plane. Therefore the normal field could not be removed, nor could the anomalous field be subsequently isolated and normalized with respect to the normal field in the manner of Porath et al. (1970). It is a priori reasonable to find the normal field of a storm much more complicated than that of a substorm.

Source field

The location of the current system (see section 1.6) which produces a polar magnetic substorm is dependent on the location of the auroral oval. During intense storms the auroral oval is known to move equatorward (Akasofu 1966). Figure 4.11 represents the relationship of the southward movement of the auroral oval to the Dst for the storm. The storm of September 20-21, 1967 has a maximum Dst of 80 gammas which means that during the event the auroral oval probably moved southward to about 56°N latitude. The current system would then be located at some time during the event within 14° of the northernmost line of the 1967 array. Figure 4.12 (Walker 1964) shows that if the current is very wide then stations located at the latitudes of the 1967 array may be on the southward-increasing side of the H component curve.

The k-indices of the storm indicate that its field was comprised mainly of substorm activity at the times of recording. However, the source currents for the geomagnetic storm of September 20-21, 1967 seem to be very complex and a simple model for these currents simply does not exist as it did for the substorm of September 1, 1967 (Oldenburg 1969).

Figure 4.11 Southern limit of the auroral arc
in relation to amplitude of $D_{st}(H)$
for storms. After Akasofu (1966).

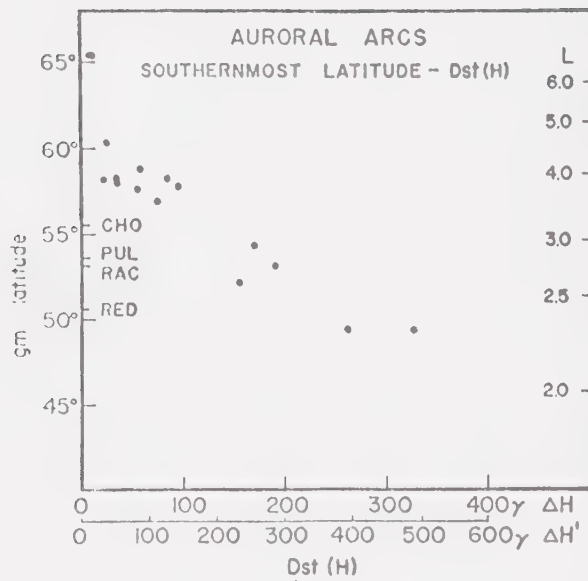
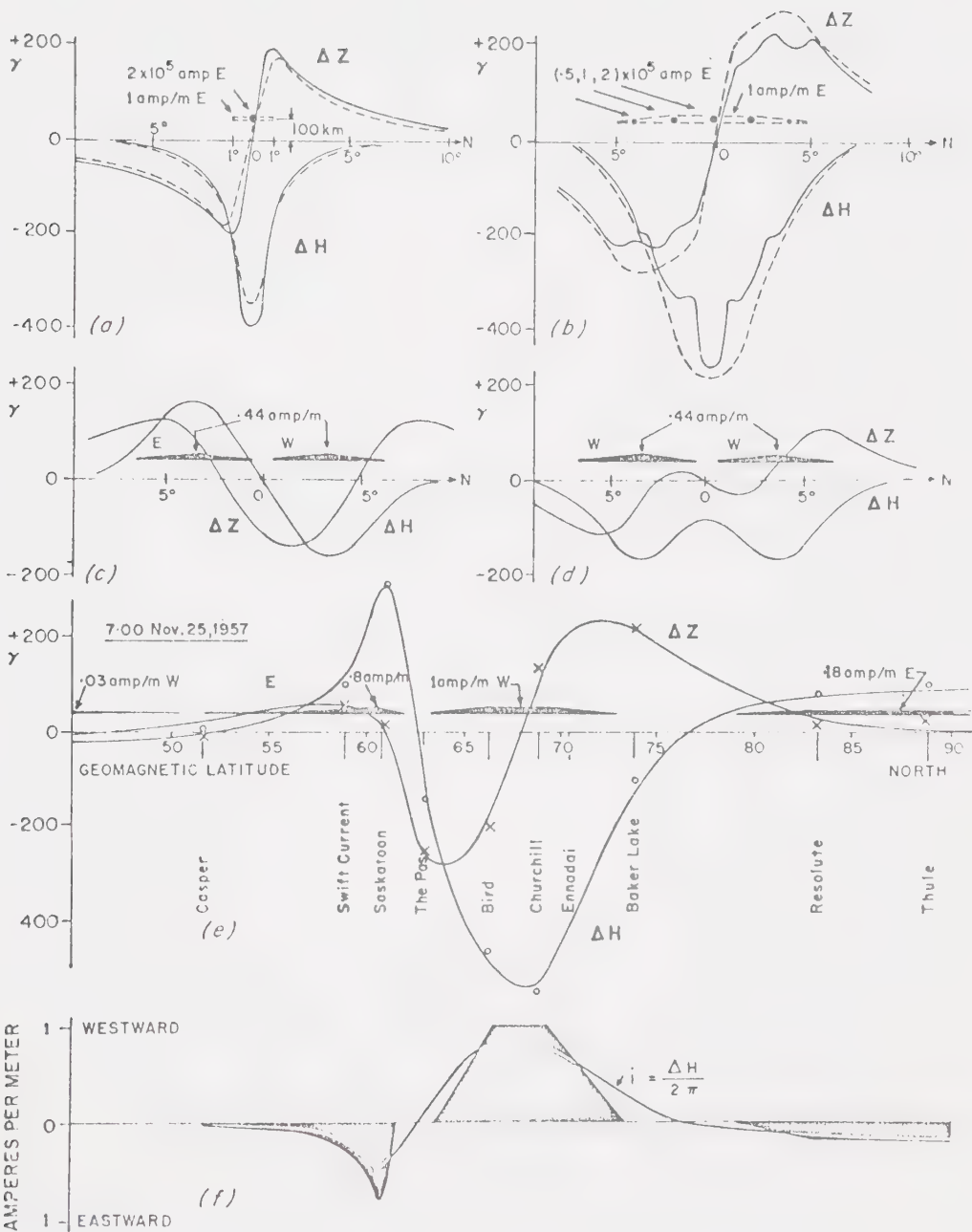


Figure 4.12 Variation of field components with
 latitude. After Walker (1964).



Scale length of the external field

As has been shown in Chapter 1, induction phenomena depend critically on the scale length ($\lambda = 2\pi/k$). The scale length will be estimated from the external fields, F_e , for the periods 89, 150 and 256 minutes.

F_e is defined as the total horizontal external field

$$F_e = \sqrt{X_e^2 + Y_e^2} \quad .$$

The parameter k is given (Schmucker 1964) by

$$k = \frac{1}{F_e} \left(\frac{\partial F_e}{\partial r} \right) \approx \frac{1}{F_e} \left(\frac{\Delta F_e}{\Delta r} \right) \quad (4.1)$$

where r is the distance in the direction of maximum gradients of F_e . The values estimated from figures 4.14 and 4.15 are:

Period (mins.)	89	150	256
$k \times 10^{-8} \text{ (cm}^{-1}\text{)}$	1.4	0.3	0.65

The values of k for the storm are

$$0.3 \times 10^{-8} \text{ cm}^{-1} \leq k \leq 1.4 \times 10^{-8} \text{ cm}^{-1}$$

$$4,500 \text{ km} \leq \lambda \leq 20,800 \text{ km}$$

with an average value of λ of 12,000 km.

Thus it can be seen that the scale length of the external field is much larger than the dimensions of the

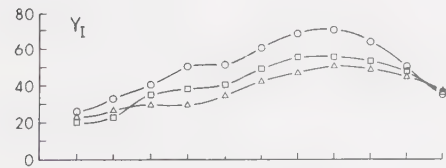
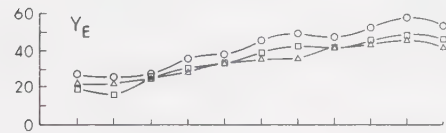
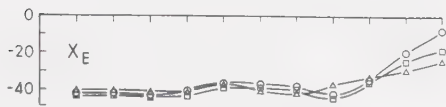
Figure 4.13 Separated field components for the
storm along three east-west profiles.
T = 89 minutes.

T = 89 minutes

SINE

COSINE

WEST EAST



PROFILES

- No 1
- No 2
- △ No 3

WEST

EAST

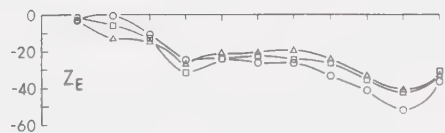
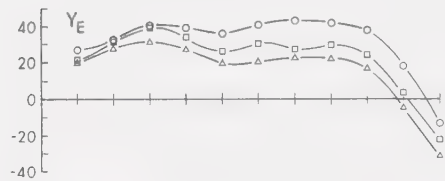
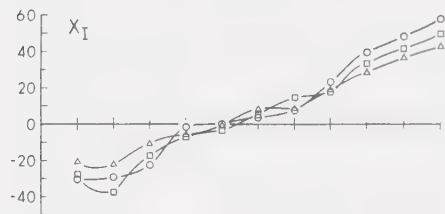
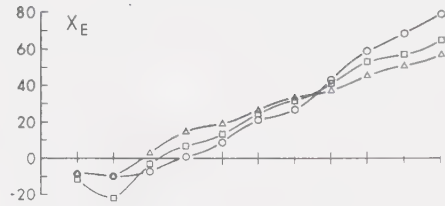


Figure 4.14 Separated field components for the
 storm along three east-west profiles.
 T = 150 minutes.

T = 150 minutes

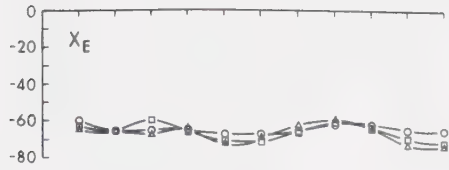
SINE

COSINE

WEST

EAST

EAST



PROFILES

- No 1
- No 2
- △ No 3

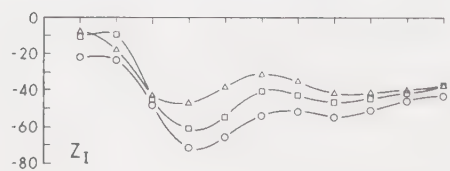
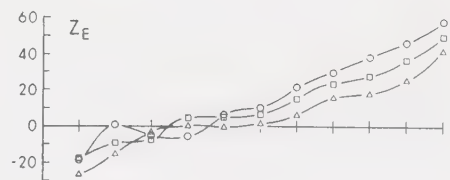
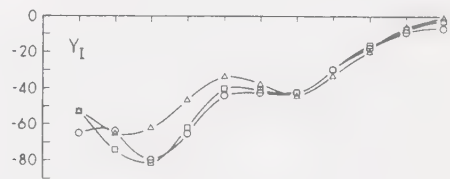
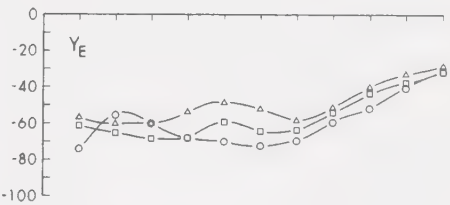
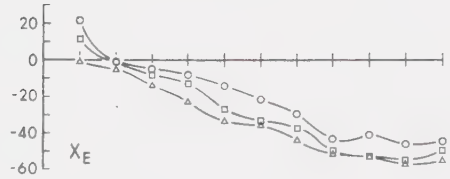
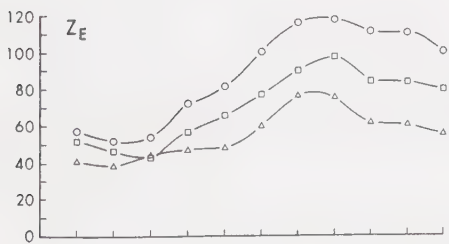
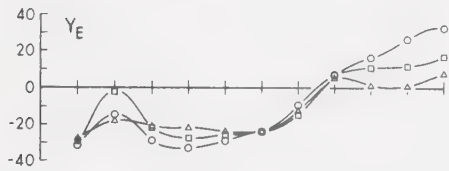


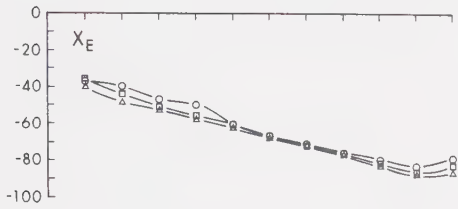
Figure 4.15 Separated field components for the
 storm along three east-west profiles.
 $T = 256$ minutes.

T = 256 minutes

SINE

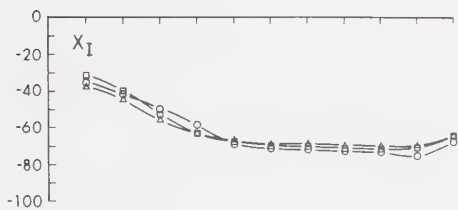
WEST

EAST



PROFILES

- No 1
- No 2
- △ No 3



WEST

EAST

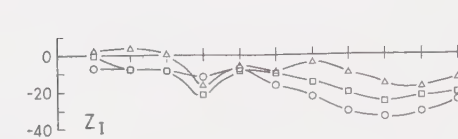
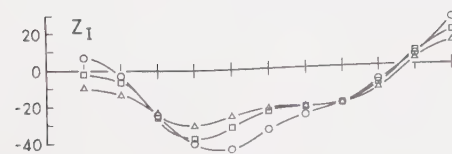
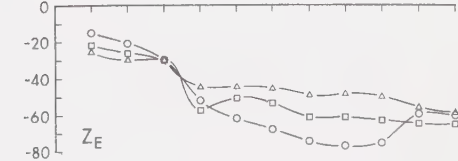
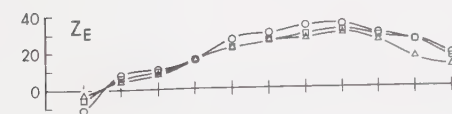
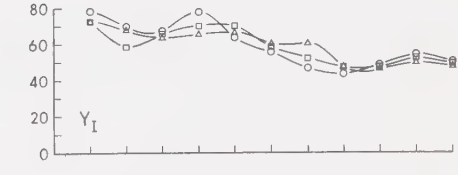
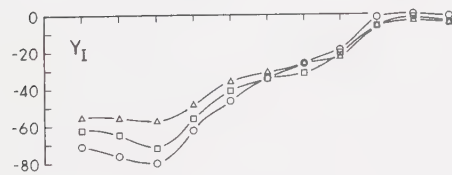
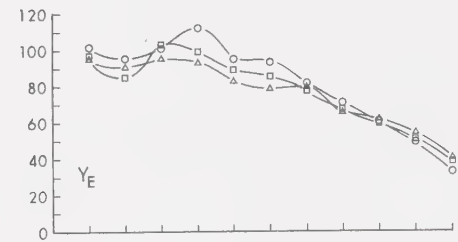
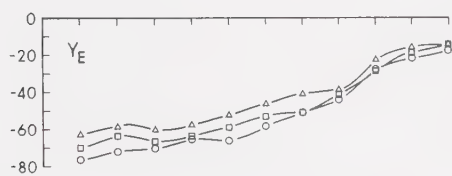
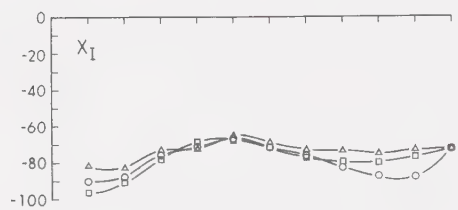
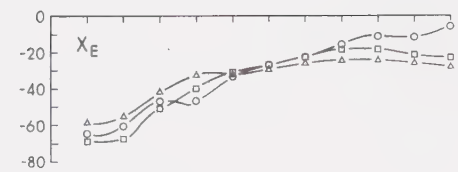
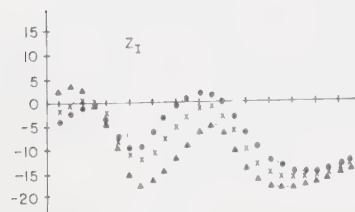
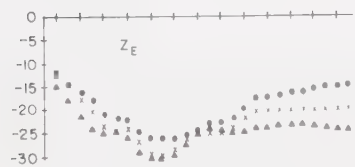
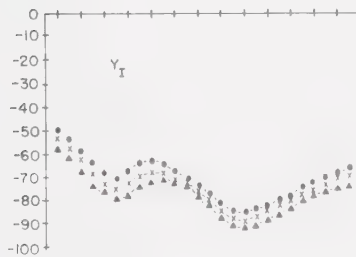
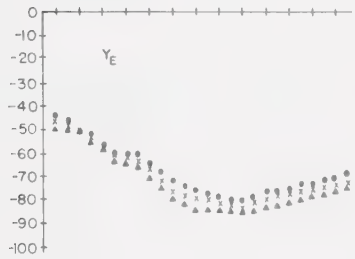
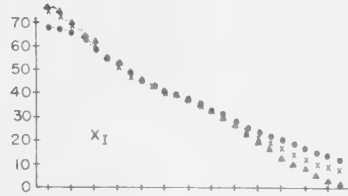
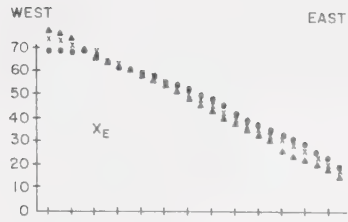


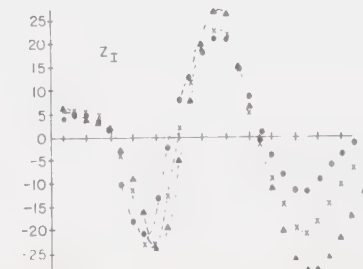
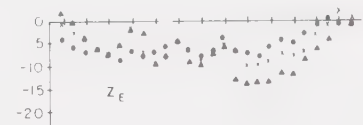
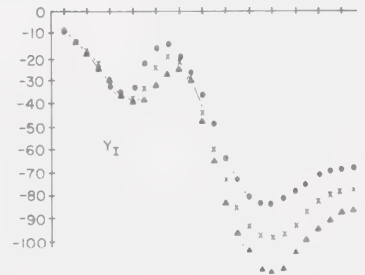
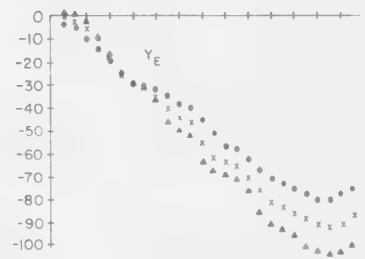
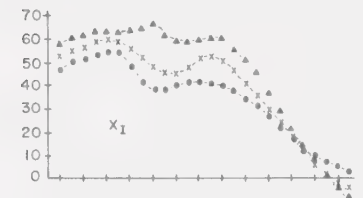
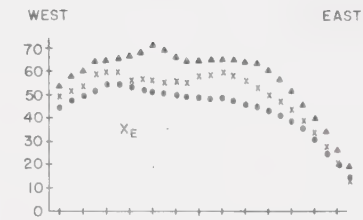
Figure 4.16 Separated field components for the
 substorm along three east-west
 profiles. $T = 89$ minutes (after
 Porath, Oldenburg and Gough 1970).

T = 89 MINUTES

SINE



COSINE



array. The values are an order of magnitude larger than the values of 600 to 800 km found by Caner et al. (1967) for his magnetic variations but compare well with the limits

$$5,000 \text{ km} \leq \lambda \leq 11,500 \text{ km}$$

found by Oldenburg (1969) for the external field of the substorm of September 1, 1967. Caner et al. (1967) were, of course, using unseparated fields and their scale lengths are doubtless related to the internal fields.

External storm fields

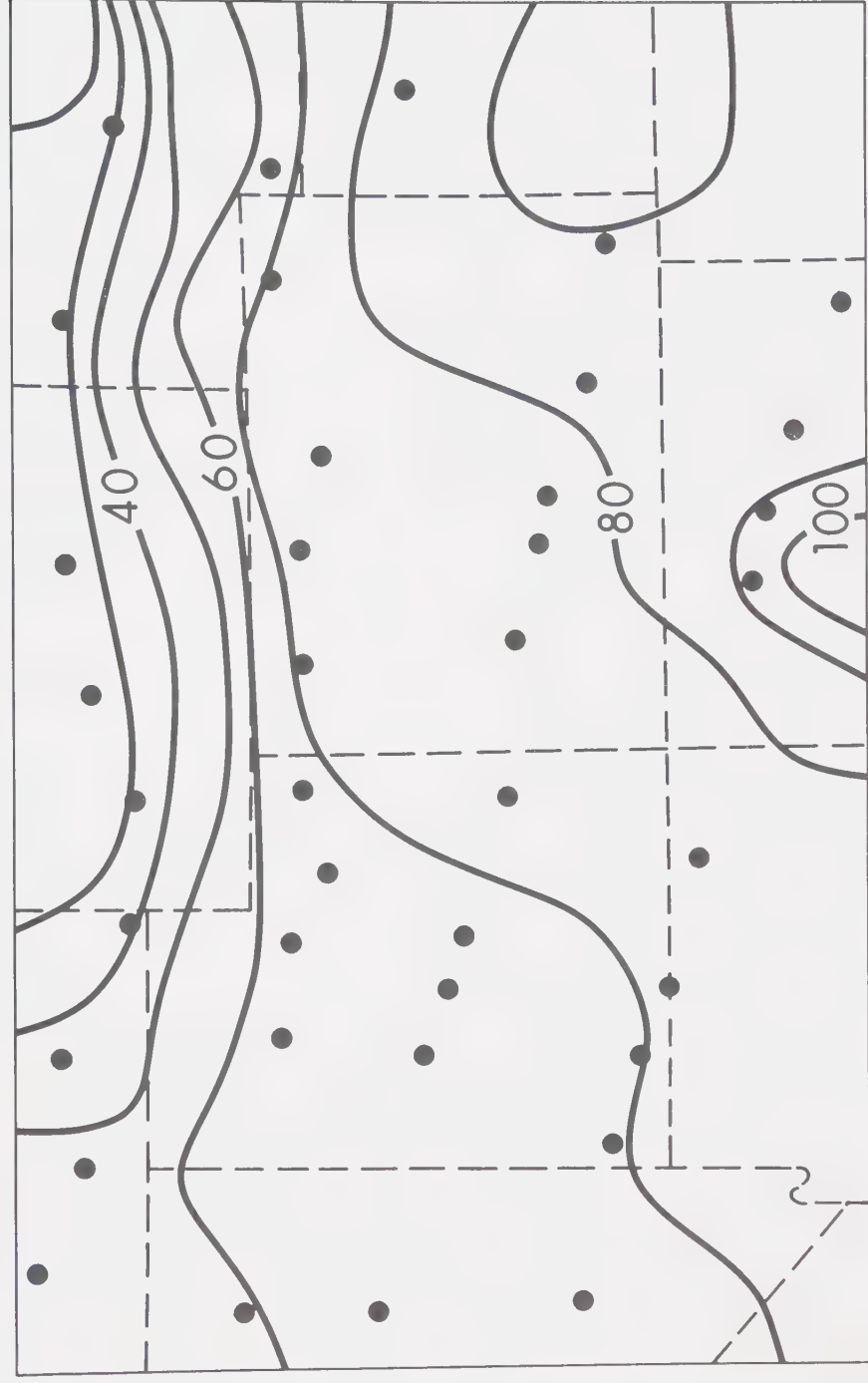
Figures 4.13 through 4.15 show how the external field of the storm varies on three lines across the array at periods 89, 150 and 256 minutes. It is obvious that the external fields must be due to complex current systems and cannot be approximated by a plane surface.

The external northward horizontal field X shows a decrease southward for periods 89 and 256 minutes. But surprisingly the X component increases southward for period 150 minutes (figure 4.17). In the paper by Reitzel et al. (1970) the X component, T=150 min., of the total field was seen to increase and this was tentatively taken to imply a rise in the upper mantle isotherms from north to south. The expected reversal of the Z component was never seen but this was attributed to lack of Z observations

Figure 4.17 Amplitude of separated external
northward horizontal field X_e of
the storm.

AMPLITUDE OF SEPARATED COMPONENTS HORIZONTAL FIELD

T=150 MINUTES CONTOUR INTERVAL 1.0 GAMMA



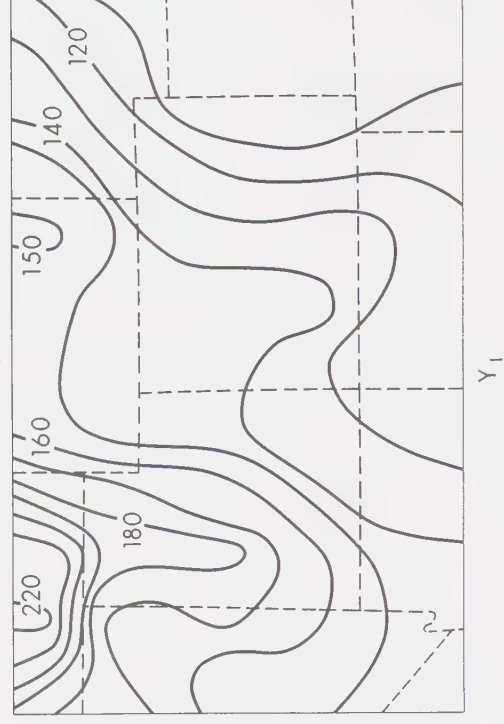
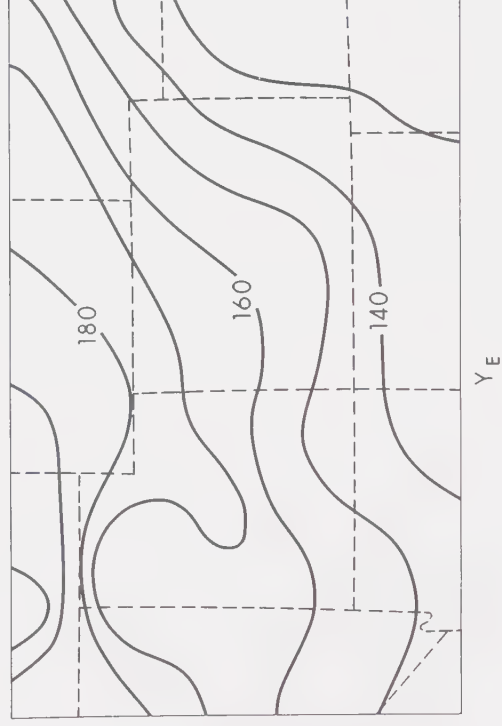
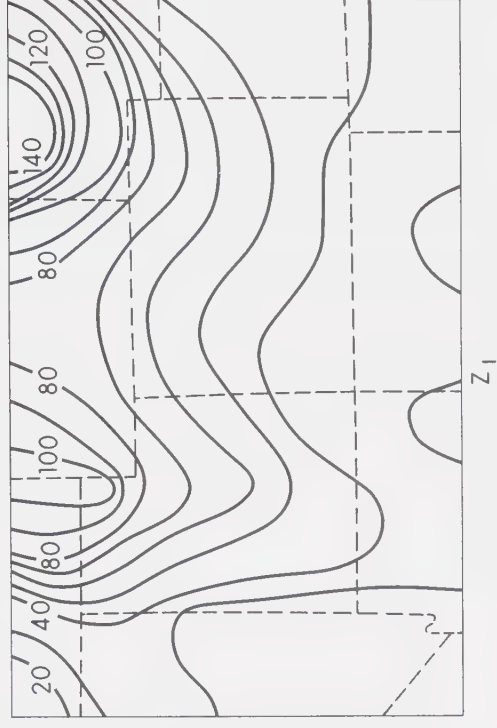
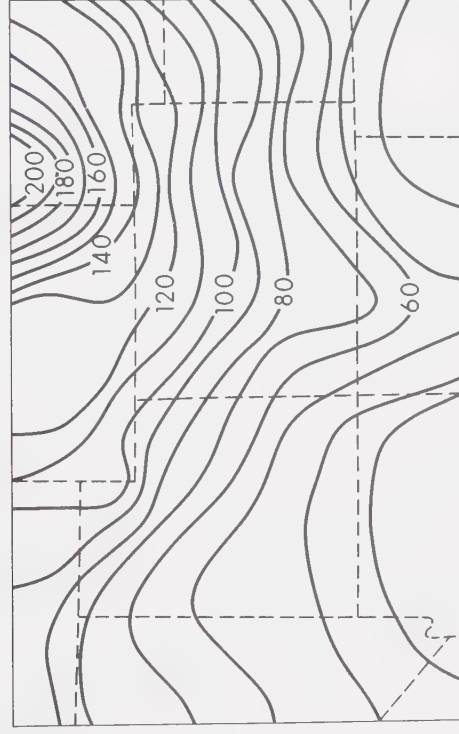
AMPLITUDE X_E

Figure 4.18 Separated vertical and horizontal
eastward storm fields at $T=150$
minutes.

AMPLITUDE OF SEPARATED COMPONENT
HORIZONTAL AND VERTICAL FIELD

T = 150 MINUTES

CONTOUR INTERVAL = 1.0 GAMMAS



in the expected area of reversal. The argument was based on the assumption that the storm external X component must decrease southward as did that of the substorm. This does not hold for $T=150$ mins., as it does for $T=89$ mins. and $T=256$ mins. It seems possible that the auroral oval came very far south and the three-dimensional current system expanded so that our array was under the southward increasing H component region of the curve of figure 4.12.

The separation was probably not complete since structure can be seen in Z_e and Y_e over the East Front anomaly in figure 4.18. This may be due to lack of information about the fields in this area. In general the external components at all three periods are smoothly varying over the Wasatch Front, where the operation of the array was more efficient.

The external phases essentially vary smoothly across the array, even though at the eastern edge there again appear spurious gradients which can be attributed to extrapolation of the maps outside the array.

Internal fields

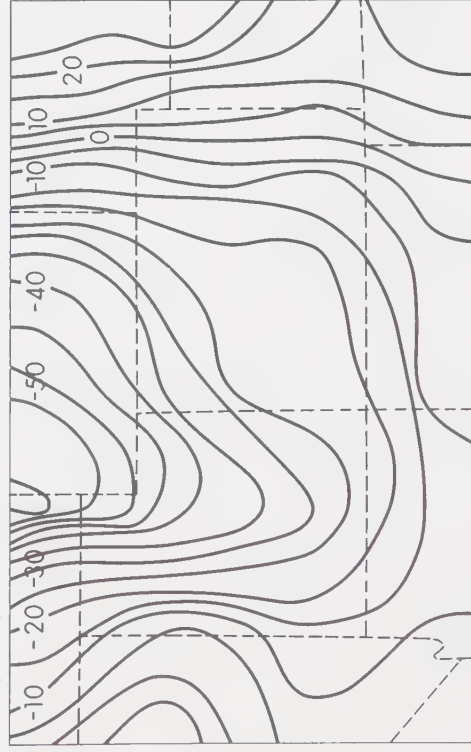
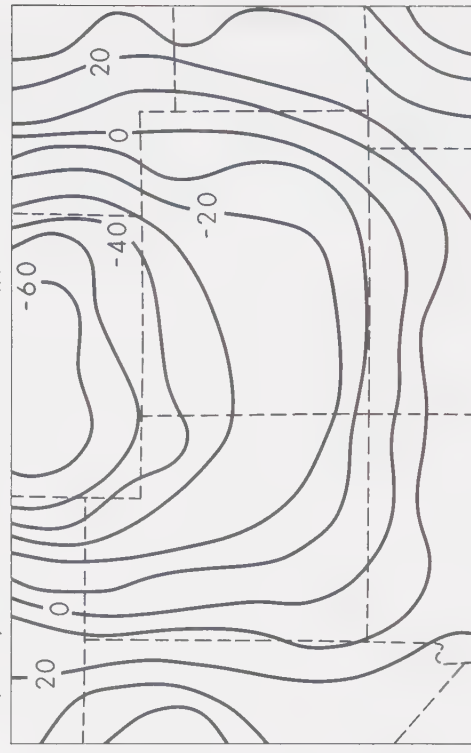
Comparison of the internal cosine and sine transform profiles of the storm and substorm can be made from figures 4.13 and 4.16. The figures represent the spatial variation of the appropriate component from west to east across central lines in the array.

In comparing the two events it must be remembered that the signs and magnitudes of the sine and cosine coefficients depend upon the starting time of the time series and features of the time series transform may be seen in either the sine or cosine transform map or in both. Inspection of figures 4.13, 4.14, 4.15 and 4.16 shows that the sine transform profile of the substorm is very similar to the cosine transform profile of the storm at T=89 minutes, while the cosine profile of the substorm bears little resemblance to the sine profile of the storm. The sine profile of the storm is essentially featureless at T=89 minutes which is most likely due to lack of energy in the sine transform.

The storm sine profiles for T=89 min. like the substorm profiles show an asymmetry over the Wasatch Front which can be clearly seen in the Z_I and Y_I components. Porath et al. (1970) have shown that this asymmetry is less prominent for the shorter periods 30 and 50 minutes. These results suggest that the Wasatch Front anomaly may be due to a ridge of conducting material superimposed on an asymmetric step in the conductive mantle down from the Basin and Range province into the Colorado Plateau. This asymmetry of Z_I and Y_I profiles over the Wasatch Front persists at periods of 150 and 256 minutes, suggesting that the upheaval and step are deep structures and may be continuous with the highly-conductive mantle below.

Figure 4.19 Separated Fourier sine transform
of storm field components Y and
Z at $T = 256$ minutes.

T = 256 MINUTES


$$Z_1$$


Z1A

Figure 4.15 shows profiles at $T=256$ minutes. Inspection of the sine profiles and the profiles at $T=89$ minutes (figure 4.16) shows that the X_E , Y_E , Z_E components are very similar. Both the X_E and Y_E components are very smooth and can be approximated by a curl-free plane. Both Z_E components show little east-west gradient which suggests that Y_n may be set equal to $2Y_{es}$ (Porath et al. 1970). The procedure to obtain Z_{ia} and Y_{ia} was then carried out on the sine transform components at $T=256$ minutes in the hope of amplifying and focusing the Wasatch Front anomaly. The results of this analysis can be seen in the maps of figure 4.19. The map of Z_{ia} shows the Wasatch Front clearly but it seems to be broadened due to the greater extent of the induced currents under the Colorado Plateau at this long period. To state this another way, the Wasatch Front anomaly at 256 minutes period would be more influenced by the East Front anomaly than, say, at 30 minutes. The map of Z_{ia} shows large gradients roughly outlining the Colorado Plateau. Particular interest resides in the large gradients in Z_{ia} in the western and southern areas of the array. These gradients may reflect the boundary of the Colorado Plateau and the Basin and Range province to the south and west of the Plateau.

The general pattern of the Z_{ia} field, in the middle of the array, increasing to the south supports the idea of a north-south isotherm under the Colorado Plateau rising up into the Basin and Range to the south. These results seem to support the findings of Reitzel et al. (1970) mentioned earlier.

The Y_I sine maps of figure 4.19 show the Wasatch Front anomaly very clearly and the trend of the gradients is located west of the trend of the Z_I gradients, which is in agreement with the results of Porath et al. (1970). Comparison of the Y_{ia} and Y_I sine maps at 256 minutes (figure 4.19) shows that the Wasatch Front anomaly is greatly enhanced by the removal of the normal internal field.

The spectrum of the Z component of the storm (figure 3.5) reveals that most of the power in the storm is concentrated near $T=150$ minutes and 110 minutes. Figure 3.5 also shows the relative amplitudes of the three components H,D,Z at various periods. It seems that the ratio of the amplitude Z/D and Z/H is greatest also at 150 minutes. Therefore 150 minutes is an ideal period at which to separate the storm because:

- (a) there is sufficient energy available in the Z component;
- (b) the ratios Z/D and Z/H are favourable.

The profiles of the cosine and sine Z_I and Y_I components at 150 minutes (figure 4.14) again show the

asymmetric fields over the Wasatch Front anomaly, but much more clearly at this more favourable period than at 89 or 256 minutes. Maps of the Z_I and Y_I amplitudes (figure 4.18) give a good representation of the Wasatch Front anomaly, while little appears in the sparsely observed eastern half of the array. The location of the maximum of Y_I is again seen to be west of the Z_I maximum over the Wasatch Front; this supports the location of an anomalous line current under the Wasatch Front. The X_E , Z_E phase maps seem to be very smooth and uneventful, while X_I , Z_I phases show definite abrupt changes in sign. Inspection of the X_I , Z_I phase maps shows that these phase changes roughly outline the western and southern boundaries of the Basin and Range and the Colorado Plateau. This outline coincides with the outline observed earlier for the Z_{ia} sine transform maps, at $T=256$ minutes.

In summary, the Wasatch Front anomaly shows in maps of the internal parts of the storm field components, particularly at period 150 minutes at which the storm spectrum has abundant energy. The results confirm the presence of an internal conductive structure in the position and azimuth indicated by analysis of the separated substorm fields.

4.6 Conductive structures

Two types of conductive structures can account for most local anomalies observed in Geomagnetic Depth Sounding investigation (Section 1.5):

(1) Surface anomalies caused by high conductivities in crustal rocks close to the surface, in many cases related to deep basins of porous sediments. The anomalous internal field should be out of phase by 60° to 90° with the inducing field since Ohmic resistance is more important than inductive reactance.

(2) Undulations of "isocons" (surfaces of equal conductivity) in a conducting medium of large extent. This type of model is representative of deep conductive structures in the Earth. These undulations have conductivities and dimensions, characteristic of upper mantle structure, such that self-inductance controls the induced currents rather than resistance. Arguments presented in Chapter 1 state that the phase differences between normal and anomalous fields associated with such structures are small (less than 40° typically).

Porath et al. (1970) estimated the real conductivity for the semi-circular upheaval under the Southern Rockies from phase differences between the normal and anomalous fields. This upheaval has the same response as an isolated cylinder (Kertz 1960, Rikitake and Whitham 1964), with an

associated induction parameter $c = r/\sqrt{4\pi\omega\sigma}$ which can be estimated from the relative magnitudes of the in-phase and out-of-phase fields. The radius r of the cylinder can be obtained from the maximum amplitude of the anomalous horizontal field $W = Y_{ia}/Y_n$ (Schmucker 1959) from the expression

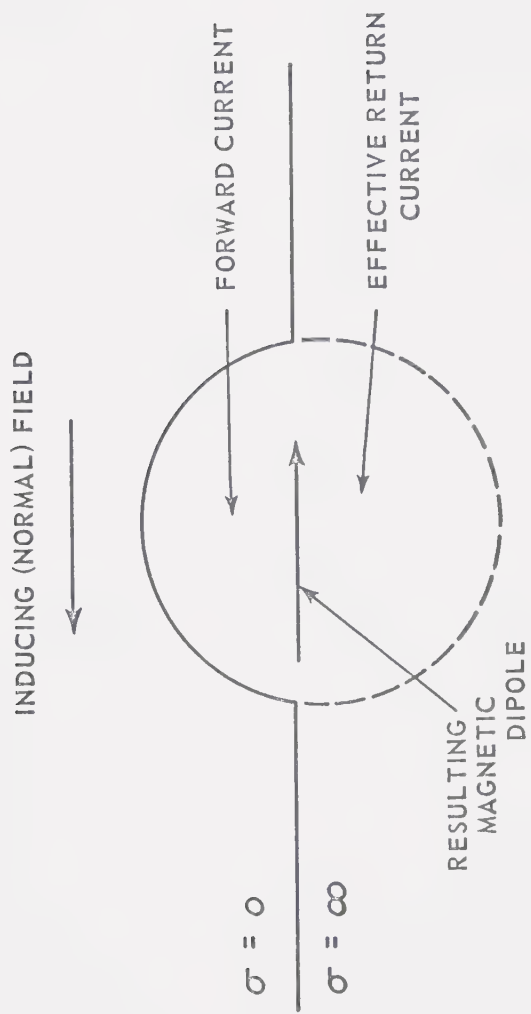
$$r = z\sqrt{W/f}$$

with f the fraction of the dipole moment of a perfectly conducting cylinder, which can be estimated from the phase differences. Thus for the Southern Rockies $z = 360$ km, $W = 0.175$ and $f = 0.6$ yielding $r = 200$ km. For the phase angle 30° , $c = 3.5$ e.m.u. which gives a conductivity of 2×10^{-12} e.m.u. for the ridge under the Southern Rockies (Porath et al. 1970).

There exist several reasons why the two north-south anomalies can be interpreted as being associated with large, deep conductors:

- (1) The general correspondence between the anomalies and heat flow results (Reitzel et al. 1970).
- (2) The inability of surface anomalies to account for phase differences of about 30° between the normal and anomalous fields (Porath et al. 1970).
- (3) The persistence of the anomaly at very long periods; this work showed persistence up to $4\frac{1}{2}$ hours, and Reitzel et al. (1970) showed persistence of the anomalies in the

Figure 4.20 Equivalence of semicylindrical ridge
on the surface of a conducting half-
space to an isolated cylindrical
conductor.



Sq daily variations, which have negligible energy in harmonics higher than the fourth ($T = 6$ hours).

The anomalous fields produced by lateral inhomogeneities in the conducting upper mantle are a second order effect superimposed upon a much larger normal field. The lateral conductivity inhomogeneities are often interpreted as upheavals in the mantle. If these upheavals are modelled as an isolated cylinder then neither the line current nor a two-dimensional dipole resulting from the induction are physically realistic for two reasons:

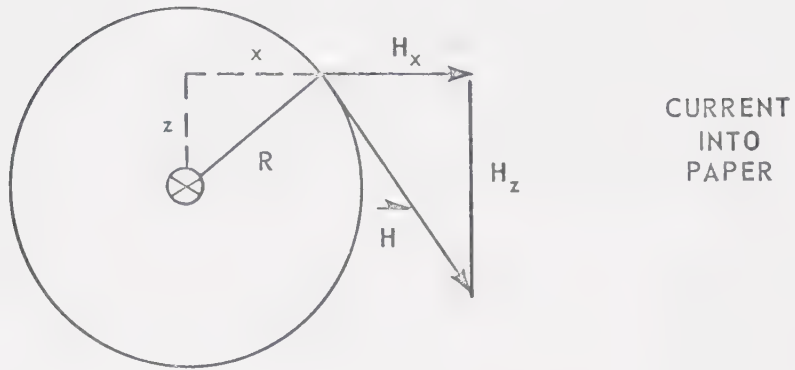
- (1) The line currents allow for no return current.
- (2) The dipole postulates the existence of two anti-parallel currents in the upheaval.

The current concentration on the elevated portion of the upheaval can be approximated by a line current, while the dilution of the current density on either side of the upheaval is equivalent to a return current under the line current. Thus a semi-cylindrical upheaval of infinite conductivity effectively has an image of the forward current under the upheaval (Rikitake and Whitham 1964), so that the half-cylinder has the same induction response as a conducting cylinder embedded in an insulator and produces the field of a two-dimensional dipole (figure 4.20).

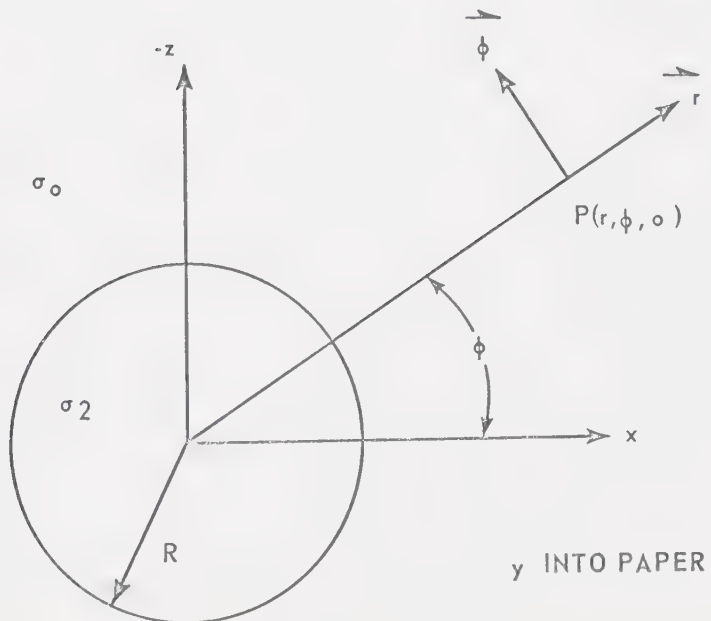
The field of a semi-cylinder on the surface of a perfect conductor can therefore be approximated by a line

Figure 4.21 Fields of a line current and double
 current in a cylinder (two-dimensional
 dipole).

LINE CURRENT MODEL



CYLINDER MODEL



of dipoles at the depth of the undisturbed surface of the conducting half-space or by a line current near the top of the upheaval. The line current then gives a maximum depth to the top of the upheaval. The two-dimensional dipole model is used to estimate depth to the undisturbed conductive surface near the ridge.

Line current

The line current model is shown in figure 4.21 where the magnetic components are

$$H_x = \frac{I_z}{2\pi r^2} \quad H_z = \frac{I_x}{2\pi r^2} \quad (4.2)$$

and the depth estimate is equal to the half-width of the H_x anomaly.

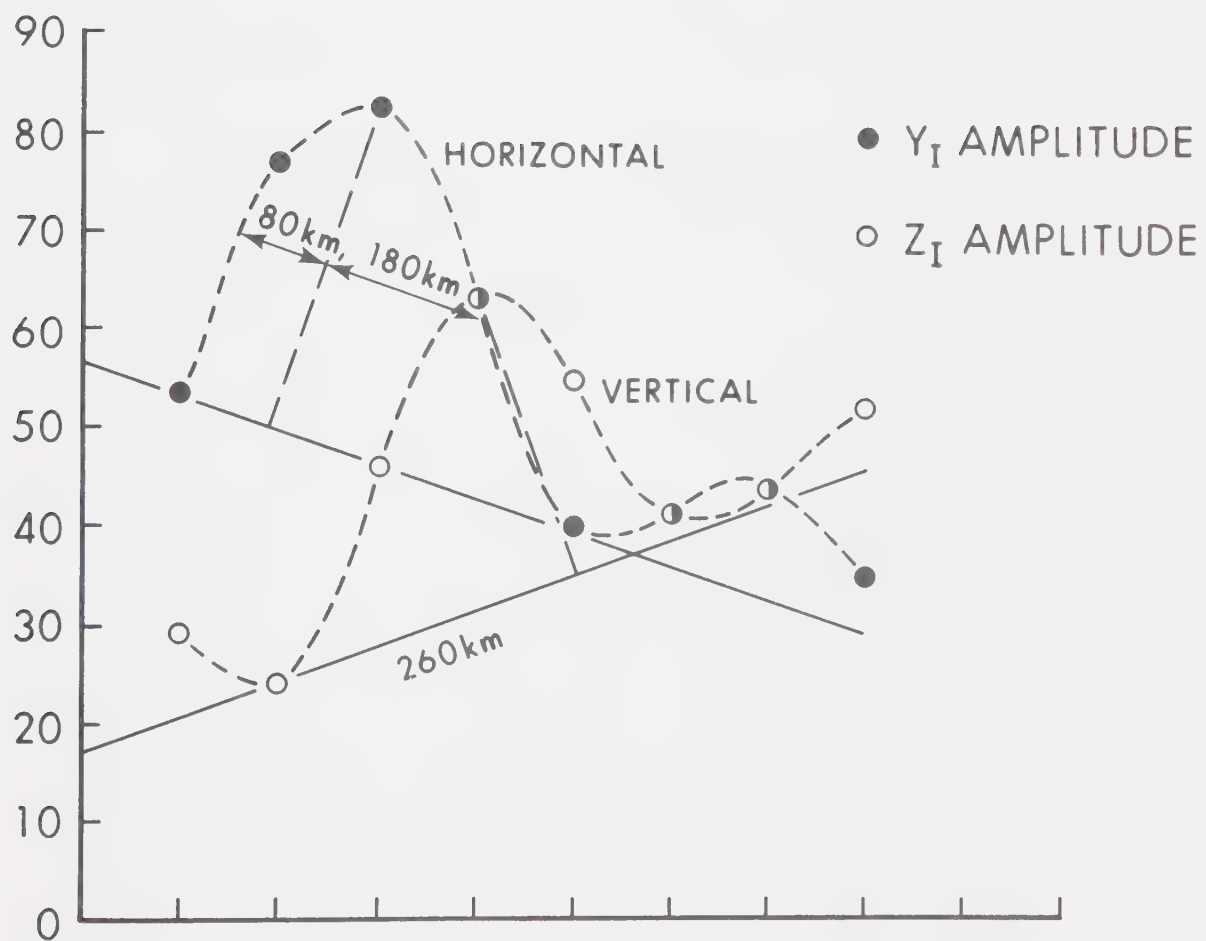
Conducting cylinder in a varying field

Kertz (1964) and Ward (1967) have derived the anomalous fields due to an isolated cylinder (figure 4.21) in a harmonically varying field. The induced fields are:

$$\begin{aligned} H_x &= \left[\frac{\alpha}{r^2} (\cos^2 \phi - \sin^2 \phi) \right] e^{-i\omega t} \\ H_z &= \left[\frac{2\alpha}{r^2} \sin \phi \cos \phi \right] e^{-i\omega t} \\ \alpha &= -R^2 (M + iN) H_0 \end{aligned} \quad (4.3)$$

Figure 4.22 Internal parts of Y and Z components
of storm field at $T = 150$ minutes.

$T = 150 \text{ min.}$



where α is the dipole moment of the two-dimensional dipole. M and N are the in-phase and out-of-phase components of the anomalous field respectively.

Equations 4.3 give the depth relations of the horizontal and vertical fields respectively:

$$Z = \pm x / (.5 - 2) \approx 2.04 x$$

$$Z = \pm \sqrt{3} x .$$

Depth estimates were obtained from the spatial half-widths of maxima of the separated magnetic fields along three centrally located east-west profiles. Figure 4.22 gives the amplitude profiles of Y_I and Z_I at 150 minutes. The depth estimates were made only for the Wasatch Front. As stated previously only in the sine transform at $T = 256$ minutes was it appropriate to isolate the anomalous field in the manner of Oldenburg (1969). All other depth estimates were made from unnormalized separated magnetic variations. Comparison of the isolated to the non-isolated fields shows that the values are within the 20% error associated with each estimate. Since the depth estimates were made from unnormalized fields a baseline representing some portion of the normal field was drawn. Depths to a line current and infinite cylinder are given in table 4.1; all estimates are taken from

magnetic anomaly profiles like figure 4.22 over the Wasatch Front. Comparison of the results above with those of Porath et al. (1970) can be made by inspection of the depth estimates they computed for the substorm, quoted in table 4.2.

The depth estimates of the postulated currents are consistent for all profiles and interestingly enough for the very long period also, giving the average maximum depth to the top of the conductive ridge under the Wasatch Front as

$$114 \text{ km} \pm 20\% .$$

Oldenburg (1969) computed a similar table to 4.1 for line current depth estimates for the substorm, and found for average maximum depths to Wasatch Front $110 \text{ km} \pm 20\%$

$$\text{East Front} \quad 230 \text{ km} \pm 20\% .$$

He also reported that depth estimates from similar profiles on maps of the sine and cosine transforms of Z_{ia} and Y_{ia} and on maps of $\text{Re}(Z_{ia}/Y_n)$ and $\text{Re}(Y_{ia}/Y_n)$ also gave maximum depths of the line current which were within the limits of the unnormalized depth estimates.

The results of Oldenburg (1969) and of the author show that good estimates to the top of an upheaval modelled as a line current can be made from the unnormalized separated fields. The consistency of the depth estimates at

Table 4.1

Depth Estimates of Wasatch Front

Period (mins.)	Depth(from half-width)km	
	Line Current	Cylinder
89	110	207
150	117	230
256	114	232

Table 4.2

Depth estimates from substorm fields

	T	Y_{ia}/Z_{ia}	Depth(from half-width)km	
			Line Current	Cylinder
Southern	32.5	0.7	180	370
Rockies	50.0	0.9	190	400
	89.0	0.9	200	410
Wasatch	32.5	1.0	110	230
Front	50.0	1.2	125	260
	89.0	1.2	-	-

long periods corroborates the conclusion of Reitzel et al. (1970) that the anomalous conductive structures are deep and may be regarded as undulations in the conducting mantle.

4.7 Models of conductive structures

Porath, Oldenburg and Gough (1970) have developed a five-step method to obtain models of conductive structures that cause two-dimensional magnetic anomalies observed across an array. The five steps are:

- (i) A line current model is used to estimate maximum depths to the tops of conducting upheavals.
- (ii) A two-dimensional dipole model is used to estimate the depth to the undisturbed conductive surface near the ridge.
- (iii) A semi-cylindrical upheaval on the surface of a perfectly conducting half-space is tried, starting with depth and radius as estimated from (i) and (ii), with necessary adjustments to improve the fit. The fields associated with such a model can be computed by the method of conformal mapping (Schmucker 1964).
- (iv) Asymmetrical anomalies can be fitted by a step in the surface of the half-space, and combined in a first approximation with the half-cylinder model if needed,

(v) Once the dimensions of the required conducting ridge are established phase differences between the normal and anomalous fields can be used to estimate the true, finite conductivity.

This thesis has completed steps (i) and (ii). The writer did not proceed to steps (iii), (iv) and (v) because the results of the storm separation do not allow quantitative modelling. The separated fields over the Wasatch Front have been compared with the models developed by Porath et al. (1970). As was pointed out previously the anomalous fields must be normalized to obtain good estimates of the conductivity using the phase differences between the normal and anomalous fields. The results of the storm separation have shown the fields to be too complex to be normalized by present methods, so that no quantitative estimate of the conductivity was obtained from the storm fields.

Porath et al. (1970) model the two anomalies by fitting the observed anomalous fields to the response of semi-cylindrical upheavals and steps in the surface of a perfectly conducting half-space. The responses were computed by conformal mapping techniques (Schmucker 1964). Figure 4.23 shows the steps involved in approximating the substorm vertical field anomaly by a conductivity model

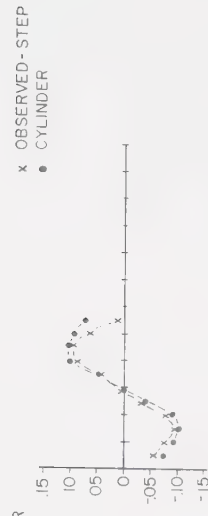
Figure 4.23 Model fitted to normalized anomalous vertical field of substorm at $T = 89$ minutes (after Porath, Oldenburg and Gough 1970).

T = 89 MINUTES

(a)



(c)



(b)

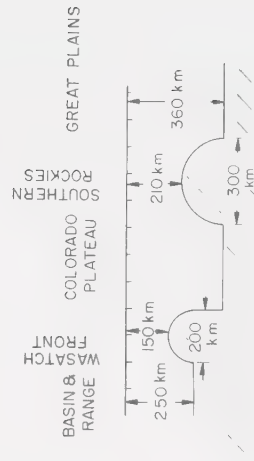
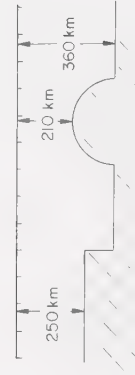
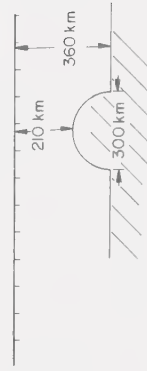
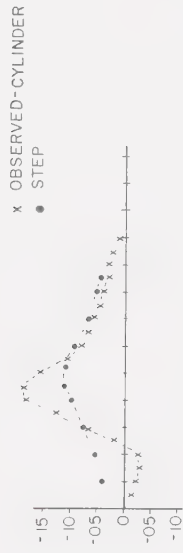
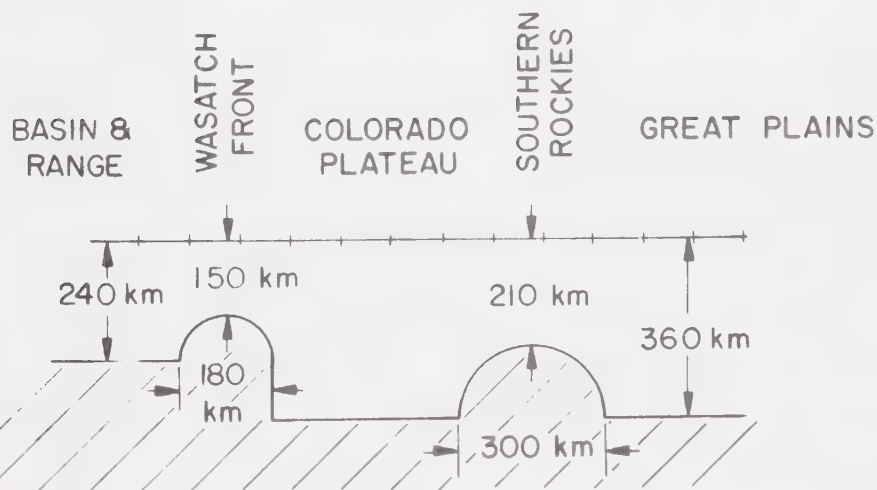
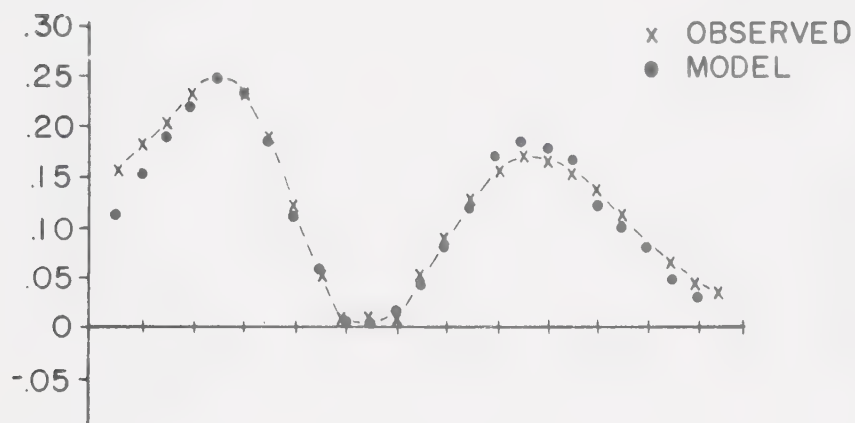
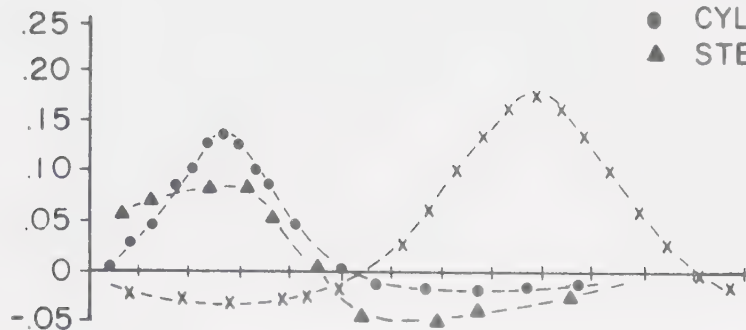


Figure 4.24 Model fitted to normalized anomalous
eastward horizontal field of substorm
at $T = 89$ minutes (after Porath,
Oldenburg and Gough 1970).

T = 89 MINUTES

Y_{ia}

- x CYLINDER (SOUTHERN ROCKIES)
- CYLINDER (WASATCH FRONT)
- ▲ STEP (WASATCH FRONT)

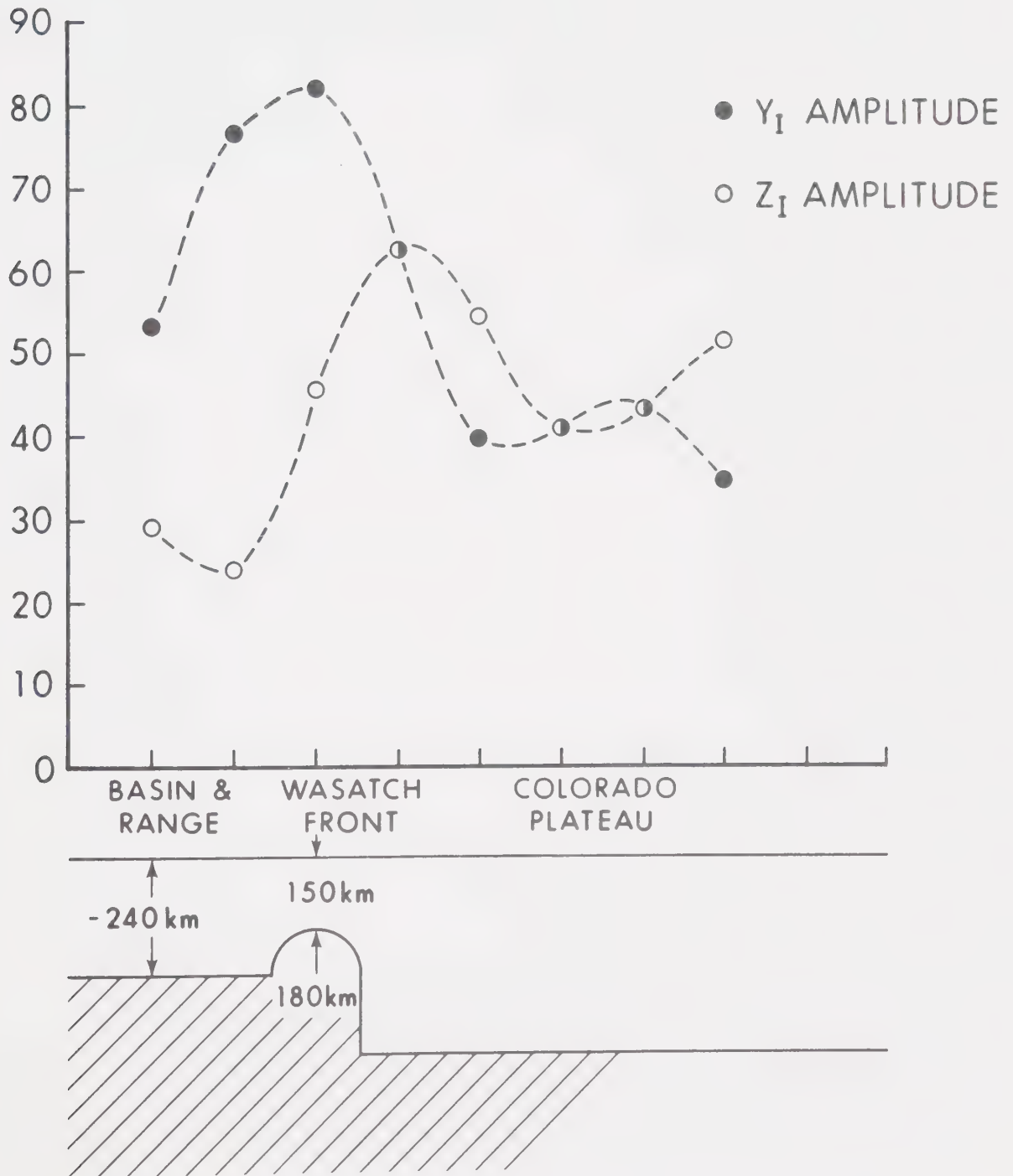


(after Porath et al. 1970). Figure 4.23a is a semi-cylinder on an infinite half-space whose dimensions were derived from results of the line current model and the dipole model. Figure 4.23b shows the response to a step model compared to the observed anomaly minus the field due to the model in figure 4.23a observed over the Wasatch Front. Figure 4.23c shows the result of superposition of the step response to the cylinder response model, which then gives a good approximate conductivity model to the observed Wasatch Front anomaly and the East Front anomaly. This procedure depends heavily on getting a good estimate of the East Front conductivity structure. Because such an estimate was not obtained by the writer for the anomalous storm fields this modelling procedure could not be completed. The work on the separated storm fields terminates with a qualitative fit of the unnormalized Y_I and Z_I amplitude components of the storm at $T=150$ minutes as profiles over the Wasatch Front. Figure 4.25 shows that within the limits of the depth estimates Y_I and Z_I fit the theoretical responses of the Y_I and Z_I components over the Wasatch Front as seen in figures 4.23 and 4.24.

Although the lack of information from the eastern half of the array and complexity of the external field of the storm prevent completion of a quantitative interpretation of structure from this variation event, the

Figure 4.25 Internal Y and Z fields of storm at
T = 150 minutes, with linear gradients
removed (compare Figure 4.22), and the
Wasatch Front model structure derived
from substorm fields.

$T = 150 \text{ min.}$



qualitative and semi-quantitative results secured for the Wasatch Front structure are important in giving independent support, from a second input field, to the conductive structure deduced from study of the substorm fields.

CHAPTER 5

GEOPHYSICS AND UPPER MANTLE STRUCTURE IN THE
WESTERN UNITED STATES

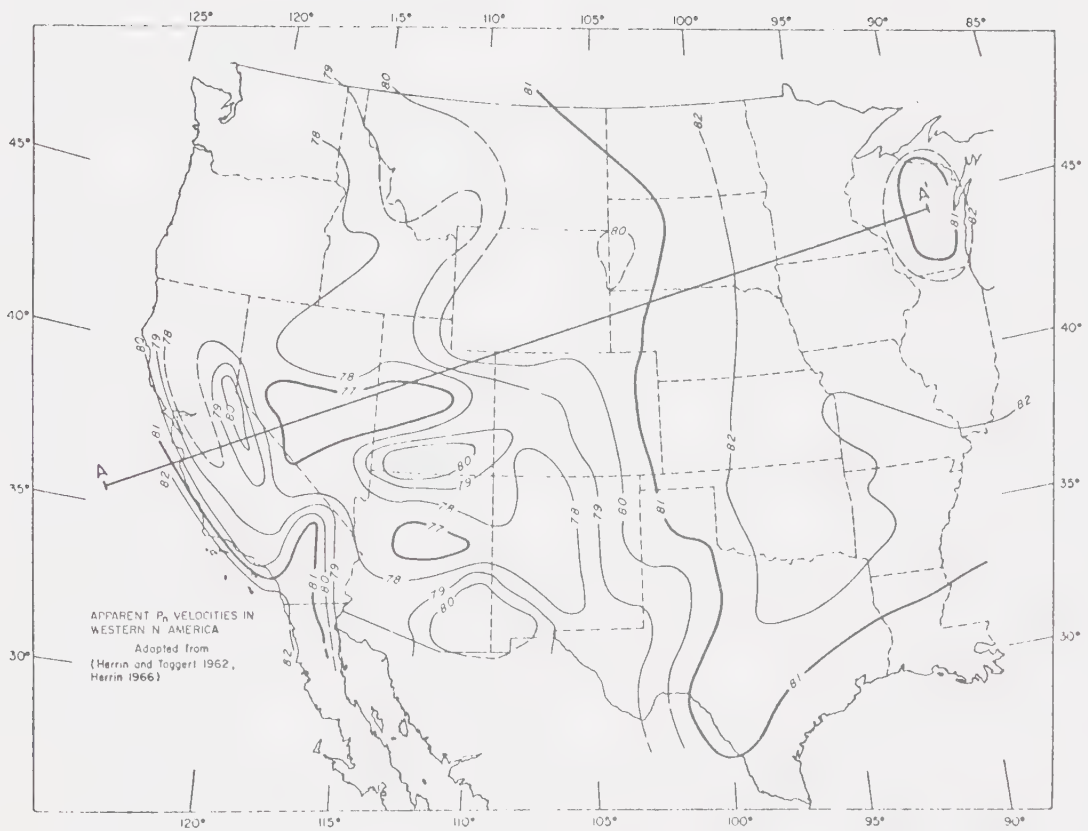
Geomagnetic deep sounding results from the 1967 array in the western United States (Reitzel, Gough, Porath and Anderson 1970, Oldenburg 1969, Porath, Oldenburg and Gough 1970, and the present thesis) provide the opportunity for correlation with other geophysical results. Such results include refraction data in seismic P_n velocity (Herrin and Taggart 1962, Archambeau, Flinn and Lambert 1969), seismic time-term studies, (Cleary and Hales 1966) extensive heat flow measurements (Roy et al. 1968a, Roy, Blackwell and Birch 1968b) and conductivity-temperature relationships (Tozer 1959, Hughes 1955, Swift 1967, Hyndman and Hyndman 1968, Warren et al. 1969, Gough and Porath 1970) with the hope of establishing a geophysically consistent areal pattern of upper mantle lateral inhomogeneities in the western United States.

5.1 Seismology

Herrin and Taggart (1962) applied a computational procedure to seismic data in the P_n range from 89 stations to determine the epicenters of the Gnome explosion and the Lake Hebgen earthquake in the United States. The investigation resulted in the first

clear evidence of significant regional differences in P_n velocity. In the detailed analysis of regional variations in P_n velocity, the P_n phase is regarded as a head wave travelling in the upper mantle just below the Mohorovicic discontinuity at distances less than 2000 km, implying that the P_n velocity does not vary systematically with distance from the source. Interval velocities were computed between stations along radial lines from the source by dividing the distance between stations along the radius by the difference in arrival times at the two stations. The validity of this method is based on the condition that the crustal thickness is the same under both stations. This condition would thus prevent the detection of the Wasatch Front where GDS results suggest that the crustal thickness changes between the Basin and Range Province and the Colorado Plateau. The assumption that interval velocities approximate the P_n velocity at the center of the spread allows the results to be contoured. Figure 5.1 illustrates the compressional velocity at the top of the mantle according to the assumptions given above. The attenuation of amplitude in the first arrival from the Gnome explosion was seen to correlate with regions of low P_n velocity. Variations in the depth of a low velocity layer in the upper mantle then may well account for the complex P_n velocity pattern

Figure 5.1 P_n velocities in the western United States, after Herrin and Taggart (1962).



in the western United States. Herrin and Taggart (1962) maintain that these variations in depth and thickness of the velocity minimum are probably related to differences in terrestrial heat flow and thus to the thermal gradients thought to be present in the upper mantle. The averaging of P_n velocities along a profile definitely limits resolution, preventing the recognition of such relatively narrow features as the Wasatch Front and Southern Rockies upper mantle ridges.

Cleary and Hales (1966) analyzed the travel times of P waves from 25 earthquakes to stations in North America, from sources at angular distances between 32° and 100° , by a least squares technique similar to the "time term" method of refraction seismology. Deviations from the Jeffreys-Bullen tables were separated from the effects of station and source residuals. The difference from the J-B tables were calculated at 20 intervals and fitted to a smooth curve. A regional trend was shown in the station arrival times with arrivals in Basin and Range Province being up to a second late and those in the central part of the United States up to a second early.

Cleary and Hales (1966) decided that data should be selected initially from stations on the North American continent to keep the effects of location errors to a reasonable minimum. Their reasoning follows: two

stations at opposite ends of the continent at a distance 30° from the source with a mislocation of 0.1° produce a difference error of 0.7 seconds and a distance of 60° with the same conditions produces a difference error of about 0.5 seconds. Earthquakes are chosen that 1) were shallow-focus, 2) had a first arrival that was sharp enough to be recognized and measured precisely at virtually all stations, and 3) were distributed in such a manner that the data from most stations would contain information from an adequate sample of distances and azimuths. The stations that provided data for the analysis were:

1. LRSM Station and Vela-Uniform Observatories
2. WSSS Stations in the U.S.
3. St. Louis Network Station
4. Caltech Network Station
5. Canadian Stations

A precision of 0.1 sec. was attained for all records. A version of Bolt's ID1 computer program was used to calculate the epicenter, or give time and focal depth for each event along with the residuals from the J-B times. The North American station residuals were extracted for analysis from the above residuals.

The method of analysis is based on evaluating the equation

$$a_{rs} + b_r + d_s = \delta t_{rs}$$

at each station r and earthquake s , where δt_{rs} is the observed residual from the J-B tables; a_{rs} , assumed to be a function of distance only, is the average difference from the tables at the distance of station r from earthquake s ; b_r is the station residual that is a perturbation in the travel time induced by conditions in the neighborhood of station r ; and d_s is a perturbation caused by conditions peculiar to earthquake s that is taken as constant within the range covered by the data. As mentioned above the analysis is similar to "time term" with the difference residing in the parameter d_s . This is not really a source term but should more properly be called an arbitrary baseline correction made necessary because only a selected group of stations were used and the mean of the residuals of this group may differ from zero.

The results from the analysis of shallow-focus earthquake data are shown as station P wave residuals (Cleary and Hales 1966) over the United States in figure 5.2. There is indeed a marked regional trend with large positive residuals in the Basin and Range Province and large negative residuals in the central United States with apparent extensions of this negative residual trend north into the Canadian Shield. Figure 5.3 was taken from a paper by Doyle and Hales (1967) where a similar

Figure 5.2 Station residuals in P arrival times
 over the United States (Cleary and
 Hales 1966).

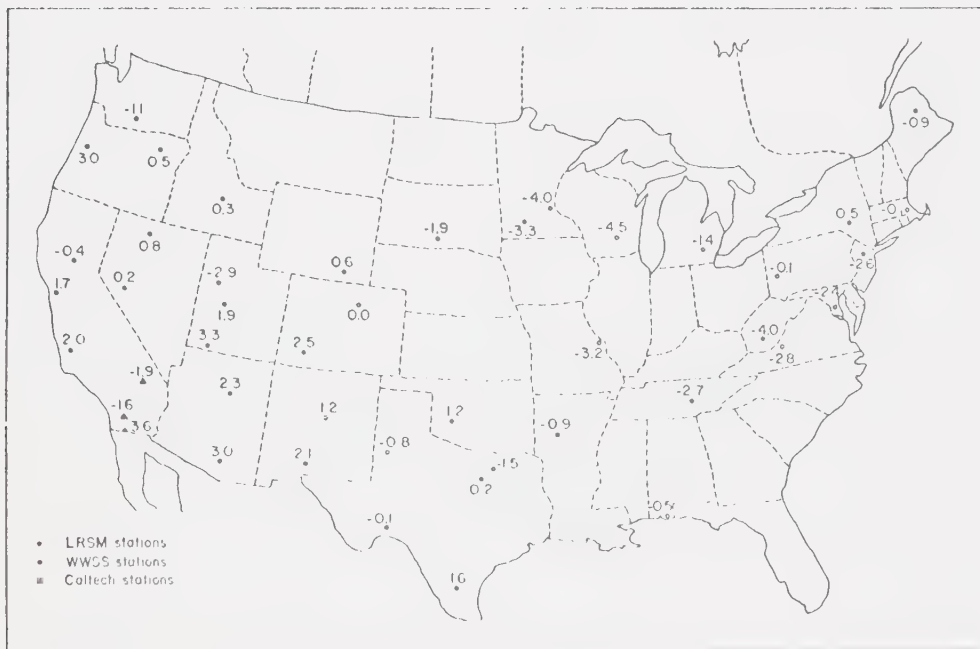
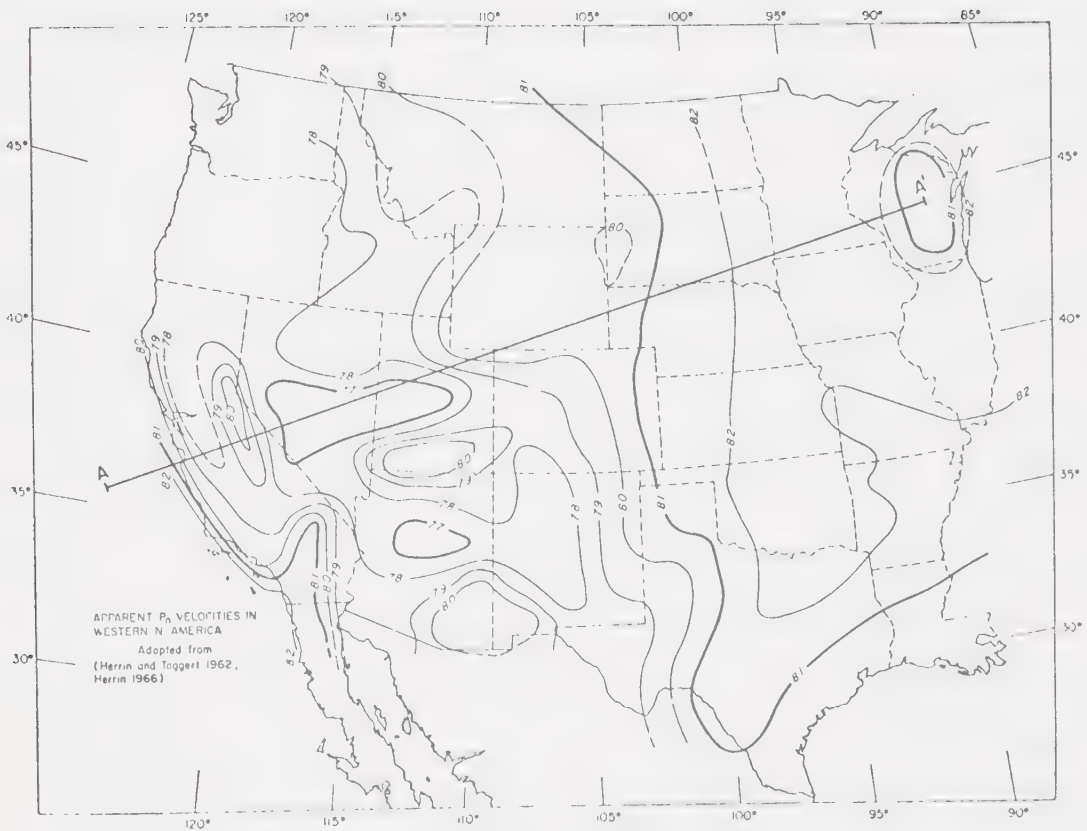


Figure 5.3 Station residuals in S arrival times
 over the United States (Doyle and
 Hales 1967).



analysis was applied to S waves as was done by Cleary and Hales (1966) for P waves.

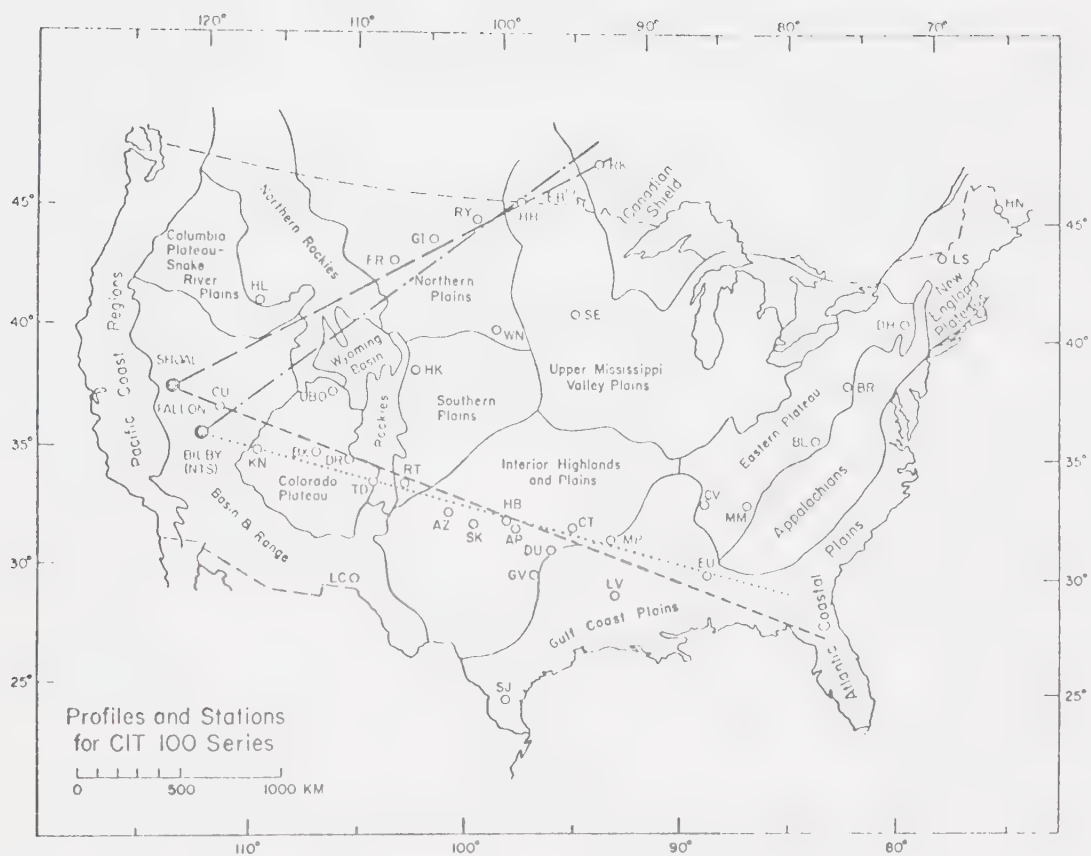
Cleary and Hales (1966) based their analysis on an earth model that had a laterally homogeneous lower mantle overlain by a laterally inhomogeneous upper mantle and crust. They have also assumed that:

- 1) the average travel time of a P wave is controlled by the homogeneous material through which the wave travels for the greater part of its path;
- 2) only inhomogeneities in the upper layer produce variations from this average time and are constant within the prescribed distance range for a specific station and source. Cleary and Hales (1966) state that the consistency of their results supports these assumptions to the first order.

The use of an array of seismometers on a regional rather than a continental basis in a Cleary and Hales "time term" method of earthquake analysis offers promise of providing a seismic technique capable of comparable lateral resolution of features to GDS array studies.

Archambeau, Flinn and Lambert (1969) attempted to determine the upper mantle structures that underlie particular continental provinces through the use of modern computer-based techniques of processing and

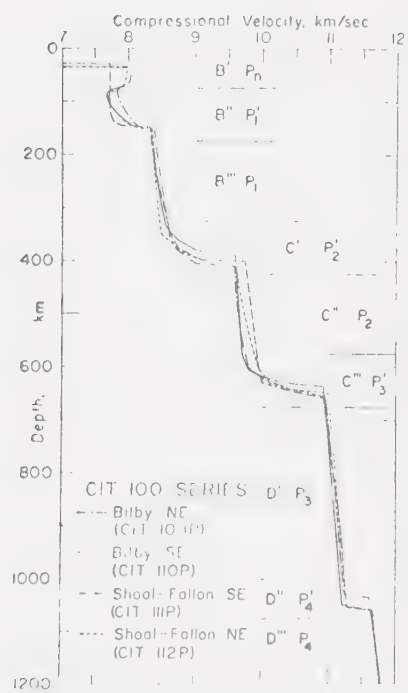
Figure 5.4 Observational profiles used by
Archambeau, Flinn and Lambert
(1969).



analyzing seismic data to systematically isolate and identify mantle body-wave phases. They state that they have been able to obtain a large amount of reliable information from a relatively small number of observations along a single profile or linear array, because their techniques allow data to be obtained from later arrivals, thus giving complete travel time and amplitude distance curves, rather than just first arrival branches. These authors obtained compressional velocity models for the North American Continent which distinguish distinct mantle structures for two tectonic regions: (i) a basin and range or rift zone mantle structure; (ii) a plateau mountain structure which may show further subdivision as more data become available.

Archambeau et al. (1969) used the compressional phases from the Shoal and Bilby nuclear explosions in Nevada and from the Fallon earthquake (which occurred at the Shoal site) observed along four basically linear profiles across the physiographic provinces of the continental United States (figure 5.4). Three profiles were expected by Archambeau et al. to provide a good sampling of the Basin and Range upper mantle, the Colorado Plateau and Southern Rocky Mountains, the Snake River plains, the Northern Rocky Mountains, and the eastern Basin and Range provinces. Because of the limited range of these stations and the probable tran-

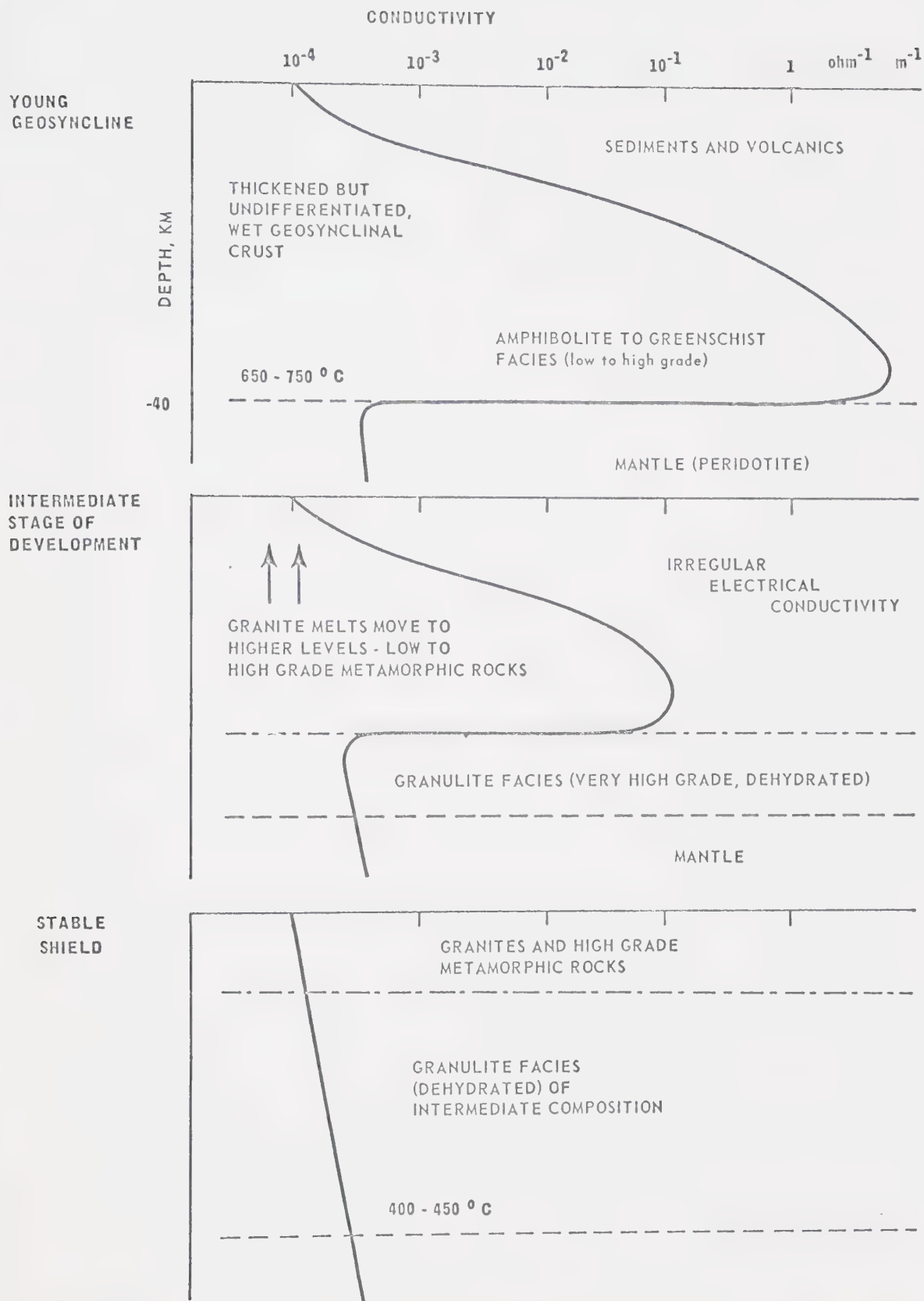
Figure 5.5 Velocity profiles found by Archambeau,
Flinn and Lambert (1969) in four regions
of the United States.



sitions in mantle structure along these profiles Archambeau et al. (1969) only hoped to observe lateral variations in mantle structure above depths of 300-400 km.

The salient results of this study can be seen in figure 5.5, pertinent to this discussion in the B zones which lie in the depth range in which lateral variations in the upper mantle properties occur. Major changes in velocity can be seen at 150 km, 400 km and 650 km. Archambeau et al. interpreted upper mantle structure appropriate to the Southern Rocky Mountains and Colorado Plateau provinces as consisting of a low velocity zone capped by a high velocity lid zone, with variations in both the lid zone and low velocity zones from province to province. The Basin and Range is said to have a very thin lid or none at all with abnormally low velocities extending from or near the base of the crust to 150 km. A pronounced low-Q zone is said to correspond to the average low velocity zone depth range for the velocity models. A major result of Archambeau et al. (1969) is the existence of laterally variable zones of the P velocity in the upper mantle, with rapid changes at both the top and bottom of the zone, as well as the decrease of low velocity values in between. This result suggests that partial melting of mantle material is occurring in this depth range.

Figure 5.6 Evolution of granites and their electrical conductivities, after Hyndman and Hyndman (1968).



This method of seismic data analysis along a profile still does not have the capability of resolution necessary to accurately map the boundaries of the upper mantle provinces, because resolution is limited by 1) the averaging process of the P velocity results and 2) the spacing of the stations on the profiles.

5.2 Conductivity and Thermal Structure as a Function of Time

Hyndman and Hyndman (1968) suggest that most of the electrical conductivity anomalies observed in the North American Cordillera and particularly that of Caner et al. (1967), which indicates that high conductivity is largely restricted to a 20 km layer at a depth of 20 to 40 km, are related to highly conducting material associated with the existence of water-saturated rocks in the lower crust. Hyndman's argument is based on the development of a geosynclinal crust. This development consists of three stages representing different instants of geological time. The results of this development with respect to conductivities and temperatures at depth are shown in figure 5.6. The alternative possibilities of electrical conductivity anomalies being due to lateral variations of conductivity in the upper mantle or being due to water-saturated rocks are

dependent on the age of the area being studied. Thus the interpretation would depend on the region being in the "Young Geosyncline", "Intermediate" or "Stable Shield" periods. The importance of the age of the rocks is caused by the decrease in time of the effects of water saturation on electrical conductivity.

Gough and Porath (1970) suggest a common origin to the ridge producing a heat flow anomaly and to the ridge producing a magnetic induction anomaly, across the Southern Rockies (Reitzel et al. 1970, Porath et al. 1970). If the origins are common then the ridges must be of considerable age, i.e. low thermal conductivities in the crust and mantle give a time constant to thermal information originating at depth in the order of 10^8 years. Gough and Porath (1970) concluded then that if the above assumptions were true then the structures could not be less than 2×10^8 years old. This conclusion rests on the assumption that the induction anomaly is caused by structure, probably thermal, in the upper mantle.

The writer suggests that the two main north-south anomalies Wasatch Front and East Front cannot be interpreted in terms of water-saturated rocks.

5.3 Electrical Conductivity, Temperature and Heat Flow

The electrical conduction in the near-surface rock formation is mainly electrolytic as a result of saline solutions filling pores and cracks. The unconsolidated sediments have conductivities between 0.1 and 1 (ohm m)⁻¹ in contrast to dense and therefore poorly conducting igneous rock (0.01-0.001 (ohm m)⁻¹). The crust is essentially a poor conductor since rocks become more and more insulating under pressure. But the conductivity does rise again at greater depths and this rise is largely attributable to increase in temperature at depth.

Ringwood (1966) produced a "pyrolite" petrological model as an approximation to the composition of the upper mantle. This model satisfies seismic, density and chemical conditions. Pyrolite has a chemical composition 75% peridotite, 80% olivine, ((Mg,Fe)₂SiO₄), 20% enstatite(MgSiO₃) and 25% basalt.

The main constituent of "pyrolite", olivine, was investigated by Hughes (1955) with respect to its conductivity as a function of temperature and pressure between 1333°K and 1513°K and between 0 and 8.5 kbar, the ambient pressure at 30 km depth.

Hughes' results indicate an exponential law for the conductivity of olivine; such a relation is typical of minerals which are semi-conductors:

$$\sigma = \sum_i \sigma_i e^{-\frac{A_i}{kT}}$$

where A_i is the activation energy for one of the semi-conduction processes, impurity, intrinsic or ionic. Tozer (1959) has shown that the predominant semi-conduction processes in the upper mantle are intrinsic and ionic. He also states that the A_i/kT exponent is large and the dependence on temperature is very strong, while the error introduced into the temperature calculations by the presence of other phases amounts to only a few tens of degrees for quite large "impurity" contents. Therefore the precision of temperature determination from electrical conductivity is highest in the upper mantle. Tozer (1959) has derived

temperature at depth from the conductivity models of Lahiri and Price (1939) and McDonald (1957). The conductivity-temperature relationships are still not too well defined in the upper mantle, mainly because of uncertainty with regard to the fayalite content of the olivine.

If the surface of the earth and that of the the highly-conducting upper mantle are assumed to be isothermal surfaces, then the coincidence of heat flow anomalies with those of electromagnetic induction should give information concerning the conductivity-temperature

relationship in the upper mantle. This was the approach taken by Warren et al. (1969) to compare their heat flow measurements along a profile coincident with Schmucker's (1964, 1969) profile of magnetic observations in Southern New Mexico, Arizona and Texas. For the coincidence of the thermal and electromagnetic anomalies to have meaning in regard to temperature, each must be shown independently to arise from the lateral inhomogeneities in the upper mantle. Schmucker (1964) has given a reasonable interpretation of the Rio Grande anomaly in terms of lateral conductivity inhomogeneities of the upper mantle, and this has been discussed in Chapter 3.

Roy et al. (1968b) have shown that major changes in heat flow taken from 38 bore-holes in plutonic rocks across the continental United States can be attributed to changes in the source of heat at depths within the upper mantle. Their analysis takes account of the heat produced by radioactive decay in the plutons by using the linear heat flow relationship $Q = a + bA$, where Q is the heat flux at the surface, A is the radioactive heat production of surface plutons, b the depth to which the radioactivity measured at the surface is constant and a the heat flow due to sources in the lower crust or upper mantle. With information about radioactive element concentration at each site of heat flow observation, the value for bA can be estimated. Roy found that b varied from 7 to 11 km across the United States thereby

allowing a standard plot of $Q = a + bA$ with coordinates Q and A to be drawn. The intercept of Q , a , would represent the contribution to Q from the lower crust or upper mantle. This shows that heat flow variations as seen on a large scale are due mostly to variation in the lower crust and upper mantle.

The combined radioactivity and heat flow measurements at the 38 localities show that the continental United States has three definite heat flow provinces: 1) eastern United States where $b=7.5$ km and $a=0.79$ $\mu\text{cal}/\text{cm}^2\text{sec}$ (H.F.U.); 2) the Sierra Nevada where $b=10.1$ km and $a=0.40$ H.F.U.; and 3) the Basin and Range Province where $b=9.4$ km and $a=1.4$ H.F.U. Roy et al. (1968b) state that the slope associated with the heat flow results of the eastern United States may have broad applicability in that it may be considered the reference curve for normal continental heat flow. The Basin and Range Province has an intercept of 1.4 H.F.U., 0.6 H.F.U. greater than the eastern United States; this heat must come from the lower crust or upper mantle, but the lower crust can be discounted as a source since this would conflict with seismic and geochemical results. This leaves the upper mantle as the source of the excess heat flux. Roy et al. (1968b) state that high temperatures causing partial melting at shallow depths in the upper mantle would be consistent with seismic, gravity

and electrical conductivity data and that the top of the partially molten zone is essentially an isotherm since the melting point gradient is only 2 to 4°C/km.

Even though the number of heat flow data locations is not as plentiful as used in other upper mantle investigation techniques in the continental United States, enough values exist in the western United States to support the concept of representing the surface or near surface of the upper mantle as an isotherm that is undulating under the physiographic provinces in the western United States.

Warren et al. (1969) with heat flow results along the same line as Schmucker (1969) were able to relate their heat flow variations with Schmucker's electromagnetic anomalies by showing that both sets of data were consistent with a 1200°C isotherm at a depth between 50 and 200 km under Southern Arizona and between 150 and 400 km under western Texas. Warren's isotherm was determined by downward continuation of heat flow data in two dimensions using Poisson's equation:

$$\frac{\partial^2 \theta}{\partial x^2} + \frac{\partial^2 \theta}{\partial z^2} = \frac{A(x,z)}{K}$$

where θ and A are the temperature and heat production at the point (x,z) . He assumed the surface of the earth also to be an isotherm. The results of this process are

Figure 5.7 Heat flow and conductive models
(after Warren et al. 1969).

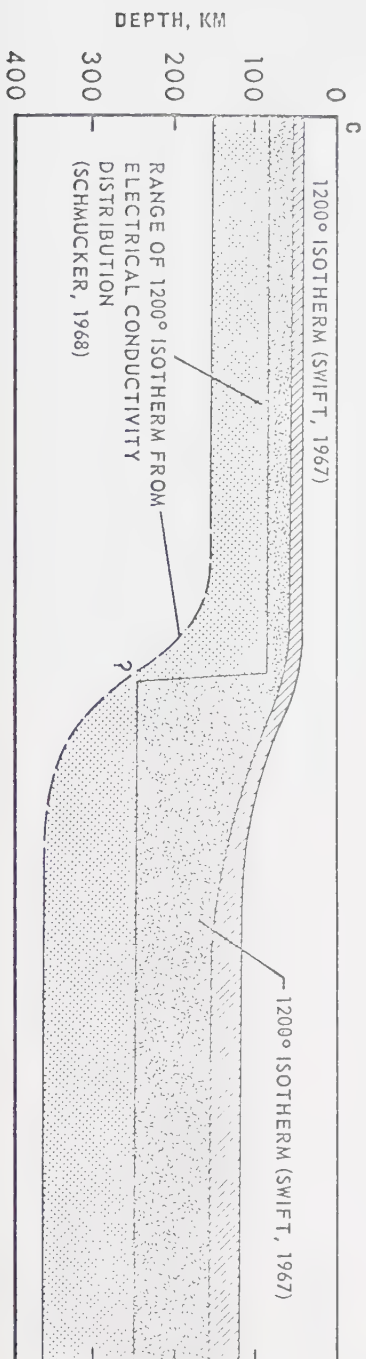
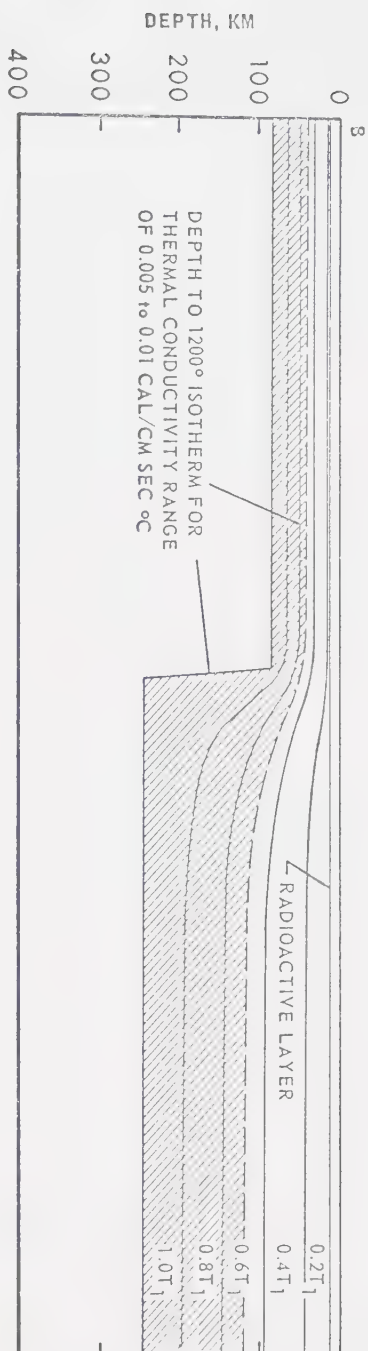
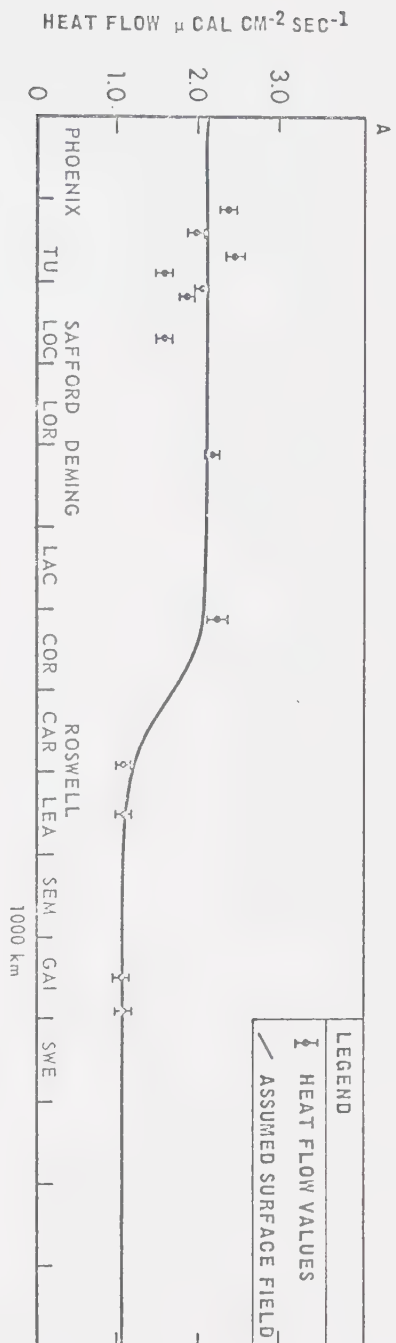


Figure 5.8 Heat flow and geomagnetic depth-sounding and magnetotelluric stations (Warren et al. 1969). The three broken lines show the approximate positions of lines 2, 3 and 4 of the 1967 array in the present study.

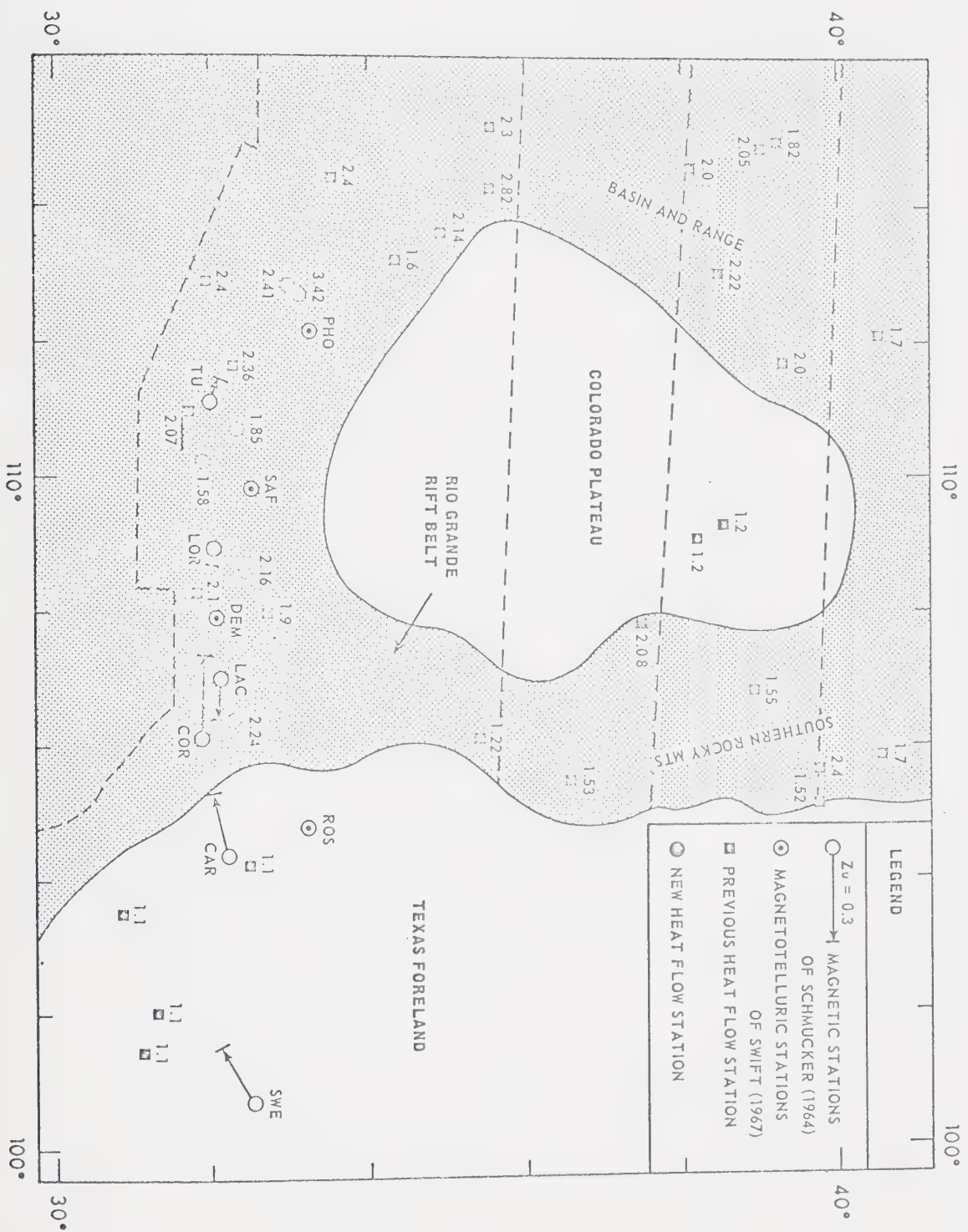
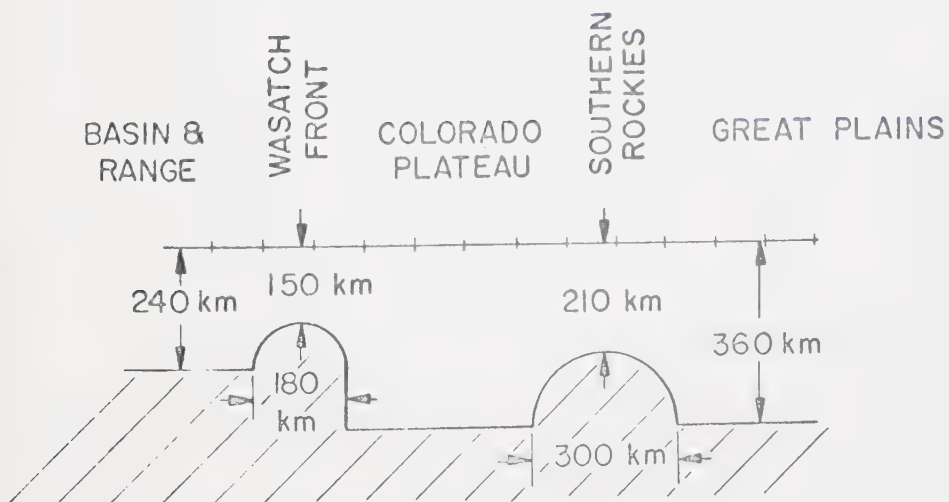
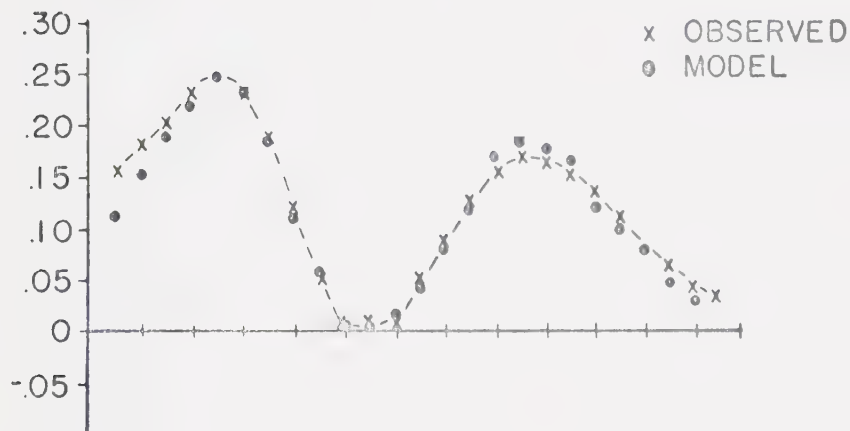
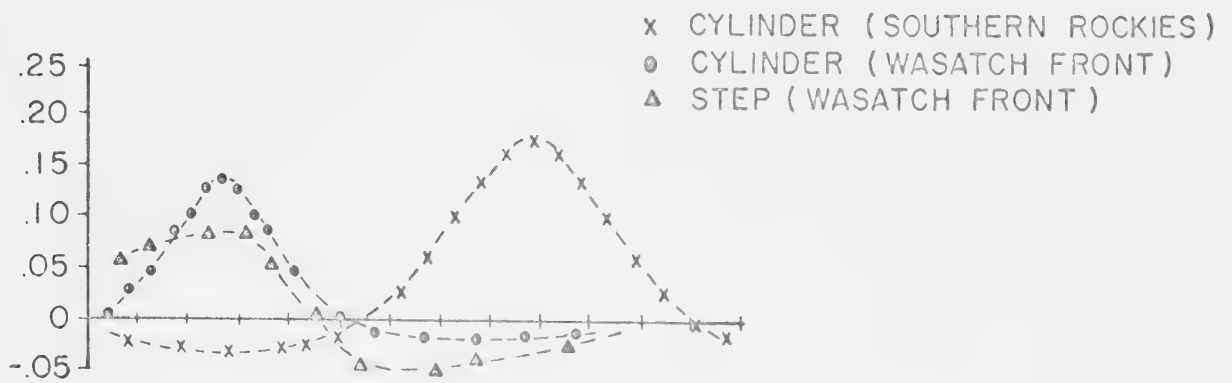


Figure 5.9 Model structure for results of 1967
array (Porath et al. 1970). Repetition
of figure 4.28.

T=89 MINUTES

Y_{ia}



shown in figure 5.7 along with the results of Schmucker (1969). Estimates can be made of the isotherm which gives best correlation of heat flow to magnetic variations along a line. The resulting temperature estimates are in agreement with estimates from other considerations within 300°C.

Figure 5.8 reproduced from Warren et al. (1969), shows the distribution of heat-flow values in a region which overlaps most of the area covered by our 1967 array. Lines 2, 3 and 4 of the array are indicated. The correlation with the conductive structures (figure 5.9) is close. The Basin and Range Province and Southern Rockies are hot, the Texas Foreland and Colorado Plateau cold. Only two heat-flow determinations suggest a lower upper mantle temperature under the Colorado Plateau, where Warren et al. obviously assume a correlation of heat flow with the structures. Here the GDS evidence of a step structure in the conductivity under the boundary between the Basin and Range and the western edge of the Colorado Plateau bears out and extends the heat-flow picture. The ridge on top of the step at the Wasatch Front (figure 5.9) is not shown in the heat-flow results, probably because the latter are too few.

An alternative presentation of the correlation between heat-flow and induction anomalies is given in

Figure 5.10 Provisional heat-flow contour map of Roy, Blackwell and Decker (private communication) superposed on Fourier spectral amplitude map of unseparated vertical component of substorm field at $T = 60$ minutes.

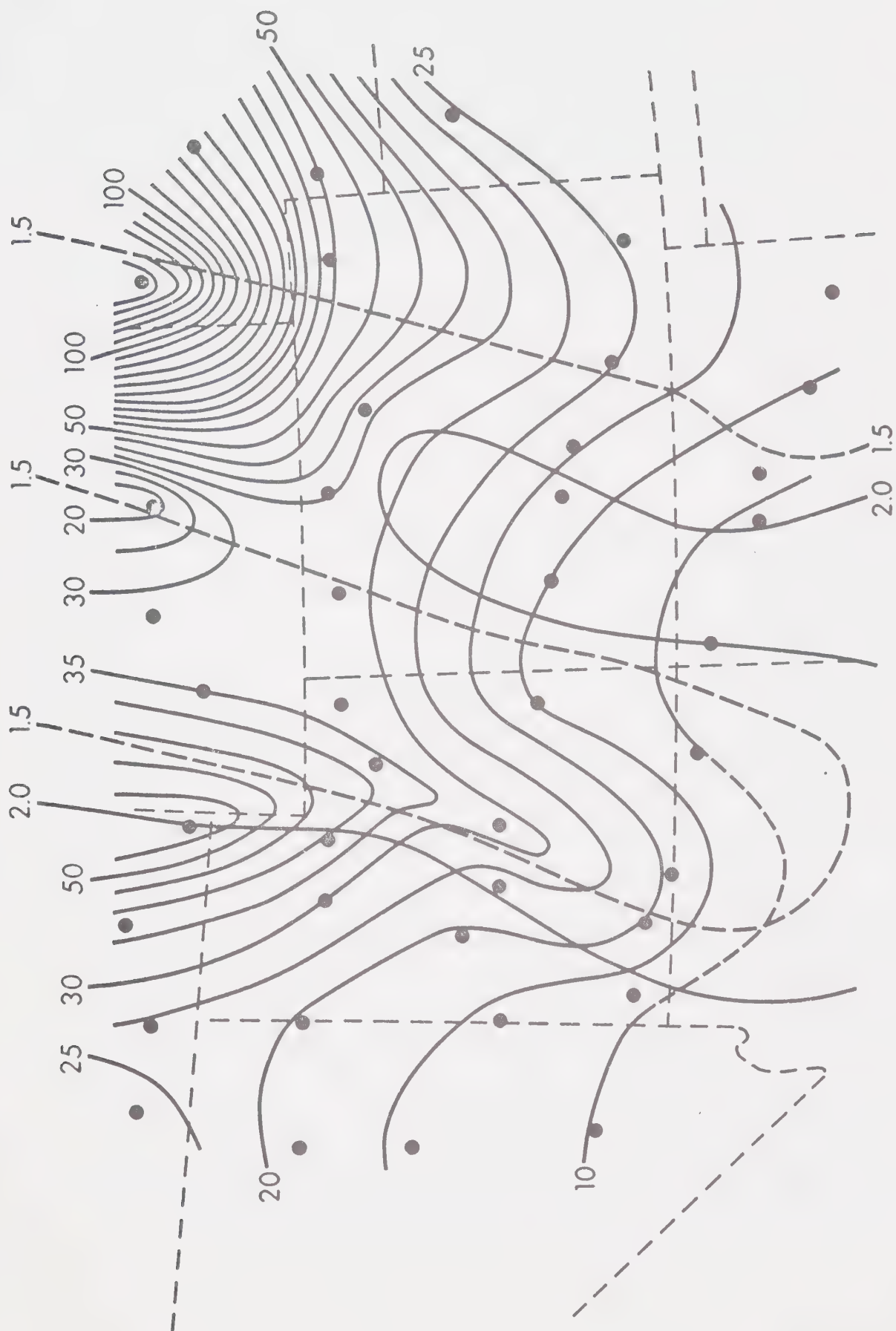


figure 5.10. Here a provisional heat-flow contour map by Roy, Blackwell and Decker (personal communication) is superposed on the unseparated Z component Fourier spectral amplitude map at $T=60$ minutes for the sub-storm field of September 1, 1967. The magnetic fields indicate the local currents under the Southern Rockies and Wasatch Front, west of the maxima in Z. The tracking of the magnetic field with the heat-flow contours is striking.

5.4 Conclusions

Seismic, heat-flow and geomagnetic depth sounding results agree in showing that the Basin and Range Province is underlain by upper mantle material at higher temperatures, at a given depth, than that under the Great Plains or the Colorado Plateau. Magnetotelluric results by Swift (1967) also fit in to this picture. Figure 5.9 presents the essential results of the 1967 GDS array study discussed in this thesis. The model there given is, of course, not unique. It is, however, consistent with all of the geophysical information, though the GDS array study resolves details not revealed by the present seismic and heat-flow data.

Other large GDS array studies have been made in 1968 and 1969, to extend the investigation of upper

mantle conductivity structure southward to the Mexico-U.S. border and northward to the Trans-Canada Highway. When results are available from these later arrays it should be possible to set limits to the structures relating those here discussed to the East Pacific Rise and to those under the Northern Rockies.

BIBLIOGRAPHY

- Akasofu, S.I., 1966. Electrodynamics of the magnetosphere, Geomagnetic Storms Space Science Reviews 6,
- Akasofu, S.I., S. Chapman, and C.I. Meng, 1965. The polar electrojet, J. Atmosph. Terrest. Phys. 27, 1275.
- Akasofu, S.I., D.S. Kimball, and C.I. Meng, 1965. Dynamics of the aurora: II. Westward travelling surges, J. Atmosph. Terrest. Phys. 27, 173.
- Akasofu, S.I., C.I. Meng, and D.S. Kimball, 1966. Dynamics of the aurora: IV. Polar magnetic substorms and westward travelling surges, J. Atmosph. Terrest. Phys. 28, 489.
- Archambeau, C.B., E.A. Flinn, and D.G. Lambert, 1969. Fine structure of the upper mantle, J. Geophys. Res. 74, 5825-5864.
- Bonnevier, B., R. Boström, and G. Rostoker. A three dimensional model current system for polar magnetic substorms (submitted for publication).
- Bullard, E.C., 1967. Electromagnetic induction in the earth, Quart. J. RAS 8, 143-160.
- Cagniard, I., 1953. Basic theory of the magnetotelluric method of geophysical prospecting, Geophysics 18, 605-635.

- Caner, B., W.H. Cannon and C.E. Livingstone, 1967.
Geomagnetic depth sounding and upper mantle structure in the Cordillera Region of Western North America, J. Geophys. Res. 72, 6335-6351.
- Cantwell, T., 1960. Detection and analysis of low frequency magnetotelluric signals, Ph.D. Thesis, Department of Geology and Geophysics, Massachusetts Institute of Technology.
- Cantwell, T. and T.R. Madden, 1960a. Preliminary report on crustal magnetotelluric measurements, JGR 65, 4202-4205.
- Chapman, S., 1919. The solar and lunar diurnal variation of the earth's magnetism, Phil. Trans. Roy. Soc. London, Ser. A, 218, 1-118.
- Chapman, S., and T.T. Whitehead, 1923. The influence of electrically conducting material within the earth on various phenomena of terrestrial magnetism, Trans. Cambridge Phil. Soc. 22, 463-482.
- Chapman, S., and J. Bartels, 1940. Geomagnetism, Oxford University Press, London, 1049 pp.
- Clark, S.P., and A.E. Ringwood, 1964. Density distribution and constitution of mantle, Rev. Geophys. 2, 35-88.
- Cleary, J.R., and A.L. Hales, 1966. An analysis of the travel times of P waves to North American Stations, in the distance range 32° to 100° , Bull. Seismol. Soc. Amer. 56, 462-489.

- Doyle, H.A., and A.L. Hales, 1967. An analysis of the travel times of S waves to North American Stations, in the distance range 28° to 82° , Bull. Seismol. Soc. Amer. 57, 461-771.
- Dyck, A.V., and G.D. Garland, 1969. Canadian Journal of Earth Sciences 6, 513.
- Gough, D.I., and J.S. Reitzel, 1967. A portable three-component magnetic variometer, J. Geomag. Geoelect. 19, 203-215.
- Gough, D.I., and J.S. Reitzel, 1969. Magnetic deep sounding and local conductivity anomalies, in the application of Modern Physics to the Earth and Planetary Interiors, edited by S.K. Runcorn, Interscience Publishers (in press).
- Gough, D.I., and H. Porath, 1970. Evidence for a long-lived thermal structure under the Southern Rocky Mountains (to be published).
- Hakura, Y., 1966. Tables and maps of geomagnetic coordinates corrected by the higher order spherical harmonic terms, Radio Research Laboratories, Kokubunjo, Tokyo, 121-146.
- Hamilton, R.M., 1965. Temperature variation at constant pressure of the electrical conductivity of periclase and olivine, J. Geophys. Res. 70, 5679-5692.
- Hartman, A., 1963. Behandlung lokaler erdmagnetischer Felder als Randwertaufgabe der Potentialtheorie, Abhandl. Akad. Wiss. Göttingen, Math Phys. K., Bertr. I.G.J. 2, 1-50.

- Hyndman, R.D., 1963. Electrical Conductivity Inhomogeneities in the Earth's Upper Mantle, M. Sc. Thesis, University of British Columbia.
- Hyndman, R.D., and D.W. Hyndman, 1968. Water Saturation and High Electrical Conductivity in the Lower Continental Crust, Earth and Planet. Sc. Letters 4, 427-432.
- Jackson, J.D., 1962. Classical Electrodynamics, John Wiley and Sons, Inc., New York.
- Kertz, W., 1964. The conductivity anomaly in the upper mantle found in Europe, J. Geomagnetism Geoch. 15, 185-192.
- Lahiri, B.N., and A.T. Price, 1939. Electromagnetic induction in non-uniform conductors, and the determination of the conductivity of the earth from terrestrial magnetic variations, Phil. Trans. Roy. Soc., London, Ser.A, 237, 507-540.
- Matsushita, S., W.H. Campbell, 1967. Physics of Geomagnetic Phenomena Vol. I, Academic Press, New York and London.
- McDonald, K.L., 1957. Penetration of the geomagnetic field through the mantle, J. Geophys. Res. 62, 117-141.
- Oldenburg, D.W., 1969. Separation of Magnetic Substorm Fields for Mantle Conductivity Studies in the Western United States, M.Sc. Thesis, University of Alberta.
- Pakiser, L.C., 1963. Structure of the crust and upper mantle in the Western United States, J. Geophys. Res. 68,

- Parkinson, W.D., 1959. Directions of rapid geomagnetic fluctuations, *Geophys. J.* 2, 1-14.
- Parkinson, W.D., 1962a. The influence of continents and oceans on geomagnetic variations, *Geophys. J.* 4, 441-449.
- Parkinson, W.D., 1964. Conductivity anomalies in Australia and the ocean-effects, *J. Geomagnetism Geoelec.* 15, 222-226.
- Peeples, W.I., 1969. Magnetotelluric Profiling over a Deep Structure, Ph.D. Thesis, University of Alberta.
- Porath, H., D.W. Oldenburg, and D.I. Gough. Separation of magnetic variation fields and conductive structures in the Western United States (In Press).
- Price, A.T., 1949. The induction of electric currents in non-uniform thin sheets and shells, *Quart. J. Mech. Appl. Math.* 2, 283-310.
- Price, A.T., 1950. Electromagnetic induction in a semi-infinite conductor with a plane boundary, *Quart. J. Mech. Appl. Math.* 3, 385-410.
- Price, A.T., 1962a. The theory of magnetotelluric methods when the source field is considered, *J. Geophys. Res.* 67, 1907-1918.
- Price, A.T., 1964. A note on the interpretation of magnetic variations and magnetotelluric data, *J. Geomagnetism Geoelec.* 15, 241-248.

Reitzel, J.S., D.I. Gough, H. Porath, and C.W.

Anderson III, 1969. Geomagnetic deep sounding and upper mantle structure in the Western United States (In Press).

Rikitake, T., 1965. Electromagnetic induction in a semi-infinite conductor having an undulatory surface, Bull. Earthquake Res. Inst. 43, 161-166.

Rikitake, T., 1966. Electromagnetism and the Earth's Interior, Elsevier Publishing Company, New York.

Rikitake, T., and K. Whitham, 1964. Interpretation of the alert anomaly in geomagnetic variations, Can. J. Earth Sci. 1, 35-62.

Rikitake, T., I. Yokoyama, and S. Sato, 1956. Anomaly of the geomagnetic Sq variation in Japan and its relation to subterranean structure, Bull. Earthquake Res. Inst., Tokyo Univ. 34, 197-235.

Rostoker, G., 1966. Mid-latitude Transition Bays and their Relations to Spatial Movement of Overhead Current Systems, J. Geophys. Res. 71, 79-95.

Rostoker, G., 1968. Macrostructure of Geomagnetic Bays, J. Geophys. Res. 73, 4217-4229.

Roy, R.F., D.D. Blackwell, and F. Birch, 1968. Heat Generation of Plutonic Rocks and Continental Heat Flow Provinces, Earth and Planetary Science Letters 5, 1-12.

- Schmucker, U., 1964. Upper mantle, Symposium, IAGA-IUGG, Berkeley, Journal of Geomag. and Geoelect. Vol. XV, No. 4, 179-293.
- Schmucker, U., 1964. Anomalies of geomagnetic variations in the South-western United States, J. Geomag. Geoelect. 15, 193-221.
- Schmucker, U., 1969. Anomalies of geomagnetic variations in the South-western United States, Monograph Scripps. Inst. Oceanography (to be published).
- Siebert, M., 1958. Die Zerlegung eines zweidimensionalen Magnetfeldes in äussern und innern Anteil mit Hilfe des zweidimensionalen Fourier-Theorems, Abhandl. Akad. Wiss. Göttingen, Math. Physik. Kl. Beitr. I.G.J. 4, 33-38.
- Siebert, M., 1962. Die Zerlegung eines zweidimensionalen Magnetfeldes in äussern und innern Anteil mit Hilfe des Cauchyschen Integralformel, Z. Geophysics 28, 231-236.
- Seibert, M., and W. Kertz, 1957. Zur Zerlegung eines lokalen erdmagnetischen Feldes in äussern and innern Anteil, Nachr. Akad. Wiss. Göttingen, II, Math. Physik. Kl. 87-112.
- Swift, C.M., 1967. A magnetotelluric investigation of an electrical conductivity anomaly in the South-western United States, Ph.D. Thesis, Massachusetts Institute of Technology.

- Taylor, J.H., 1944. On the determinations of magnetic vertical intensity Z , by means of surface integrals, *Terrest. Magnetism Atmospheric Elec.* 49, 223-237.
- Tozer, D.C., 1959. The electrical properties of the earth's interior. In: L.H. Ahrens, F. Press, K. Rankama and S.K. Runcorn (Editors), *Physics and Chemistry of the Earth*, Pergamon, London 3, 414-436.
- Upper Mantle Project, 1964. Symposium, IAGA-IUGG, *Berkeley Journal of Geomag. and Geoelect.* Vol. XV, No. 4, 179-293.
- Vestine, E.H., 1941. On the analysis of surface magnetic fields by integrals, I. *Terrest. Magnetism Atmospheric Elec.* 50, 1-36.
- Vozoff, K., and C.M. Swift, 1968. Magnetotelluric measurements in the North German Basin, *Geophys. Prosp.* 16, 454-473.
- Wait, J.R., 1951. The magnetic dipole over the horizontally stratified earth, *Can. J. Phys.* 29, 577-592.
- Wait, J.R., 1960. Some solutions for electromagnetic problems involving spheroidal, spherical, and cylindrical bodies, *J. Res. Natl. Bur. Std. B.* 64, 15-32.

- Walker, J.K., 1964. Space-time associations of the aurora and magnetic disturbance, *Journal of Atmospheric and Terrestrial Physics* 26, 951-958.
- Ward, S.H. Mining Geophysics Vol. II, the Society of Exploration Geophysicists, Tulsa, Oklahoma.
- Warren, R.E., J.G. Scalter, V. Vacquier, and R.F. Roy, 1969. A comparison of terrestrial heat flow and transient geomagnetic fluctuations in the Southwestern United States, *Geophys. J.* 34, 436-478.
- Weaver, J.T., 1963. On the separation of local geomagnetic fields into external and internal parts, *J. Geophys.* 29-36.
- Whitham, K., 1963. An anomaly in geomagnetic variations at Mould Bay in the Arctic archipelago of Canada, *Geophys. J.* 8, 26-43.
- Whitham, K., 1964. Anomalies in geomagnetic variations in the Arctic archipelago of Canada, *J. Geomagnetism Geoelec.* 15, 227-240.
- Whitham, K., and F. Andersen, 1962. The anomaly in geomagnetic variations at Alert in the Arctic archipelago of Canada, *Geophys. J.* 220-243.

B29943